UNIVERSITY OF BELGRADE

FACULTY OF PHYSICS

Mohsan S. A. Eldakli

# TRANSFER OF KNOWLEDGE FROM SCIENTIFIC EXPERIMENT TO STUDENT LABORATORY - HOLLOW CATHODE DISCHARGE AND OPTOGALVANIC EFFECT

Doctoral Dissertation

Belgrade, 2017

УНИВЕРЗИТЕТ У БЕОГРАДУ

ФИЗИЧКИ ФАКУЛТЕТ

Мохсан С. А. Елдакли

# ТРАНСФЕР ЗНАЊА ОД НАУЧНОГ ЕКСПЕРИМЕНТА ДО СТУДЕНТСКЕ ЛАБОРАТОРИЈЕ – ЛАМПА СА ШУПЉОМ КАТОДОМ И ОПТОГАЛВАНСКИ ЕФЕКАТ

Докторска дисертација

Београд, 2017.

**Thesis advisor, Committee member:**

dr Bratislav Obradović, Associate professor

University of Belgrade, Faculty of Physics

**Committee member:**

dr Milorad Kuraica, Full professor

University of Belgrade, Faculty of Physics

**Committee member:**

dr Mićo Mitrović, Full professor

University of Belgrade, Faculty of Physics

**Committee member:**

dr Milivoje Ivković, Principal Research Fellow

University of Belgrade, Insitute of Physics

**Committee member:**

dr Nikola Cvetanović, Assistant professor

University of  Belgrade, Faculty of Transport and Trafing Engeniring

# Acknowledgement

I am grateful to my family on provided love, understanding and support, as well as on everything it could not even be counted.

I would like to thank the mentor Prof. dr Bratislav Obradović for the leading, voice of reason and numerous advices during research work and doctoral thesis as well as for numerous discussions about research, as well as physics in general.

I would like to thank to all the friends who have directly or indirectly contributed to this achievement.

# TRANSFER OF KNOWLEDGE FROM SCIENTIFIC EXPERIMENT TO STUDENT LABORATORY - HOLLOW CATHODE DISCHARGE AND OPTOGALVANIC EFFECT

**Abstract**: This thesis presents a study of two commercial hollow-cathode lamps (HCLs) with the intention of demonstrating different phenomena in gas discharges. The optogalvanic effect in both HCLs is produced by a laser diode radiated at the wavelength that corresponds to neon transition $1s^2$–$2p^2$ at 659.89 nm. The voltage–current characteristics of the lamps are explained using a classical theory of hollow-cathode discharge, while the optogalvanic signal is treated as a small perturbation of the discharge current. For certain values of voltage self-sustained current oscillations are observed in one of the HCLs. In the same HCL laser-induced optogalvanic dumped oscillations are detected. A phenomenological model that includes the effective circuit parameters of the discharge is used to explain the oscillation characteristics.

The main goal of this thesis is to present the results of the mentioned work as a foundation for experimental exercises for ungraduated or master students in physics. The experiments proposed in the thesis use HCLs and current/temperature controlled laser diode. Out of the thesis, four experimental exercises are given as potential work for students at the universities studying plasma physics. Each exercise is conducted in step-by-step manner; the theory related to the experiment is presented at first, experimental setup is given as a second part of the exercise, in the third part students are guided how to conduct experiments. After the laboratory work is done, students should use a program for graphical presentation for comparing, analyzing and plotting the results. Finally, they have to comment presented results.

This thesis shows that using affordable and simple equipment, experiments for undergraduate students can be formed in the field of physics of ionized gases.

**Research area:** Didactics

**UDC number:** 507.8

# ТРАНСФЕР ЗНАЊА ОД НАУЧНОГ ЕКСПЕРИМЕНТА ДО СТУДЕНТСКЕ ЛАБОРАТОРИЈЕ – ЛАМПА СА ШУПЉОМ КАТОДОМ И ОПТОГАЛВАНСКИ ЕФЕКАТ

**Сажетак**: Ова теза представља истраживање две комерцијалне лампе са шупљим катодама са намером да се демонстрирају различити феномени у електричним гасним пражњењима. Оптогалвански ефекат у обе лампе добијен је озрачивањем шупље катоде зрачењем ласерске диоде на таласној дужини 659,89 nm која одговара прелазу $1s^2$–$2p^2$ атома неона. Струјно-напонске карактеристике коришћених лампи објашњене су класичном теоријом електирчног гасног пражњења шупље катоде, док је оптогалвански сигнал третиран као мала пертурбација струје пражњења. На одређеним вредности напона једне од лампи детектоване су само-одживе сопствене осцилације. У истој лампи су детектоване и ласерски индуковане амортизоване оптогалванске осцилације. Феноменолошки модел који укључује параметре ефективног електричног кола пражњења искоришћен је за објашњење карактеристика детектованих осцилација.

Главни циљ ове тезе се састоји у коришћењу резултата поменутог истраживања као основе за експерименталне вежбе за студенте основих или мастер студија из физике. У експериментима предложеним у тези се користе лампа са шупљом катодом и ласерска диода контролисана струјом /температуром. Из ове тезе су произашле четири вежбе погодне за рад са студентима који на универзитетима изучавају физику плазме. Свака вежба се одвија корак по корак: на почетку је дат теоријски опис феномена на која се односи експеримент, затим је дата поставка експеримента као други део вежбе, док у је трећем делу дато упутство за извођење експерименте. Након завршетка лабораторијског рада, студенти су упућени да користе програм за графичко представљање, упоређивање и анализу експерименталних резултата. Коначно, студенти морају коментисати добијене резултате.

Ова теза показује да се употребом приступачне и једноставне опреме могу формирати студентски експерименти из области физике јонизованих гасова.

# Contents

# 1 Introduction

Plasma physics or more precisely, physics of ionized gases and plasma is the study of charged particles and fluids interacting with electric and magnetic fields. It is a basic research discipline that has many different areas of application - space and astrophysics, controlled fusion, accelerator physics, and industrial processing. Basic research in plasma physics is carried out and applied to all areas by three broad categories - theoretical, computer simulation and experimental studies. Scientific expertise, in all of these areas, is guideline for both undergraduate and graduate education in plasma physics, providing research opportunities for students. There are many problems related to teaching and learning of plasma physics which are related to the lack of facilities in insufficiently equipped laboratories, and the extent to which the university is conductive for practical activities. It is also a fact that many universities cannot afford to perform research in plasma physics with their own resources. In plasma, most of equipments are too expensive (vacuum pumps power supplies…), so it is difficult to arrange low cost experiments. However, there exists equipment some of which is not so expensive, designed for purposes other than demonstration of plasma phenomena, which can be used for student's exercise. Cheap and easy to use commercial hollow cathode lamps (HCLs) are one of the mentioned equipment and a reason to conduct the experiments on the glow discharge. Also, HCLs offer spectral purity, stable operation, low noise, long life, and high output intensity.

Electric discharge in gases occurs when the applied voltage between two electrodes establishes field strength that exceeds breakdown by passing current through a noble gas. The potential drops rapidly close to the cathode, varies slowly in the plasma and changes again close to the anode. The electric fields in the system are restricted to sheaths at each of the electrodes. Electrons originating at the cathode are accelerated by the electric field, collide with the surrounding gas molecules, transfer energy, leave by diffusion and recombination, slowed by the anode and transferred into the outside circuit. The luminous glow is produced because the electrons have enough energy to generate visible light by excitation collisions. Since there is a

continuous loss of electrons, there must be an equal degree of ionization going on to maintain the steady state.

A special type of glow discharge is a hollow cathode discharge (HCD) that has been the subject of investigations by physicists and chemists for almost a century. Several hundred references may be found concerning various aspects of the HCD. Ever since, they have received considerable attention, and have been used in a variety of applications [1-8]. HCDs are glow discharges with the cathode fall and negative glow confined in a cavity within the cathode. The discharge generation depends upon various parameters (current, voltage, charge), operating conditions (pressure, temperature), geometry, material, and the filling gas. In a HCD, at low gas pressure, in the high-voltage regime and bore diameter of the cathode, the negative glows from opposite walls to inner surface of the hollow cathode coalesce to produce neutral and excited atoms and ions of high densities at the center of the hollow cathode. Two hollow cathode geometries have been used to investigate the properties of discharges: parallel plate and cylindrical hollow cathode. First one has the advantage that the potential of each cathode can be adjusted independently. However, higher plasma densities are achieved with cylindrical hollow cathode, in which discharge is generated within a structure composed of an anode, a cup-shaped cathode, and a buffer gas at low pressure encased in a glass enclosure. The most important parameter of cylindrical hollow cathode is its radius. Geometry leads to a higher density of sputtered atoms from the cathode material with the lower ionization potential, which influences the secondary processes at the cathode.

Optogalvanic effect (OGE) is the electrical response to an optical perturbation induced by laser beam [9]. Gas impedance changes due to the resonant light absorption at an optical transition. Atoms and molecules populate the various energy levels of the species present in the discharge plasma, followed by collisions that result in redistribution of the plasma species in energetically favorable states. Many studies reported in the literature identify and quantitatively characterize the dominant physical processes that follow OGE [10-15]. In 1920s, Penning observed change of gas discharge conductivity due to resonant light absorption at an optical transition [16,17]. OGE has been used as a tool to investigate different characteristics of atoms and molecules in discharge environments [18], has been widely studied and exploited through multiple experiments for different purposes such as plasma diagnostics

[19,20], atomic and molecular spectroscopy [21,22], oscillatory behavior of discharge current [23], etc. For the purpose of this research, the phenomenon, characteristics and the potential applications of the OGE are explored in a broad set of experiments to gain a better insight into the physical process of hollow cathode discharge. The transient response and steady states response of OG signals [24] are analyzed. DC and oscillation current in the dynamic of the HCD [25,26] are also observed.

This thesis aims to correlate and compare some of mechanisms contributing to the HCD in relation to a varied range of operating conditions and parameters. Main objective is to study the voltage-current characteristics, OG signals and self-sustained and laser induced current oscillations in two commercial HCLs. The purpose of this dissertation is to use relatively simple and accessible devices like HCLs and current/temperature controlled laser diode to present the mentioned phenomena to undergraduate students. The research in this context is based on tracking down the current oscillations from the occurrence until they decrease to zero. The laboratory work itself consisted of registering I-V and frequency-current (f-I) dependence. From this processing one can determine the points of stability and current oscillations.

The main goal of this study is to present the results of this work as an experimental exercise for motivated graduated students in physics, thus deepening students' knowledge on the OGE. The simplest object for such studies is presented with research in various laboratory conditions and with different hollow cathode lamps. In order to follow experiments one requires knowledge of the discharge, techniques and devices used for the experiments. Students are expected to be familiar with software for recording and processing data.

The OGE is investigated during laboratory work. Firstly, students set up the experiment. They use Ca-Ne and Sb-Ne HCLs, first one to generate current pulse for driving the laser diode and the second for the OGE observation and investigation. The laser diode is tuned to the appropriate wavelength (659.9 nm), and directed to enter of the HC discharge lamp filled with Ne gas. Atoms absorb those photons whose energies correspond to certain atomic transitions; the light directed at plasma results in an impedance change only when the frequency of the light matches the transition of the atoms in the plasma. The discharge current is controlled by adjusting the voltage on power supply. The resulting OG signal is recorded, and displayed on a digital oscilloscope. After the setup, students observe the discharge, oscillation current, and

voltage. The stored data from the oscilloscope is converted to the ASCII format and further analysis performed on collected data.

After the laboratory work is done, students used some (commercial) computer program for fitting (e.g. Origin), comparing, analyzing and plotting the results. Students use this tool to analyze the nonlinear fits of the observed time-resolved OG waveforms.

The thesis is organized as follows. Glow discharge is presented in the following section. The chapter is also a theoretical introduction to the process of a HCD. Pre-discharge, discharge and transitions are explained in details. Also, a review of the hollow cathode effects is given in this chapter. Chapter 3 describes mechanism of OGE. Chapter 4 discusses both self-generated and laser induced oscillations in the gas discharge. Chapter 5 outlines experimental setup. Measurements of electrical properties of the HC discharge for both steady states and transient phases during formation of the discharge induced by laser beam are described. In Chapter 6, the experimental results are presented. By varying the discharge current, and therefore relaxation rate, a set of time-resolved OG waveforms is compiled in order to reveal the effects of varying the discharge currents. Current oscillations were observed in two ranges, and experimental results compared with fits. Fits are based on the electrical circuit analysis which is given in this chapter. Exercises for the students are suggested and given in Chapter 7, finally summary and conclusions are given in Chapter 8.

Contents of this thesis are based on the following papers of the author:

1) M. S. A. Eldakli, S. S. Ivković, B. M. Obradović,Optogalvanic effect and laser-induced current oscillations in hollow-cathode lamps, European Journal of Physics, 38 (2017) 025210

2) D. V. Redžić, M. S. A. Eldakli, M. D. Redžić, Image charge inclusion in the dielectricsphere revisited, European Journal of Physics, 33(2012) 1751-1759

## 2 Glow discharge

Electric discharge in gases occurs when electric current flows through a gaseous medium due to ionization of the gas. Depending on several factors, the discharge may radiate ultraviolet, visible or infrared light. The properties of electric discharges in gases are studied in connection with design of lighting sources and in the design of high voltage electrical equipment. The glow discharge is a self-sustaining discharge with a cold cathode emitting electrons due to secondary emission mostly due to positive ion bombardment. A distinctive feature of this discharge is a layer of large positive space charge at the cathode, with a strong field at the surface and considerable potential drop of $100 - 400$ V (or more). This drop is known as cathode fall, and the thickness of the cathode fall layer is inversely proportional to the density (pressure) of the gas.

When the applied voltage exceeds the breakdown voltage, the gas ionizes, and begins conducting electricity, causing it to glow with a light. Several regions can be observable in a discharge, ones described as glows emit significant light, while others labeled as dark spaces do not (see Figure 2.1).
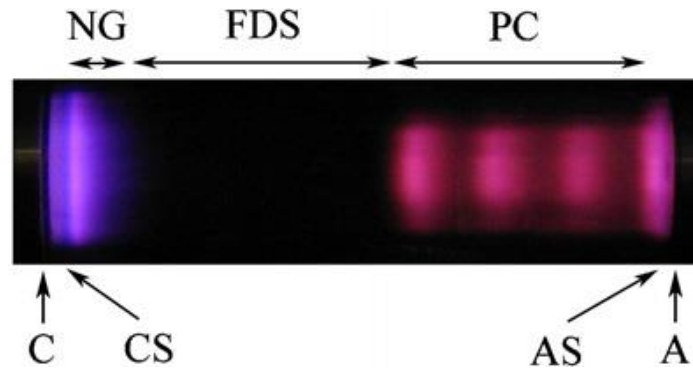


Figure 2.1. Regions in DC glow discharge [37]. C – cathode, CS – cathode space, NG – negative glow, FDS – Faraday dark space, PC – positive column, AS – anode space, A – anode.

Three major regions can be distinguished in the discharge: the cathode region, the glow regions, and the anode region, and eight different sub-regions can be observed. The Aston dark space is a thin region close to the cathode. It has a negative space charge, meaning that electrons outnumber the positive ions in this region. The

electron density and energy is too low to efficiently excite the gas, it consequently appears dark. In the cathode glow, next to the Aston dark space, the electrons are energetic enough to excite the neutral atoms during collisions. The cathode dark space is a dark region that has a strong electric field, a positive space charge and a relatively high ion density. In this region the electrons are accelerated by the electric field. Positive ions are accelerated towards the cathode. They cause the sputtering of the cathode material and the emission of secondary electrons. These electrons will be accelerated and cause the creation of new ions through collision with neutrals. The voltage drop between the two electrodes develops almost entirely in a narrow region near the cathode. The negative glow has the brightest intensity of the entire discharge. Electrons carry almost the entire current in the negative glow region. Electrons that have been accelerated in the cathode region to high velocity produce more electrons though ionization of the surrounding gas. Slower electrons that have had inelastic collisions already induced atom or molecular excitations. The negative glow is predominantly generated by the slow electrons. The negative glow is the region where most exciting and ionizing collision processes occur because of the high density for both negative and positive charged particles in this area. Hence, this zone is the source of light. In this region, positive and negative space charge values are close to each other. At the end of the negative glow, the electrons have lost most of their energy; excitation and ionization processes cease to exist. This is the start of the Faraday dark space which separates the negative glow from the positive column. The electron energy is low in this region. The positive column is a luminous region that prolongs the negative glow to the anode, and it is characterized charge neutrality. The electric field in it is just large enough to maintain the degree of ionization to reach the anode. The anodic glow is slightly brighter than the positive column. It is not always observed. The anode glow is the boundary of the anode sheath. The anode dark space (anode sheath) is the space between the anode glow and the anode itself. It has a negative space net charge density due to electrons traveling towards the anode.

As the discharge becomes more extended (stretched horizontally in the geometry of the Figure 2.1), the positive column may become striated, which means alternating dark and bright regions that may form. Compressing the discharge horizontally will result in fewer regions. The positive column will be compressed while the negative

glow will remain the same size, and with small enough gaps the positive column will disappear altogether.

## 2.1 Hollow cathode discharge - overview

In case that cathode with the cylindrical structure replaces single plane cathode in a glow discharge (see Figure 2.2), the negative glow rises inside the hollow structure of the cathode in a specific range of operating conditions. The product (pd) of the pressure p and the distance between anode and cathode d obeys the Paschen's law, which determines the required breakdown voltage, given values of p and d, $V_B=f(p,d)$ as well as the identity of the operating gas. The breakdown condition contains coefficient two parameters, which characterize the reflecting action of the electric field and the lifetime of the electrons in the discharge. Under such conditions and constant current, the voltage is found to be lower and if the voltage is kept constant the current is found to be orders of magnitude larger than for the plane cathode. This effect is known as hollow cathode effect (HCE) [27]. It is generally accepted, that the pendular motion of high-energy electrons and the efficient collection of ions are key elements in most of the HCDs [28-31].
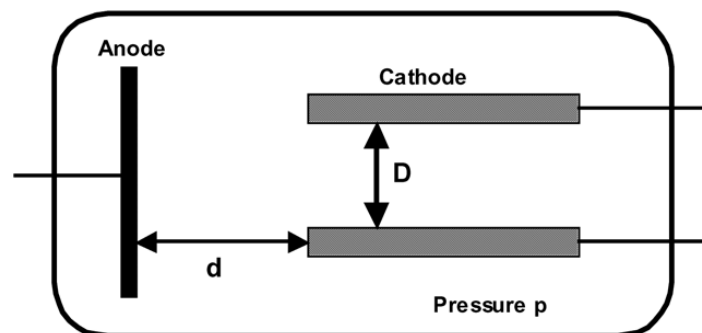


Figure 2.2 General diagram of hollow cathode discharge device [32]

A calling law, unique to the HCD, involves the product of the pressure and dimension of an aperture to the cathode pd, ranging from 0.1–10 Torr cm. In this case the discharge develops in stages, with each stage having its distinctive V–I

characteristic. At low currents one observes a pre-discharge, a glow discharge with the cathode fall region outside the cathode structure. Throughout this stage the electrons follow trajectories determined by the electric field between the cathode and anode in the absence of a discharge, in a single region of positive space charge. With increasing current, the positive space charge region moves closer to the cathode and eventually enters the cavity in the cathode. Transition from the pre-discharge to a discharge is accompanied by a drop in the sustaining voltage, as the current is increased, which is a region of operation that is traditionally referred to as the hollow cathode mode. V–I characteristic becomes essentially flat for further growth of current while the cathode layer expands across the surface outside the cavity [32].

Temporal evolution of the HCD can be separated into four different parts: pre-discharge (electron beam), development of discharge, high-current main discharge and decay of the discharge plasma, which is shown in Figure 2.3. Before the pre-discharge phase, the potential distribution is determined by the geometry of the electrodes. At low currents, a pre-discharge is observed. It is a glow discharge, whose cathode fall region is generally outside the cathode structure. There is a single region of positive space charge disc and electrons follow a path that is essentially determined by the by the direction of the electric field between the anode and the cathode in the absence of a discharge. Evolution of the electric field configuration and change in the gap potential is instantaneously reflected in charge distribution. As the current increases, the positive space charge region moves closer to the cathode and enters a hollow cathode structure. The electrical field, which was initially axial, becomes radial and a potential 'trough' is created within the cavity. This causes the acceleration, which leads to the oscillatory motion of electrons. In the transition from a pre-discharge to the discharge, sustaining voltage drops as current increases. The ion density increases which leads to the formation of a positive space charge, then starts to shift towards the cathode and deforms the initial electrical field configuration. This precedes the formation of the sheath at the cathode. In this phase of the discharge development electron avalanches, which is initiated by the seed electrons, contribute to the build-up of the ion density in the hollow cathode cavity. This phase is characterized by a large increase in the current density and discharge light density followed by a drop of a sustaining voltage. As the current is increased further I-V characteristics show constant voltage at increasing current. When the cathode layer

reaches the boundaries of cathode, any further increase of current requires an increase in discharge voltage and the discharge changes from normal into an abnormal.
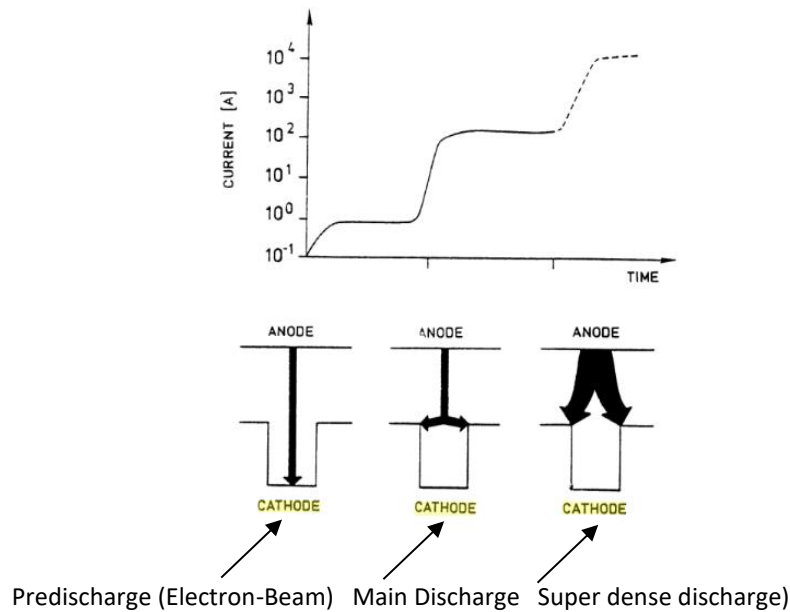


Figure 2.3 Stages of the discharge development [33]

## 2.2 Hollow cathode discharge - theory

In this part it an elementary theory of the glow discharge is presented, applied on a hollow cathode configuration. It is based on using Townsend's ionization equations with suitable boundary conditions in conjunction with Poisson's equation. Though outdated, this old approach looks in methodology more accessible to undergraduate students than more accurate methods like fluid model, kinetic Boltzmann equation or some of numerical simulations (Monte Carlo and Particle-in-cell). However, numerical simulations are often indispensable in areas where the gap between a simple theory and experiment is large.

A number of glow discharge regions (the Crooks dark space, the negative glow, Faraday dark space, positive column, anode region) are in the case of the hollow cathode discharge reduced to the Crooks dark space and the negative glow. Also, the hollow cathode lamps are designed to work as an abnormal glow discharge i.e. an increase in current causes an increase in cathode fall voltage and in current density. The dark space is characterized by non-homogeneous electrical properties. The electric field created by the voltage difference between electrodes has a largest

(absolute) value at the cathode surface and drops to zero at the end of the dark space. Absolute value of the electric field approximately linearly decreases from the cathode as:

$$E = E(0)\left(1 - \frac{x}{d}\right) \tag{2.1}$$

Where $E(0)$ is the electric field at the cathode i.e. for $x = 0$, $x$ is the distance from the cathode, $d$ is the cathode fall length. Equation (2.1) is an experimental fact although it is confirmed by calculation using experimental data of ion velocities [28]. The potential $V$ at distance $x$ is then

$$V = V_c\left[\frac{2x}{d} - \left(\frac{x}{d}\right)^2\right] \tag{2.2}$$

Where $V(0) = V$ at $x = 0$ i.e. at the cathode. The total current density at any position in the discharge is:

$$j = j^+ + j^e \tag{2.3}$$

Where $j^+$ and $j^e$ are ion and electron current densities.

Poisson's equation in MKS system for net space charge densities $\rho^+ - \rho^e$ is:

$$\frac{dE}{dx} = \frac{\rho^+ - \rho^e}{\varepsilon_0} \tag{2.4}$$

Neglecting the negative space charge in the dark space one can obtain:

$$\frac{dE}{dx} = \frac{\rho^+}{\varepsilon_0} = \frac{j^+(0)}{\varepsilon_0 v^+(0)} \tag{2.5}$$

Where $j^+(0)$ and $v^+(0)$ are ion current density and ion drift velocity at the cathode. On the other hand from (2.1) stands

$$\frac{dE}{dx} = -\frac{E(0)}{d} = \frac{2V(0)}{d^2} \tag{2.6}$$

Where $V(0) = \frac{E(0)}{2d}$ and finally

$$j^+(0) = \varepsilon_0 v^+(0)\frac{2V(0)}{d^2} \tag{2.7}$$

Ions of high energy (of the order of $e \cdot V(0)$) can be observed at the cathode what can only be a consequence of subsequent charge transfer processes. If the mean free path for the charge transfer is $\lambda$ than the potential $V'$ at the distance $\lambda$ from the cathode is

$$V' = V(0)\left[\frac{2\lambda}{d} - \left(\frac{\lambda}{d}\right)^2\right] \tag{2.8}$$

As the kinetic energy of the ions arriving at the cathode is

$$\frac{1}{2}mv^+(0)^2 = eV' \tag{2.9}$$

then, for ion of mass m and for $\lambda \ll d$, from (2.8) and (2.9) one obtains

$$v^+(0) \approx \sqrt{\frac{4e}{m}\frac{\lambda}{d}V(0)} \tag{2.10}$$

The ion current density at the cathode surface is obtained by combining (2.7) and (2.10):

$$j^+(0) \approx 2\varepsilon_0\sqrt{\frac{e\lambda}{m}}\frac{V(0)^{\frac{3}{2}}}{d^{\frac{5}{2}}} \tag{2.11}$$

Now, it is needed to find a connection between the total and the ion current density and for that, it is necessary to include all processes that lead to the emission of electrons from the cathode. The electron current density at the cathode surface is:

$$j^e(0) = \gamma_i j^+(0) + D_p j_d^e + G_p j_g^e + D_m j_d^e + G_m j_g^e \tag{2.12}$$

where $\gamma_i$ is coefficient which represents efficiency of the secondary electron emission from the cathode surface for the impact of ions; $j_d^e$ and $j_g^e$ are the electron current densities in the dark space ($0 < x < d$) and the negative glow ($d<x$); $D_p$ and $G_p$ are photon coefficients for the dark space and negative glow, respectively. Metastable atoms act in the same way as photons and, by analogy, $D_m$ and $G_m$ are metastable coefficients for the mentioned regions. The photon and metastable coefficients are:

$$D_p = f_d\gamma_p n_p^d$$

$$G_p = f_g\gamma_p n_p^g$$

$$D_m = d_d \gamma_m n_m^d$$

$$G_m = d_g \gamma_m n_m^g$$

where $\gamma_p$ and $\gamma_m$ are coefficients which represents efficiency of the secondary electron emission from the cathode surface for the impact of photons and metastable atoms, respectively. The photons which have energies larger than the work function of the cathode material are often named as "energetic photons". $n_p^d$ and $n_p^g$ are numbers of energetic photons created by each electron entering the dark space and the negative glow; $f_d$ and $f_g$ are geometric factors for their collection at the cathode i.e. fractions of photons which strike the cathode. In the hollow cathode configuration almost all emitted energetic photons got the cathode surface, so $f_d$ and $f_g$ are nearly equal to one. $d_d$ and $d_g$ describe mutual and integrated influence of geometrical factors and diffusion for metastable atoms. $n_m^d$ and $n_m^g$ are numbers of metastable atoms created by electrons in the dark space and in the negative glow. If it is assumed that the current in the negative glow is the total current $j_g^e \approx j$ than from (2.12) one can obtain:

$$\frac{j^+(0)}{j} = \frac{1 - D_p - G_p - D_m - G_m}{1 + \gamma_i - D_p - D_m} \tag{2.13}$$

Since the number of energetic photons in the dark space is negligible in comparison to their number in the negative glow, $D_p$ can be neglected. Similarly, the metastable atom concentration in the dark space is much lower than in the negative glow and consequently $D_m$ also can be neglected. Finally

$$\frac{j^+(0)}{j} = \frac{1 - G_p - G_m}{1 + \gamma_i} \tag{2.14}$$

The $G_p$ as the secondary emission coefficients due to radiation from the glow and the $G_m$ as the secondary emission coefficients due to metastables produced in the negative glow must depend on the parameters of the dark space. Electrons are multiplied from the cathode to the negative glow and the number of ionizing collisions of fast electrons entering the glow is:

$$\bar{s}d\left(1 - \sqrt{\frac{V_e}{V(0)}}\right) \tag{2.15}$$

where $\bar{s}$ is the average ionization coefficient in the dark space and $V_e$ is a minimal energy for fast electron, characteristic of the working gas (for neon $V_e > 50$ eV). It can be shown that the relation stands:

$$f_g \gamma_p \eta_p b V(0) e^{\bar{s}d\left(1-\sqrt{\frac{V_e}{V(0)}}\right)} j^e(0) = G_p j_g^e \tag{2.16}$$

Where $\eta_p$ is a number of active quanta per one volt produced by one electron in the glow and $b_p V(0)$ ($b_p < 1$) is the average energy of fast electrons at the entrance of the glow.

As $j_g^e = j^e(0) e^{\bar{s}d}$ for the $G_p$ it is obtained

$$G_p = f_g \gamma_p \eta_p b_p V(0) e^{-\bar{s}d\sqrt{\frac{V_e}{V(0)}}} \tag{2.17}$$

Analogously for metastable atoms, the $G_m$ is obtained as:

$$G_m = d_g \gamma_m \eta_d b_m V(0) e^{-\bar{s}d\sqrt{\frac{V_e}{V(0)}}} \tag{2.18}$$

Combining (2.13) and (2.11) one can get:

$$j = 2\varepsilon_0 \sqrt{\frac{e\lambda}{m}} \frac{V(0)^{\frac{3}{2}}}{d^{\frac{5}{2}}} \frac{1 + \gamma_i}{1 - G_p - G_m} \tag{2.19}$$

Equation (2.19) gives a fitting function for I - V graphs for the hollow cathode lamps in the forms:

$$I(V) = k_1 V^{\frac{3}{2}} \frac{1}{1 - G} \tag{2.20}$$

$$G(V) = k_2 V e^{-k_3 \sqrt{\frac{1}{V}}} \tag{2.21}$$

where $k_1 = 2\varepsilon_0 \sqrt{\frac{e\lambda}{m}} \frac{1+\gamma_i}{d^{\frac{5}{2}}} S$ (S –the cathode surface), $k_2 = \gamma_p \eta_p b_p + d_g \gamma_m \eta_d b_m (f_g \approx$ 1 for the hollow cathode discharge) and $k_3 = \bar{s}d\sqrt{V_e}$. Here it is assumed that the dark space thickness d and average ionization coefficient $\bar{s}$ dependence on V is of secondary importance (insignificant) in comparison with G dependence on V (e.g. $d \sim \ln G$).

## 2.3 Hollow Cathode Lamps

A hollow cathode lamp is one of the most important components in atomic absorption spectroscopy. Atomic absorption spectroscopy is a common technique to determine the concentration of a particular analyte in a sample. This can be done since the absorption spectrum, molar absorbance of the sample and the amount of energy that passes through the atomized sample are known in advance. Hollow cathode lamps, as light sources in which radiation is produced by electrical discharges in gases at low pressure, have different internal geometries. Hollow cathodes can take cylindrical (Figure 2.4a-2.4c), spherical (Figure 2.4d), parallel plates (Figure 2.4e-2.4f), slit (Figure 2.4g), and helical forms (Figure 2.4h).
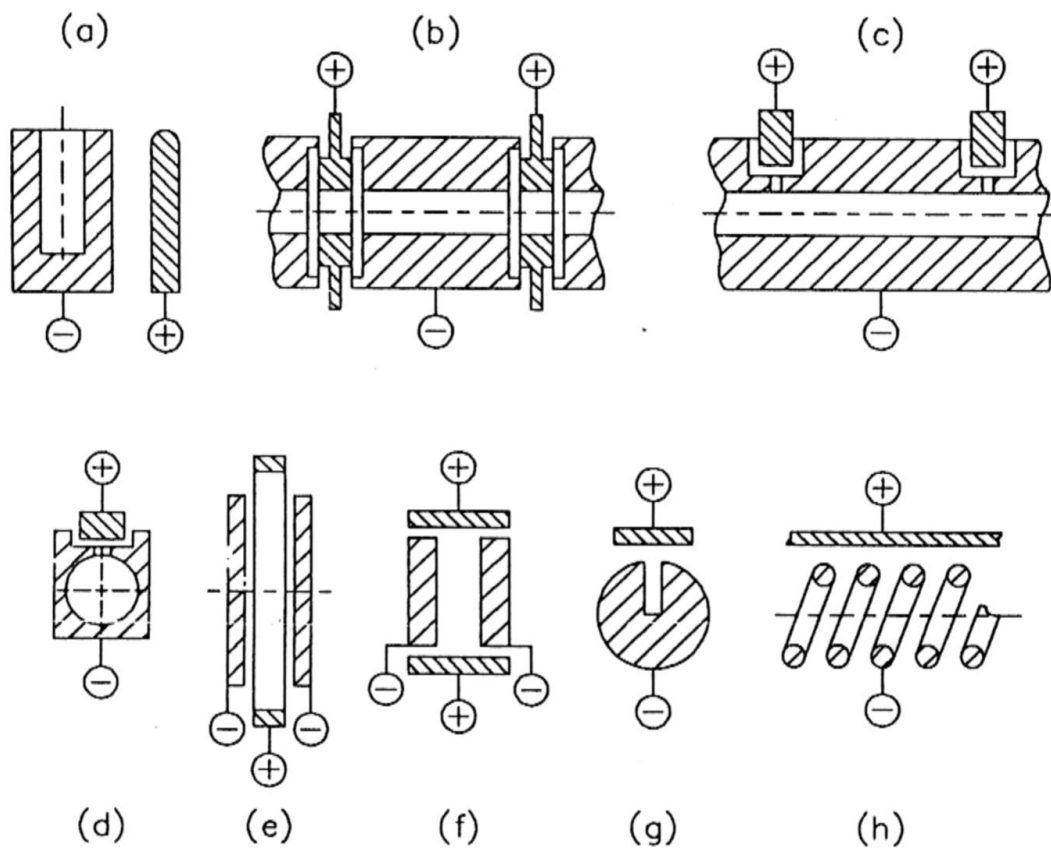
Figure 2.4 Hollow cathode lamp geometries [38]

The performances of a HCL vary with the cathode composition, gas fill pressure, bore diameter of the hollow cathode and the operating current, while pressure, voltage and current are interdependent parameters that can be controlled. The end window of the lamp is usually made of quartz that transmits the light of spectral lines of the elements

to be determined. A lamp is connected to a regulated low voltage low current DC power supply, having specified current settings, to assure and adjust the DC power supply to be within the operational parameters. The cylindrical HCL (Figure 2.5) used in this thesis consists of anode and cylindrical cathode sealed in a glass tube containing neon gas at low pressure.
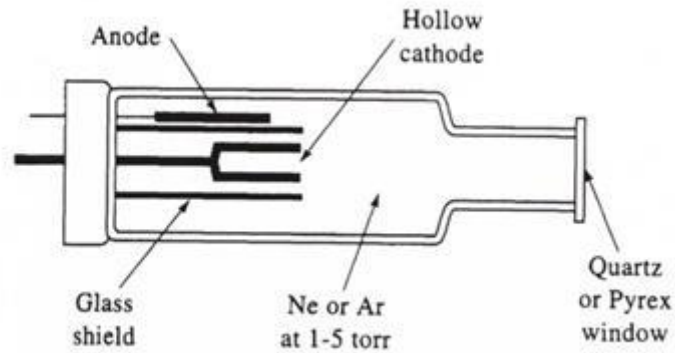


Figure 2.5 Hollow cathode lamp

The emission from the HCL is a process that consists of five steps: (1) ionization of rare gas atoms, (2) acceleration of gas into the cathode, (3) sputtering the metal atoms of the cathode into gas, (4) collision of sputtered atoms with gas atoms or electrons and (5) decay to lower energy levels by emission of light. Electrons and photons with sufficient energy collide with the neutral atoms and molecules in the feed gas, while the energy supply for plasma generation can be generated by adiabatic compression or via energetic beams that moderate in a gas volume. Scheme of processes caused atomic emission is presented in Figure 2.6. The resultant output is unique line spectrum, suitable for highly specific and sensitive material analysis, since the different materials give different wavelengths of light.
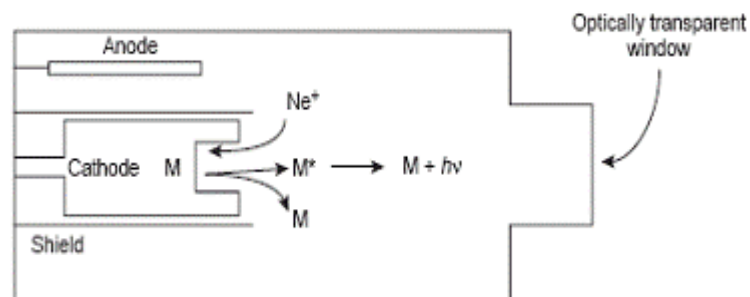


Figure 2.6 Scheme of process caused atomic emission of cathode material [39].

There are several producers of HCL. Hamamatsu offers 66 types of single element HLCs and 7 types of multi element HCLs, Heraeus produced 70 single element HCLs and more than 120 multi element HCLs [41], SpectroLamps offers lamps that are designed for optimal performance, chemical sensitivity, emit high intensity at the recommended current resulting in low S/N ratio. Capital Analytical offers variety of single and multi- elements HLC [1]. Figure 2.7 presents Ne-Sb HCL, developed by Hamamatsu.
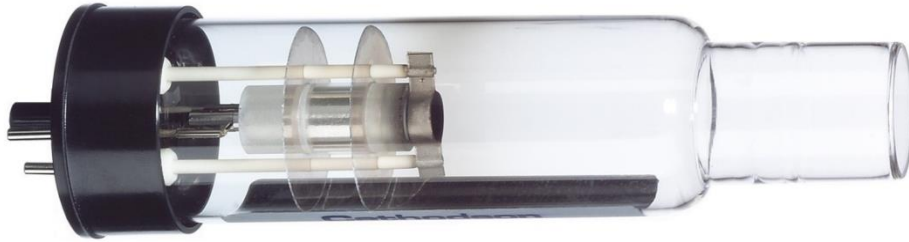


Figure 2.7 Hollow cathode lamp (Ne-Sb) [43]

# 3 Optogalvanic effect

The flow of electricity through gases induces a great variety of luminous phenomena, which are typical for various electrical discharges. Changes in electrical properties of a self-sustained gas discharge can be noticed when gas is illuminated by radiation which is resonant with an atomic or molecular transition of a species contributing to the discharge mechanisms. This phenomenon is called the optogalvanic effect (OGE). OGE is a direct consequence of the laser excitation of the atoms populating the various energy levels of the species present in the discharge plasma, followed by collisions and redistribution of the plasma species in energetically favorable states. This change is observed as an increase or decrease in the conductivity of the discharge, which can be recorded by illuminating the gas discharge using a tunable light source.

There are two different mechanisms proposed for the origin of the OGE. First, excited atom becomes ionized and the conductivity of the discharge increases as a laser excitation. This leads to electron impact ionization from higher atomic levels that have a larger cross section for this process. Second, the laser excitation of atoms to higher electronic states perturbs the equilibrium established between the electron temperature and the atomic excitation temperature. Super-elastic collisions between the electrons and the atoms restore the equilibrium, which ends up the excess energy in an increased electron temperature and increases conductivity of the discharge. Both mechanisms proceed simultaneously [1]. The atom excitation in the discharge allows the observation of transitions starting from the metastable or excited state. Specific collision state dynamics of a particular species can be investigated since the rate of ionization undergoes changes due to collisions within the discharge plasma and depends on the probability of atomic ionization which occurs when the atom is hit by an electron [2]. The very high intensity of OGE in the cathode region is explained by changing of the secondary electron emission caused by change of photon and/or metastable atom concentration by resonant laser irradiation.

## 3.1 History of optogalvanic effect

The first publications related to OGE were published in 1920 when Foote and Mohler [3] observed ionization of Cesium vapor that has occurred after the sample had been irradiated with light of wavelength resonant to wavelengths at which Cesium emits light. In 1928, Penning observed the same phenomenon by detection of variation in the impedance associated with the discharge of an element irradiated with the emission of an identical discharge. In 1930, Terenin observed the OGE in molecules while studying the photo-ionization of salt vapors [4]. In 1940, Joshi also discovered OGE while studying Chlorine in a discharge tube and noted that as the sample was irradiated with energies equal to the difference in energy between the ground and excited states the current through the discharge was changed [5]. While the OGE was observed through various experiments for more than 50 years, the serious investigations on OGE were not explored until the development of tunable dye lasers that were excellent as light sources as well as sensitive detection methodologies which opened many new possibilities [6,7]. In this way the wavelength of the laser beam that passes through an electrical discharge are finely tuned, changes in the impedance correspond directly to the wavelengths, which induce transitions between the exact energy levels of the various atomic, ionic or molecular species in the discharge. Since one can get an OG spectrum by monitoring the discharge current as a function of wavelength, the OGE is considered as a useful detection method for obtaining spectroscopic data without the use of absorption or emission spectroscopy, discharge diagnostics, laser calibration and stabilization, saturation intensity measurements of excited state transitions, isotope radio spectrometry, laser OGS and more [6, 44-47].

## 3.2 Optogalvanic effect in neon

Green et al. [6] have measured a change in the voltage across the discharge tube while irradiating the sample at the laser wavelength corresponding to a transition of the sample. This type of research illustrated the usefulness and applications of a HCL as the gas discharge environment, which allowed not only excited state transitions but resonance transitions as well. The result of theoretical and experimental study of the resonant OGE in Ne discharges conducted by Shuker, Ben-

Amar and Erez in 1983 [48], illustrates the experiments for various Ne transition, including some Ca cathode Penning effects (Figure 3.1).
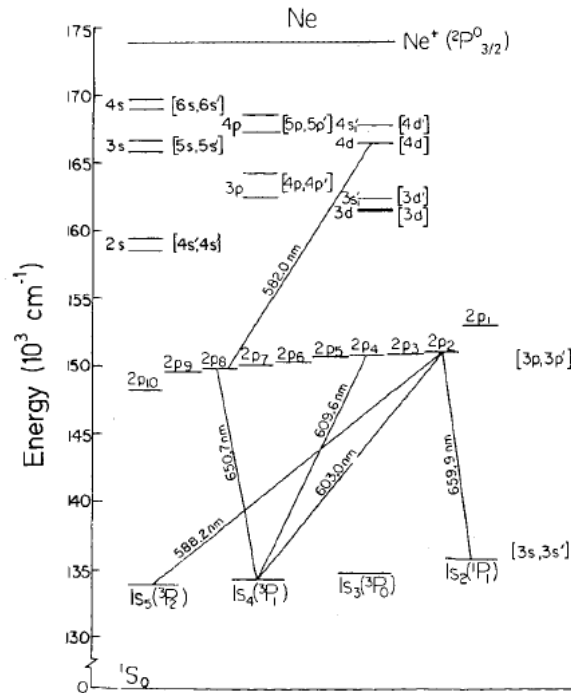


Figure 3.1 Energy levels of Neon (simple Ne transitions) [39].

In pulsed experiments the light is "On" for a short time ($\sim 10^{-8}$s) and the voltage is followed (without light) for tens of microseconds.

Pulse response: Let K be the "multiplication factor", i.e. the number of electrons ejected from the cathode by ions, photons, etc., created by a single electron ejected one generation previously and let T be the mean time of a generation. The current I in the discharge is given with the following formula

$$I(t) = I_0 \exp\left((K-1)\frac{t}{\tau}\right) \qquad (3.1)$$

For the steady state, K is equal to unity while any change in the plasma affects K, which is followed by a rapid change in current.

Transitions from the meta-stable Ne levels ($1s_i$-2p): A systematic study of the 1s-2p Ne transition reveals the following: a) the amplitude ratios are independent of DC current; b) the amplitudes are proportional to the current; c) the relaxation rates depend linearly on the current; d) the integrated signal behaves irregularly. It can be

19

said that statements a) and b) are consistent with one determined from the properties of the levels and are linear in the initial conditions, while statement c) implies that increments in the relaxation rates are proportional to the current, i.e. the main effect of increased current is an increase in the electron density rather than an increase in their velocity. Figure 3.2 presents the results related to the statement d).
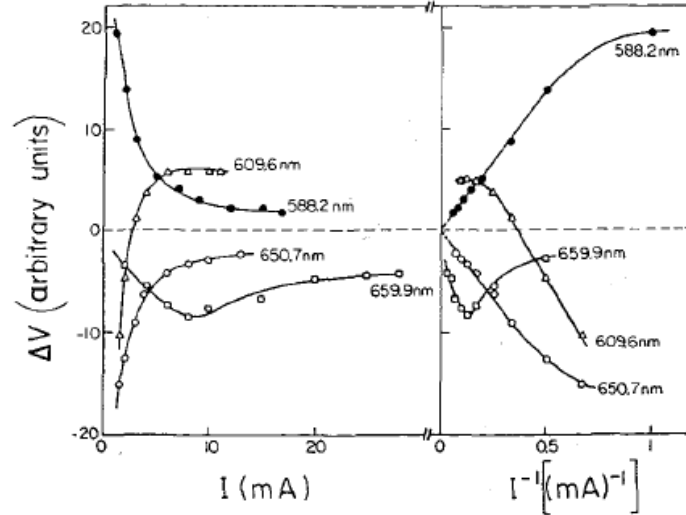


Figure 3.2 Integral of OGE signal as a function of current I (part a) and its inverse (part b) for various $1s_i$-$2p_j$ transitions [39].

Population inversion: The fast dipole transition from the $1s_2$ level to the ground states permits an inversion to be achieved on $1s_2$-$2p_j$ transitions; $n_1 - n_2$ is negative, inverting the initial OGE conditions. (Figure 3.3)
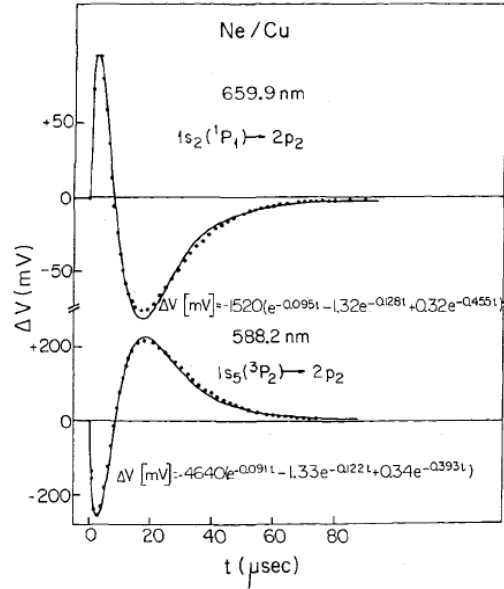
Figure 3.3 OGE signals for the two Ne transitions, 659.9 nm and 588 nm (4 mA) [39].

Ben-Amar et al. [24] have studied, by the pulsed technique, transient effects in the discharge plasma such as fast relaxation of level population density and population inversion. The experimental results were correlated with a four states phenomenological model of the pulsed optogalvanic effect taking into account lumped relevant levels of the 3s and 3p manifolds of neon. The time Integration of the pulsed optogalvanic signals (OGS) yielded the previously measured cw signals and explained their sign changes.

From an analysis of the OG signals observed for laser irradiation at different positions within the cathodic region, DeMarinis and Sasso [49] have shown that different mechanisms are strictly related to the OG spatial dependence, where a dominant role in sustaining the glow discharge and producing the OG signal was played by the bombardment of the cathode surface by metastables, VUV photons, and ions. The depletion of the metastable atoms by laser excitation to a level cascading to the neon ground state was the source of the negative OG signals, as pointed out also for the neon obstructed glow. The increase of UV photons by neon atoms in the so-called radiative levels is the source of the positive OG signals.

A damped oscillation at about 5 kHz was observed on the optogalvanic signals of a Ne hollow-cathode discharge on illumination by a pulsed dye laser at the resonant frequency of the Ne $2p_s$-$^1s_5$ transition [61]. The signal fitted the formula $\Delta V(t) = V_0 e^{-t/\tau} sin(\omega t + \theta)$, and the values of the parameters were determined for several positions

of illumination and discharge currents. The oscillation originated from the ionization wave in the positive-column region, and a qualitative interpretation was presented based on the theory of striation.

Laser-induced optogalvanic (OG) signal oscillations were also detected in a miniature neon glow discharge plasma and are investigated using a discharge equivalent-circuit model [57]. The damped oscillations in OG signal were generated when a pulsed dye laser is tuned to a specific neon transition ($1s_5 \rightarrow 2p_2$) at 588.2 nm under the discharge conditions where dynamic resistance changes its sign. Penning ionization via quasi-resonant energy transfer collisions between neon gas atoms in metastable state and sputtered electrode atoms in ground state was explained by the negative differential resistance properties of discharge plasma that were attributed to oscillations in the OG signal.

## 3.3 Theory of the optogalvanic effect in the hollow cathode discharge

For modeling of the OG signal we have used the method proposed in Ref [49]. This method which used generalized theory of Little and von Engel [28] for a hollow cathode discharge, previously mentioned, treated OG signal as small perturbation of the discharge current. The complete knowledge of an OGE mechanism is restricted only to several cases [28]. One of them is the OGE in the positive column of a DC neon discharge. The OGE in this regime is modeled by applying perturbation theory to key rate equations that describe the discharge [50]. In the positive column the electric field is weak and constant, while it is large and spatially variable in the cathode region. The secondary electron emission from the cathode has a great direct influence on cathode region's characteristics while its influence on the positive column is only indirect and weaker. As explained above, the high intensity of OGE in the cathode region is caused by the change of the secondary electron emission, which caused by change of photon and/or metastable atom concentration by resonant laser irradiation [28]. In our case when the laser radiation excites 3s – 3p neon transition (659.89 nm), the population of radiative level $2s^2 2p^5(^2P^\circ_{1/2})3p$ is modified. Consequently, the variation of energetic photon densities $\Delta n_p^d$ and $\Delta n_p^g$ and the variation of the metastable density $\Delta n_m^d$ and $\Delta n_m^g$ induce a perturbation $\Delta I$ of the discharge current:

$$\Delta I = \frac{\partial I}{\partial n_p^d} \Delta n_p^d + \frac{\partial I}{\partial n_p^g} \Delta n_p^g + \frac{\partial I}{\partial n_m^d} \Delta n_m^d + \frac{\partial I}{\partial n_m^g} \Delta n_m^g \tag{3.2}$$

It seems reasonable that during the change of the radiative level population the variation of metastable densities $\Delta n_m^d$ and $\Delta n_m^g$ can be neglected. Also, during the irradiation of the negative glow region of the hollow cathode lamp, the variation of the energetic photon density in the dark $\Delta n_p^d$ can be neglected, too. Finally the current perturbation i.e. OG signal is:

$$\Delta I = \frac{\partial I}{\partial G_p} \Delta G_p \tag{3.3}$$

where $\Delta G_p = \gamma_p \Delta n_p^g$. It is supposed that changes of $\bar{s}$ and d, and consequently $k_1$ and $k_3$ are negligible. Using eq. (2.20) one obtains

$$\Delta I = I \frac{1}{1-G} \gamma_p \Delta n_p^g \tag{3.4}$$

To use of the eq. (3.4) for fitting it is necessary to estimate the value $\Delta n_p^g$. It can be estimated by measuring the laser light absorption caused by radiative level population in the discharge [28]. Configuration of the commercial HCL (the hollow cathode with one end closed) does not allow this kind of measurements. In that case the dependence of $\Delta n_p^g$ on the discharge current $I$ can be used for creating the fitting function. To establish this dependence one can consider that for a discharge in a steady state, the population of an excited state is determined by a balance between the rates of radiative and collisional processes. Those processes depend upon the number density of electrons and their energy distributions, and the relevant excitation and de-excitation cross-sections. Furthermore, the electron number density is directly related to the discharge current. Here we suppose that the change of energetic photons has the same dependence on current as the intensities of emitted atomic lines in the neon hollow cathode discharge [50].

$$\Delta n_p^g = \frac{AI(1 + CI)}{1 + BI} \tag{3.5}$$

Where $A$, $B$ and $C$ are the constants. This equation is deduced by balancing likely excitation and de-excitation processes. Constant $A$ depends on one-stage excitation, $C$ on the relative importance of two and one-stage excitation, and $B$ on the relative

importance of collisional and radiative de-excitation. Finally, the fitting function for OG signal is:

$$\Delta I = I \frac{1}{1 - G} \gamma_p \frac{AI(1 + CI)}{1 + BI} \tag{3.6}$$

In the above equation the $G$ function is specified by equation (2.21).

# 4 Oscillations in the gas discharge – self-generated and laser induced

The low-current oscillations usually occur in the transition region between the Townsend and the normal glow regimes, i.e. in the subnormal region [52]. In Townsend discharges the space charge is negligible due to the very low discharge current and applied external electric field is not disturbed, so the discharge electric field is approximately homogeneous in the whole region between electrodes. On the other side, the normal glow discharge is characterized by a higher current density and space charge disturbs the external electric field make it localized in the so called cathode fall region. The DC discharge is usually unstable in the subnormal region where it has a negative differential resistance and the current exhibits relaxational oscillations. Beside the self-sustained oscillations, which are formed for some ranges of the discharge current, damped oscillations can be induced by the application of external voltage pulses [53], photoelectron initiated avalanches [54] and resonant laser light absorption i.e. OGE [55-57].

Two different approaches are used to explain the discharge oscillations [58]. The first one is based on a model which attempts to correlate the observables with the physical parameters such as ionization and secondary electron yield coefficients and their dependence on the reduced electric field E/N. Models of the plan-parallel discharge for low to moderate current explained the oscillatory behavior taking into account the dependence of the secondary electron emission coefficient $\gamma_i$ on the discharge voltage and current (both influencing the energy of positive ions impinging on the cathode surface) [59]. Model developed to explain the oscillation phenomena in hollow cathode discharge in subnormal glow region includes the space charge deformation of the electric field [52]. This model is, probably, the most appropriate for the commercial hollow cathode lamps that work in abnormal glow regime, but it is based on numerical simulation and does not give any functional dependence useful for fitting of the experimental data.

The second approach is based on the phenomenological model in which some of the physical phenomena are connected to the effective circuit parameters of the discharge. Here we use the phenomenological model developed in [59] but modified

for the hollow cathode discharge. The basis for the model is an idea that the secondary electron yield may be represented as a function of both voltage and current:

$$\gamma = \gamma_{pot} + k_V V + k_I I \tag{4.1}$$

where $\gamma_{pot}$ represents the "potential ejection" of electrons, the $k_V$ term is an approximation to the contribution of "kinetic" ejection of electrons, and the $k_I$ term represents the first-order effects of space charge on the electric field and, thereby, the electron yield at the cathode. The voltage dependence of gamma is easily understood, while the second requires further explanation. The current dependence of gamma is due to the fact that increasing of the current leads to an increased space charge shielding effect and consequently to a higher field close to the electrode. Thus, in principle, both dependencies are associated with the field close to the cathode. Though $\gamma$ in Eq. (4.1) is defined in [55] as the coefficient for secondary electron emission caused by ions i.e. as $\gamma_i$ , this dependence on voltage and current can be applied also on coefficients $G_m$ and $G_p$ for metastables and photons, using the mentioned argument – change of the electric field close to the cathode which changes the electron energy and, consequently, number of the metastable atoms and the energetic photons. Another assumption of the model is that the changes occur on the time scales greater than the average ion and metastable transit time T. Thus it is possible to associate the electron current I, at the cathode (at time t+T) with the current at the time t by equation:

$$
\begin{aligned}
I^e(0, t + T) = I^p(0, t + T) &+ \gamma_i I^e(0, t)\left(e^{\alpha_i(t)d} - 1\right) \\
&+ G_m I^e(0, t)\left(e^{\alpha_m(t)d} - 1\right)
\end{aligned}
\tag{4.2}
$$

where $I^p(0, t + T)$ is the photoelectric current produced by irradiation of the cathode, $\gamma_i$ is the effective yield of electrons per ion arriving at the cathode, $G_m$ is the effective yield of electrons per metastable atom arriving at the cathode, $\alpha_i(t)$ and $\alpha_m(t)$ are ionization and metastable excitation coefficients. Ions produced by backscattered electrons arriving at the anode could be neglected in the electrode configuration of the commercial HCL. The electron current at the cathode can also be written as an expansion in time about the time t.

$$I^e(0, t + T) = I^e(0, t) + T \frac{dI^e(0, t)}{dt} \tag{4.3}$$

Elimination of $I^e(0, t+T)$ gives

$$\frac{dI^e(0,t)}{dt} = \frac{I^p(0,t)}{T} + \frac{g-1}{T} I^e(0,t)$$

(4.4)

Where $g = \gamma_i\left(e^{\alpha_i(t)d} - 1\right) + G_m\left(e^{\alpha_m(t)d} - 1\right)$ is electron number gain.

From

$$I(t) = I^e(0,t) + I^+(0,t)$$

(4.5)

and eq. (2.14) expressed for currents, relation for the total current at the cathode is:

$$I^e(0,t) = I(t)\frac{\gamma_i + G_m + G_p}{1+\gamma_i}$$

(4.6)

By deriving Eq. (4.6) it is obtained:

$$\frac{dI^e}{dt} = \frac{dI}{dt}\frac{\gamma_i+G_m+G_p}{1+\gamma_i} + I\frac{1}{(1+\gamma_i)^2}\left[\left(\frac{\partial\gamma_i}{\partial V}\frac{dV}{dt} + \frac{\partial\gamma_i}{\partial I}\frac{dI}{dt}\right)\left(\gamma_i + G_m + G_p\right) + (1+\gamma_i)\left[\left(\frac{\partial\gamma_i}{\partial V} + \right.\right.\right.$$

$$\left.\left.\left.\frac{\partial G_m}{\partial V} + \frac{\partial G_p}{\partial V}\right)\frac{dV}{dt} + \left(\frac{\partial\gamma_i}{\partial I} + \frac{\partial G_m}{\partial I} + \frac{\partial G_p}{\partial I}\right)\frac{dI}{dt}\right]\right]$$

(4.7)

After using Eqs. (4.4) and substitution of $I^e$ with $I$ by using (4.6) we obtain:

$$\left[\frac{\gamma_i+G_m+G_p}{1+\gamma_i} + \frac{1}{(1+\gamma_i)^2}\left[(1-G_m-G_p)k_{iI} + (1+\gamma_i)(k_{mI}+k_{pI})\right]I\right]\frac{dI}{dt} = \frac{I^p}{T} + $$

$$\frac{g-1}{T}\frac{\gamma_i+G_m+G_p}{1+\gamma_i}I - \frac{1}{(1+\gamma_i)^2}\left[(1-G_m-G_p)k_{iV} + (1+\gamma_i)(k_{mV}+k_{pV})\right]I\frac{dV}{dt} \quad (4.8)$$

Where $k_{iI}, k_{iV}, k_{mI}, k_{mV}, k_{pI}, k_{pV}$ are coefficients from (4.2) for ions, metastable atoms and photons.

Another equation which connects the discharge voltage V and the discharge current I with the circuit components shown in Fig. 4.7a is:

$$\frac{dV(t)}{dt} = \frac{1}{RC}[V_0(t) - V(t) - RI(t)]$$

(4.9)

where $V_0$ is a power supply voltage, R is a series resistance and C includes the capacitance of cables, high voltage connections and the discharge electrodes.
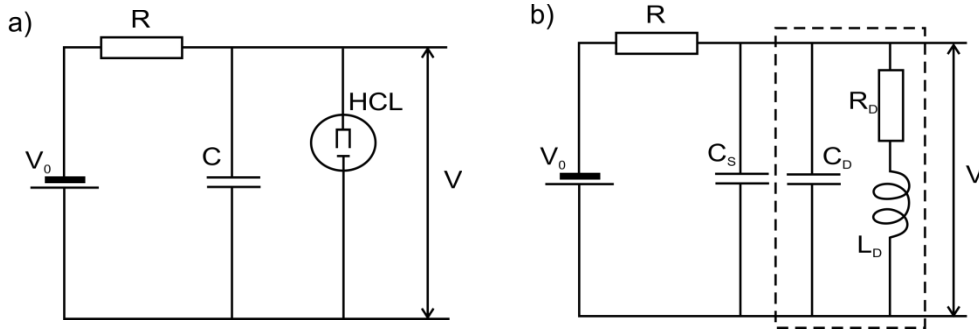
Figure 4.1 (a) Schema of the electrical circuit with an idealized discharge tube. HCL – hollow cathode lamp (b) Schema of the electrical circuit with an approximate equivalent circuit of the discharge enclosed in the dashed rectangle.

The transient model represented by (4.8) and (4.9) can be numerically solved for arbitrarily large changes of current and voltage. For obtaining the numerical solutions, empirical data such as ionization coefficient, metastable excitation coefficient and second electron emission coefficients for ions, metastable atoms and photons are needed. The numerical solutions can be obtained using a personal computer and routines or commercial codes that solve sets of first-order differential equations. Analytical solutions of the mentioned equations may be obtained for small changes of voltage and current about their steady-state values $V_{SS}$ and $I_{SS}$. For small changes of voltage and current it can be written

$$V(t) = V_{ss} + \beta v(t) \tag{4.10}$$

$$I(t) = I_{ss} + \beta i(t) \tag{4.11}$$

and also for electron number gain

$$g(t) = 1 + \beta \frac{\partial g}{\partial V} v(t) + \beta \frac{\partial g}{\partial I} i(t) \tag{4.12}$$

Where β is the perturbation parameter, v(t) and i(t)are time dependent components of current and voltage, and

$$V_{ss} = V_0 - I_{ss}R \tag{4.13}$$

As our interest is only the functional dependence, we reduced Eq. (4.8) to a simpler form

$$(a + b_I I)\frac{dI}{dt} = \frac{I^p}{T} + \frac{g-1}{T}aI - b_V I \frac{dV}{dt} \tag{4.14}$$

where

$$a = \frac{\gamma_i + G_m + G_p}{1 + \gamma_i}, \quad b_I = \frac{1}{(1+\gamma_i)^2}\left[(1 - G_m - G_p)k_{iI} + (1 + \gamma_i)(k_{mI} + k_{pI})\right],$$

$$b_V = \frac{1}{(1+\gamma_i)^2}\left[(1 - G_m - G_p)k_{iV} + (1 + \gamma_i)(k_{mV} + k_{pV})\right]$$

Substituting Eqs. (4.10) to (4.13) into Eqs. (4.14) and (3.15) for $I^p(t) = 0$ and retaining only terms that are first order in β, we obtain

$$(a + b_I I_{SS})\frac{di}{dt} = \frac{\frac{\partial g}{\partial v}}{T}aI_{SS}v - \frac{\frac{\partial g}{\partial i}}{T}aI_{SS}i + b_V I_{SS}\frac{dv}{dt} \tag{4.15}$$

$$\frac{dv}{dt} = -\frac{1}{RC}v - \frac{1}{C}i \tag{4.16}$$

Equations (4.15) and (4.16) are coupled linear first-order differential equations and are readily solved for i(t) and v(t). For our present purposes we need only the roots of the determinant which occurs, for example, when solving the equations using the Laplace transform technique.

Laplace transform of real "good" function from the real variable t>0:  f=f(t), by definition  (s is a complex variable) is

$$I(f(t)) \equiv f_l(s) = \int\limits_{0+}^{\infty} dt f(t)e^{-st} \tag{4.17}$$

Then 4.15 and 4.16 are

$$(a + b_I I_{SS})(si_L(s) - i(0))$$
$$= \frac{1}{T}\frac{\partial g}{\partial V}aI_{SS}v_L v - \frac{1}{T}\frac{\partial g}{\partial V}aI_{SS}i_L + b_V I_{SS}(sv_L(s) - v(0)) \tag{4.18}$$

$$(sv_L(s) - v(0)) = -\frac{1}{RC}v_L - \frac{1}{C}i_L \tag{4.19}$$

System of appropriate linear equations is

$$\left[(a + b_I I_{SS})s + \frac{1}{T}\frac{\partial g}{\partial V}aI_{SS}\right]i_L - \left[\frac{1}{T}\frac{\partial g}{\partial V}aI_{SS} + b_V I_{SS}s\right]v_L$$
$$= (a + b_I I_{SS})i(0) - b_V I_{SS}v(0) \tag{4.20}$$

$$\frac{1}{C}i_L + \left[s + \frac{1}{RC}\right]v_L = v(0) \tag{4.21}$$

Methods of determinants for system of linear equations give results

$$i_L = \frac{\Delta_i}{\Delta}, v_L = \frac{\Delta_v}{\Delta} \tag{4.22}$$

where

$$\Delta = \begin{vmatrix} (ab_I I_{SS})s + \dfrac{1}{T}\dfrac{\partial g}{\partial I}aI_{SS} & \left[-\dfrac{1}{T}\dfrac{\partial g}{\partial V}aI_{SS} + b_V I_{SS}s\right] \\ \dfrac{1}{C} & \left[s + \dfrac{1}{RC}\right] \end{vmatrix} \tag{4.23}$$

And

$$\Delta_i = \begin{vmatrix} (ab_I + I_{SS})i(0) - b_V I_{SS}v(0) & \left[-\dfrac{1}{T}\dfrac{\partial g}{\partial V}aI_{SS} + b_V I_{SS}s\right] \\ v(0) & \left[s + \dfrac{1}{RC}\right] \end{vmatrix} \tag{4.24}$$

$$\Delta_v = \begin{vmatrix} (ab_I + I_{SS})s + \dfrac{1}{T}\dfrac{\partial g}{\partial V}aI_{SS} & (ab_I + I_{SS})i(0) - b_V I_{SS}v(0) \\ \dfrac{1}{C} & v(0) \end{vmatrix} \tag{4.25}$$

Also needed relations

$$L(e^{-\alpha t}\sin(\omega t)) = \frac{\omega}{((s+\alpha)^2 + \omega^2)} \tag{4.26}$$

$$L(e^{-\alpha t}\cos \omega t) = \frac{s+\alpha}{((s+\alpha)^2 + \omega^2)} \tag{4.27}$$

Solutions of equations (4.16) and (4.17) without the method of Laplace transform, directly, then received the system of linear differential equations:

$$C(a + b_I I_{SS})\frac{d^2v}{dt^2} + \left[\frac{(a + b_I I_{SS})}{R} + \frac{C}{T}\frac{\partial g}{\partial I}aI_{SS} + b_V I_{SS}\right]\frac{dv}{dt}$$
$$+ \frac{aI_{SS}}{T}\left[\frac{\partial g}{\partial V} + \frac{1}{R}\frac{\partial g}{\partial I}\right]v = 0 \tag{4.28}$$

$$i = -\frac{v}{R} - C\frac{dv}{dt} \tag{4.29}$$

First of above equations presents the model of damped harmonic oscillator. At intermediate Iss the roots are complex and the current i (t) and voltage v (t) vary as

$$i(t) = i(0)e^{-\alpha t} \sin(\omega t + \phi_1) \tag{4.30}$$

$$v(t) = v(0)e^{-\alpha t} \sin(\omega t + \phi_2) \tag{4.31}$$

where

$$\alpha = \frac{aT + \left(Tb_I + aRC\frac{\partial g}{\partial I} + b_V RT\right)I_{SS}}{2RCT(a + b_I I_{SS})} \tag{4.32}$$

$$\omega^2 = \frac{\left(\frac{\partial g}{\partial I} + R\frac{\partial g}{\partial V}\right)aI_{SS}}{RCT(a + b_I I_{SS})} - \alpha^2 \tag{4.33}$$

$\alpha$ and $\omega$ are the damping constant and the angular frequency. $\phi_1$ and $\phi_2$ are phase shifts that will be not measured in the experiment. $\omega^2$ and $\alpha$ have to be expressed as functions on $I = I_{ss}$ in intention to use them for fitting of the experimental data:

$$\alpha(I) = \frac{a_1 + a_2 I}{1 + a_3 I} \tag{4.34}$$

$$\omega(I) = \sqrt{\frac{b_1 I}{1 + b_2 I} - \alpha(I)^2} \tag{4.35}$$

Formulas (4.34) and (4.35) are obtained for the assumption of small current and voltage oscillations; otherwise a system of first order differential equations (4.8) and (4.9) has to be used. Here we will apply another approach for describing the self-sustained current oscillations, which are not significantly lower than the steady state current. The current and voltage oscillations can be described presenting the discharge in an approximate form of an equivalent resonant circuit. From a viewpoint of a simple resonant circuit model, capacitance and inductance elements have to be included [56-59]. As mentioned earlier, the capacitance has two components: self-capacitance of the discharge and the stray capacitance of wiring $C_S$. The self-capacitance is higher than the geometrical capacitance between the electrodes due to the space charge formation in the discharge. The inductance $L_D$ is caused by finite drift velocity of the ions. Based on the above considerations the electrical circuit of our experiment can be presented by Fig 4.1b. The discharge is represented by the

equivalent circuit inside the dashed box where $R_D$ and $L_D$ are the discharge resistance and inductance, respectively. $C_D$ is the discharge capacitance and R is the ballast resistor. In the limit of low currents, Eqs (4.32) and (4.33) can be written in terms of equivalent circuit elements [56-59]:

$$\alpha = \frac{1}{2}\left(\frac{1}{RC} + \frac{R_D}{L_D}\right) \tag{4.36}$$

$$\omega^2 = \frac{1}{LC}\left(1 + \frac{R_D}{R}\right) - \alpha^2 \tag{4.37}$$

The self-sustained oscillations are undamped and this means that $\alpha = 0$ what is possible only if $R_D$ is negative. The negative resistance $R_D$ some authors associated with the negative slope of I – V characteristic of the discharge [55-57].

Phelps et al. [59] have investigated the oscillatory and negative differential resistance properties of low to moderate-current discharges in a parallel-plane geometry behavior in the $H_2$ gas discharge by laser-induced photoelectron pluses, while Donahue and Dieke [60] discussed the oscillatory phenomena in a direct current glow discharge of argon. The OG effect is used to study a similar type of oscillations in discharge tubes and hollow cathode lamps [55, 56, 61].

# 5 Experimental setups

Since the goal of the thesis is the transfer of knowledge from a scientific experiment to the student laboratory three types of measurements and three different types of experimental setup are used. These setups are: current and voltage measurements of the discharge, optical emission spectroscopy measurements and optogalvanic effect and laser induced current oscillation in commercial neon hollow cathode discharge.

The schematic of the experimental setup for current-voltage discharge characteristics measurements is shown in Figure 5.1. Hollow cathode lamps with Ca (Oriel) as well as Sb cathodes (PyeUnicam) are filled with neon at low pressure (< 3.5 mbar). The hollow cathode dimensions are Ca HCL (D = 3.5 mm, L = 12 mm) and Sb HCL (D = 3.0 mm, L = 11 mm). To run the discharge, a 0 – 1000 V and 0 – 100 mA voltage stabilized power supply is used.
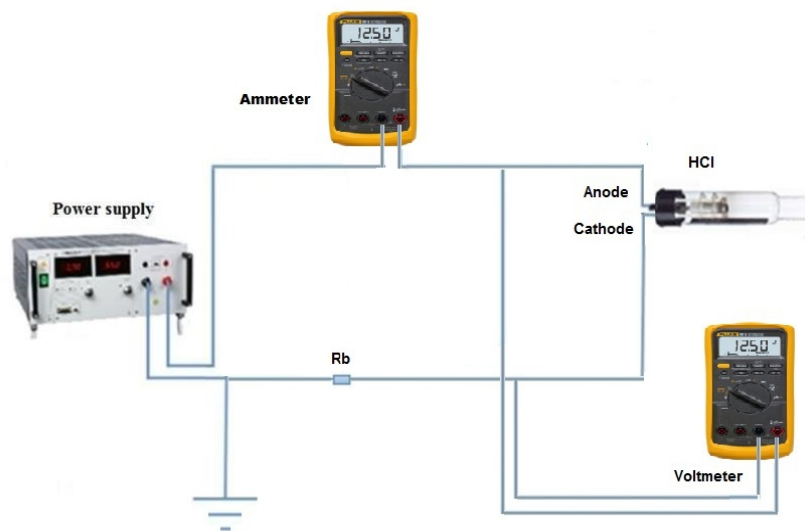


Figure 5.1 Experimental setup of current-voltage discharge characteristics measurements.

A ballast resistor of 9.85 kΩ is placed in series with the discharge and power supply. The same resistor is used for monitoring the current oscillations. Current and voltage changes are measured by ammeter and voltmeter. By increasing current by regular known steps, changes in voltage between HCL electrodes are recorded, giving current-voltage discharge characteristics. Measurement procedure includes ignition of

the discharge, decreasing voltage to the minimal current value then increasing voltage to the maximal allowed current value.

Figure 5.2 presents the experimental setup for optical emission spectroscopy measurements of the neon hollow cathode discharge. The overall emission spectra in a wide range of 300–900 nm, was recorded using a low resolution spectrometer Ocean Optics USB4000. Using quartz lens (f = 150 mm) image of the negative glow region of the HCL discharge (central part of the hollow cathode) is projected on the entrance of the quartz optical fiber. Optical emission spectra are recorded for different current values using the HCLs with Ca and Sb hollow cathodes. Recorded spectra are processed by a PC.
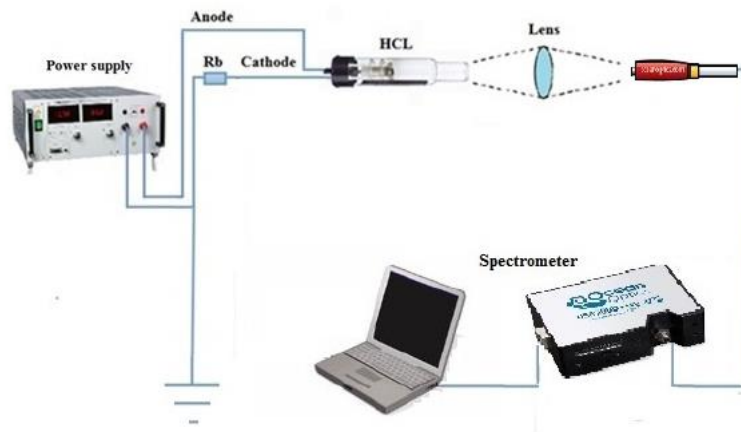


Figure 5.2 Experimental setup for recording optical emission spectra from neon HCLs.

The schematic of the experimental setup of optogalvanic effect in neon hollow cathode discharge is shown in Figure 5.3. HCLs with the cathode made of Ca and Sb and filled with neon at low pressure are used. To run the discharge, a 0 – 1000 V and 0 – 100 mA voltage stabilized power supply is used.
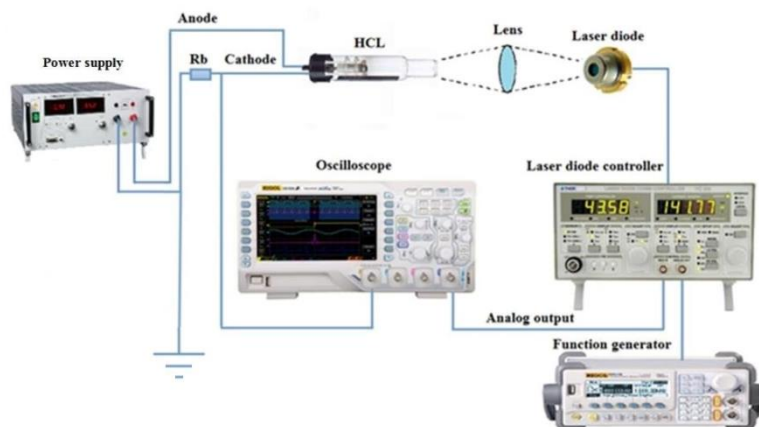
Figure 5.3 Experimental setup for researching optogalvanic effect and laser induced current oscillations in neon HCLs.

A ballast resistor of 9.85 kΩ is placed in series with the discharge and power supply. The same resistor is used for monitoring the current oscillations and the OG signal. Laser diode controller THORLABS ITC 502 is used for controlling temperature and current of the laser diode (ALGalnP Sanyo DL3147-060). For more information on laser diode as optical source for optogalvanic spectroscopy see Appendix 1. For tuning the laser wavelength a function generator RIGOL DG1022A is used to generate saw tooth signal and square pulse for modulation of the laser diode current. The LD radiation is tuned around the wavelength that corresponds to the neon transition 3s – 3p at 659.89 nm. The laser wavelength adjusts using the current tuning. The laser beam is focused by a lens (f = 250 mm) to the hollow cathode, filling all its interior space. Four-channel, wideband oscilloscope RIGOL DS1074Z is used for measurement and recording of the signals. The OG signals and the current oscillations have much lower values than the current so they had to be recorded using the oscilloscopes AC coupling. Experiment on OGE was performed using the Ca HCL (maximal current 6 mA), while the current oscillations were observed in Sb HCL (maximal current 15 mA). It has to be mentioned that Ca HCL works properly while Sb HCL at some current values exhibits oscillations. That was the reason why this specific HCL was no longer used as a light source in an atomic absorption spectrometer in a chemistry laboratory. On the other hand, that HCL is very useful for demonstration of the current oscillations – self-sustained and the laser induced.

# 6 Results and discussion

Results are presented following the order in the theoretical part of the thesis.

## 6.1 Measurement of electrical characteristics using hollow cathode lamps and obtaining the curve for differential resistivity

The current-voltage (I-V) characteristics in Figures 6.1-6.3 show the electrical responses of Ne HCLs with Antimony cathode, Calcium cathode, Lead cathode and Thallium cathode. I-V characteristics generate negative resistance in short spans of discharge current. In figures the negative dynamic resistances were calculated. The dynamic resistance and changes in its sign is observed when the current is incremented, for each of HCLs.
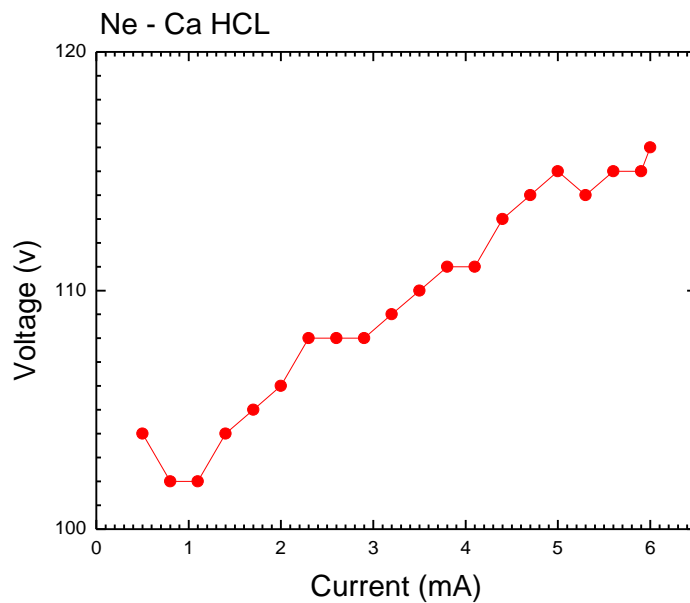


Figure 6.1 I-V characteristic of the neon discharge HCL with calcium cathode. R = 9.85 kΩ, maximal current 6 mA.
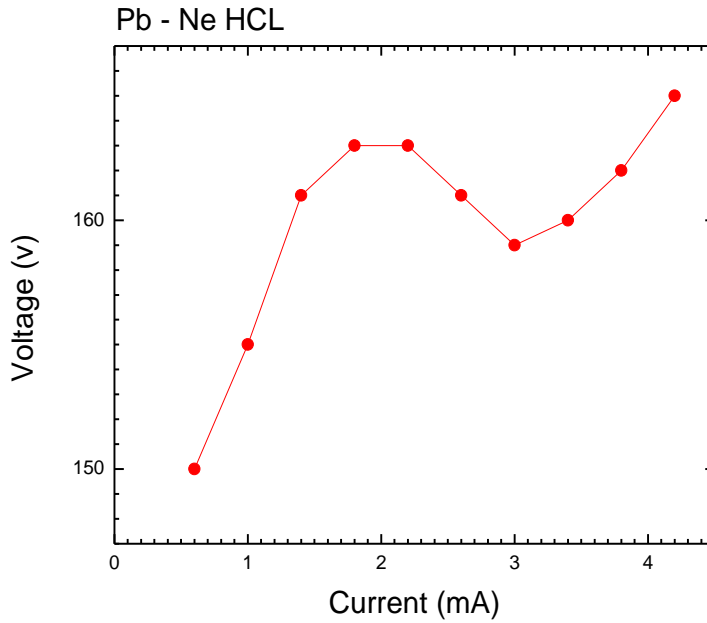
Figure 6.2 I-V characteristic of neon discharge HCL with lead cathode. R = 9.85 kΩ, maximal current 6 mA.
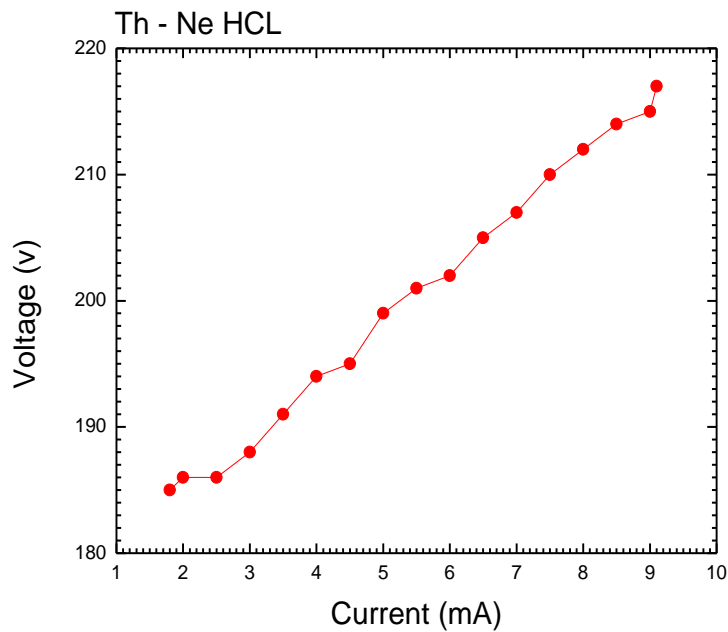


Figure 6.3 I-V characteristic neon discharge HCL with thalium cathode. R = 9.85 kΩ, maximal current 10 mA.

Hence, when the first derivative is calculated from the results, the presence of change in the sign of the differential resistivity displays the occurrence of current oscillations in the HCL. Looking at I-V characteristic of the calcium cathode neon discharge HCL (Figure 6.1) it can be noticed that there are 2 current oscillations

occurring at 2.2 mA and 5mA, one for Pb HCL occurring at 1.8 mA and one for Th HCL occurring at 4mA.

Figure 6.4 shows the I-V characteristics for the Sb-Ne HC discharge, for this particular experiment. As the voltage increases from 153 to 185 V, the current oscillations are observed as current reached 3.3 mA and 7.4 mA.

Sb - Ne HCL
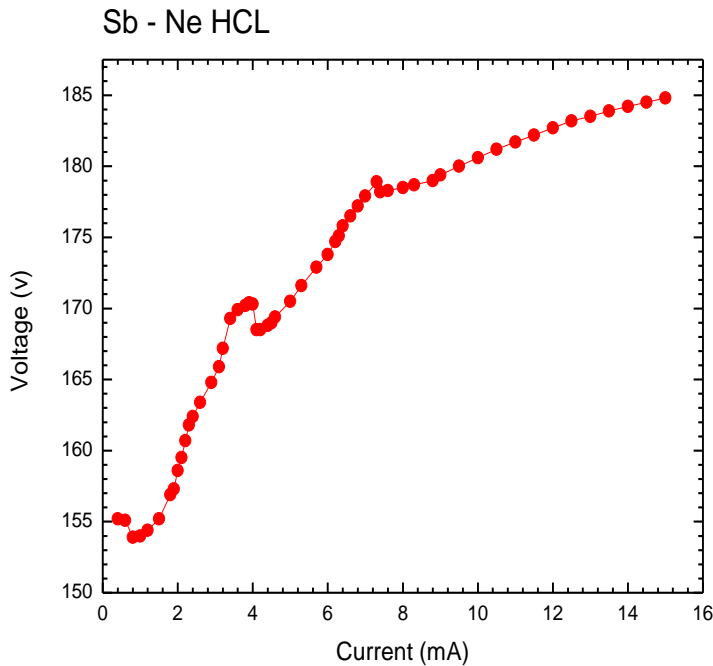
Figure 6.4 I-V characteristic of the Antimony cathode Neon discharge HCL.

I - V graphs for Ca-HCL and Sb-HCL are presented in Figure 6.5. Both graphs present current vs. voltage dependence typical for an abnormal glow discharge i.e.an increase in the discharge current results in the increase in the current density, requiring an increase in the discharge voltage. Analyzing the experimental data one can notice that the graph for Sb-HCL has irregularities, which can be seen as curvatures on the graph. These irregularities show that Sb-HCL operates improperly (without stable current) in the entire operational range. The Sb-HCL is an old lamp and it is known that after a long working time some lamp will fail to operate, mostly due to decrease of the fill gas pressure. Namely, the fill gas is absorbed into the internal surfaces of the lamp falling to a level that can no longer sustain the proper work of the electrical discharge. The experimental data for both lamps are fitted using

the equations 6.1 and 6.2, and fitting curves, together with obtained parameters $k_1$, $k_2$ and $k_3$ are presented at the Figure 6.5 [64].

$$I(V) = k_1 V^{\frac{3}{2}} \frac{1}{1 - G} \tag{6.1}$$

$$G(V) = k_2 V e^{-k_3 \sqrt{\frac{1}{V}}} \tag{6.2}$$

where $k_1 = 2\varepsilon_0 \sqrt{\frac{e\lambda}{m}} \frac{1+\gamma_i}{d^{\frac{5}{2}}} S$ (S – the cathode surface), $k_2 = \gamma_p \eta_p b_p + d_g \gamma_m \eta_d b_m (f_g \approx$ 1 for the hollow cathode discharge) and $k_3 = \overline{s} d \sqrt{V_e}$. Here it is assumed that the dark space thickness d and average ionization coefficient $\overline{s}$ dependence on V is of secondary importance (insignificant) in comparison with G dependence on V (e.g. $d \sim lnG$).
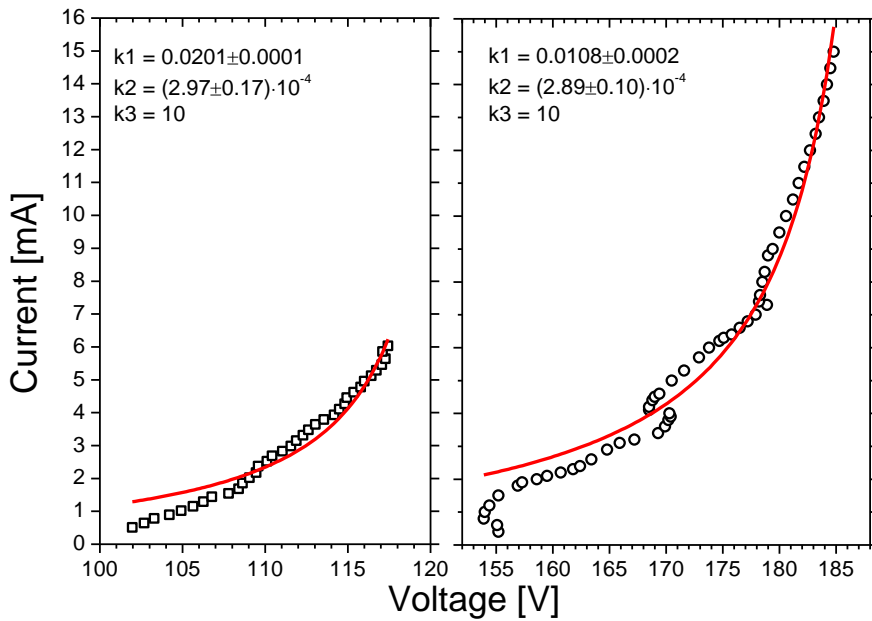


Figure 6.5. Current-voltage characteristics of the hollow cathode lamps with appropriate fits [64].

The largest difference between the two fits is in the parameter $k_1$ and this is probably due to the difference in the cathode surface area and the secondary electron emission coefficient. Parameter $k_3$ is fixed to a value which seems reasonable for the

neon at ~ 4 mbar pressure and it should not depend on the cathode material and size. It is evident that for lower current values the fits deviate from experimental data, while in a broader region the proposed hollow cathode discharge model gives a good fit. It has to be mentioned that the described model for a hollow cathode discharge was tested for much broader current regions.

## 6.2 Emission spectra from the HCLs

As it is already mentioned, the HCL is a type of a glow discharge tube that uses a hollow cathode to enhance the emission intensity. Due to the hollow cathode effect current density increases (in comparison with parallel plate electrode configuration) and consequently emission line intensity significantly increases. Each specific HCL has the hollow cathode made of characteristic materials (metals or alloys) with specific current settings. Emission spectrum of a HCL contains atomic lines specific to the element from which the cathode is comprised and from the gas filled the lamp (argon or neon). Intensity of a particular spectral line depends on excitation and de-excitation processes connected to its upper and lower atomic energy levels. In general intensity of atomic line in a HCL has the form [50]:

$$I(i) = \frac{Ai(1 + Ci)}{1 + Bi} \qquad (6.3)$$

where *A* depends on the magnitude of single-step excitation, *B* on the relative importance of collisional and radiative de-excitation and *C* on the relative importance of two-stage and single-stage excitation. Namely, for a discharge in a steady state the population of an excited state is determined by a balance between the rates of radiative and collisional processes. The latter depend upon the number density of atoms in the ground state, the number density of electrons, their velocity and energy distributions, and the relevant excitation and de-excitation cross-sections. The number density of electrons is, at a given pressure and discharge configuration, approximately proportional to the discharge current. If an energy level may be populated from the ground state, in a single step by electron collisions, and if it is de-populated by radiation, than intensity of the line originated from this level is proportional to the discharge current. This is often characteristic of atomic line of gas filled the HCL. On the other side, intensity of atomic line of cathode material depends on a two-step process – sputtering of the cathode material and excitation of sputtered atom's line. As each of two processes is approximately proportional to the discharge current it is

expected that the intensity of the sputtered atom's line is proportional to the square of the current. The purpose of spectroscopic measurements is to investigate the line intensity – discharge current relations in Ca-Ne and Sb-Ne HCLs.
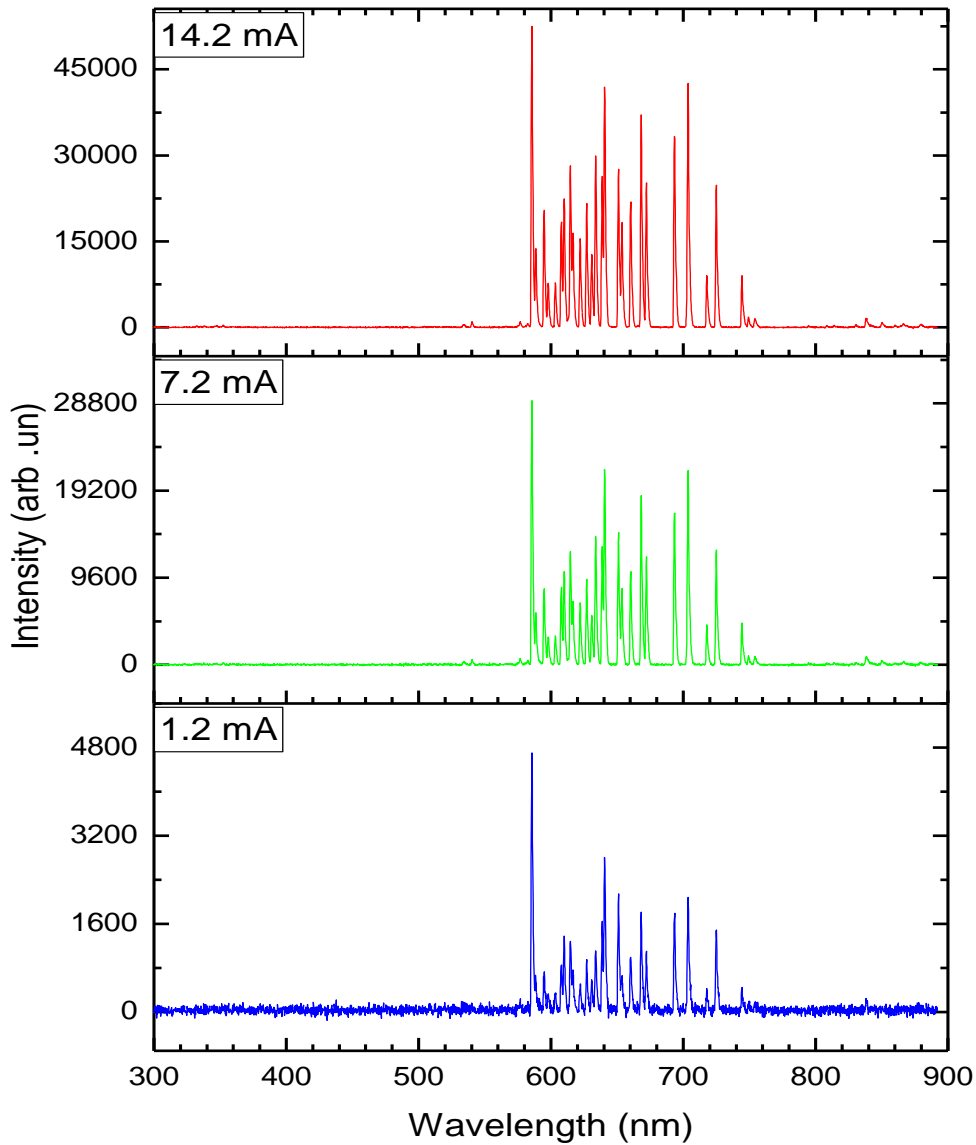


Figure 6.6 Emission spectra from Ca-Ne HCL.

Neon contains a lot of lines in the red region of the spectrum, which results with emission spectra that can be seen in the graphs below. The results of the intensity of light for various currents are presented in Figure 6.6 for Ca-Ne HCL, and in Figure 6.7 for Sb-Ne HCL. Peaks of the emission lines can be observed at the wavelengths

which correspond to the neon transitions. It can be noticed that the intensity of the peaks differs for different current intensities. For the lower current values, and consequently smaller energy transfers by electrons some of the spectral lines are not visible, while by increasing energy transfer spectral lines are more pronounced. By comparing figures 6.6 and 6.7 one can see that the same Ne I spectral lines are present in both Ca-Ne and Sb-Ne HCLs, but their intensities are different. Figure 6.8 shows an example of the spectrum with noted peaks of spectral lines emitted by Ca-Ne HCL. The upper graph shows peaks of ultimate Ca I line at 422.67 nm. For the lines
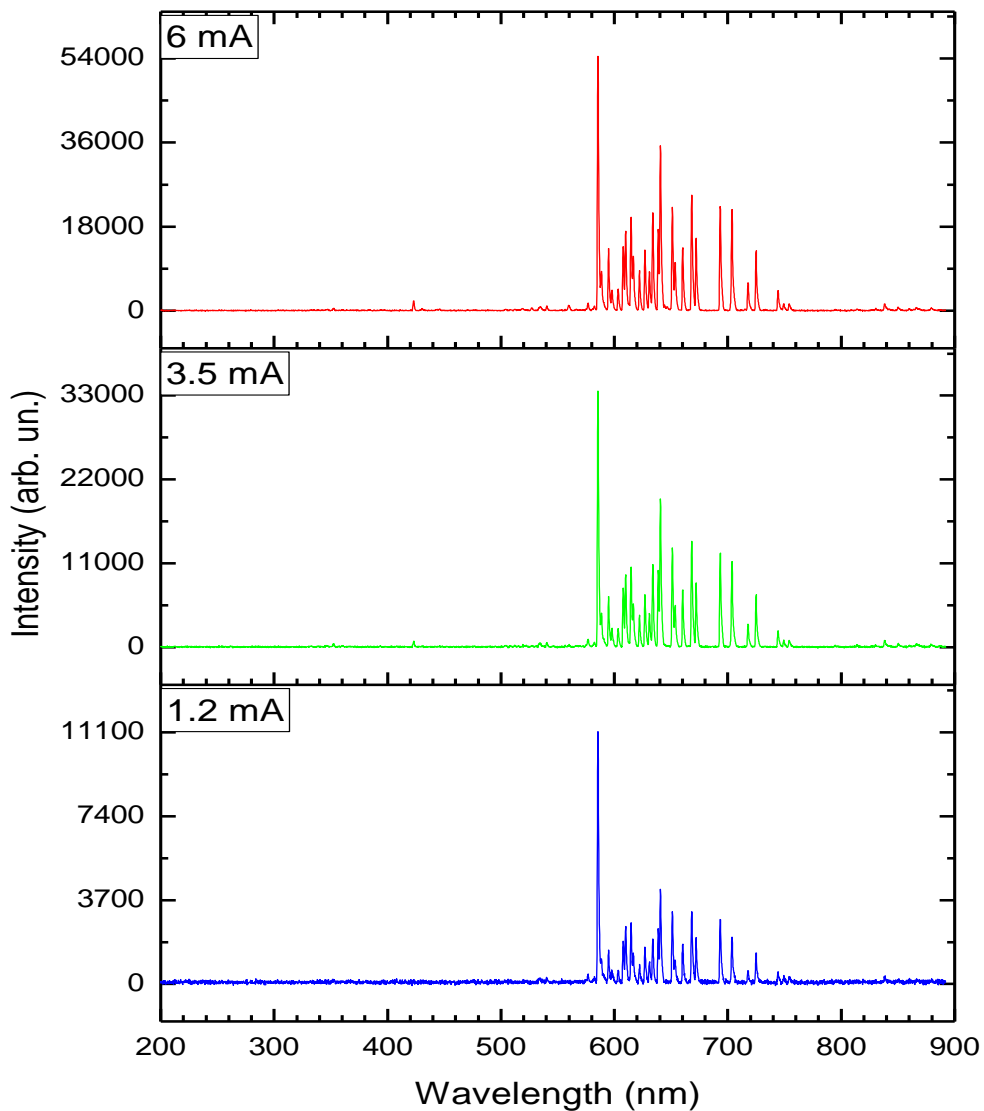


Figure 6.7 Emission spectra from Sb-Ne HCL.

identification the NIST database is used and the most of Ne I lines identified in the spectra are listed in Table 1, while in Table 2 are shown the Ca I lines.
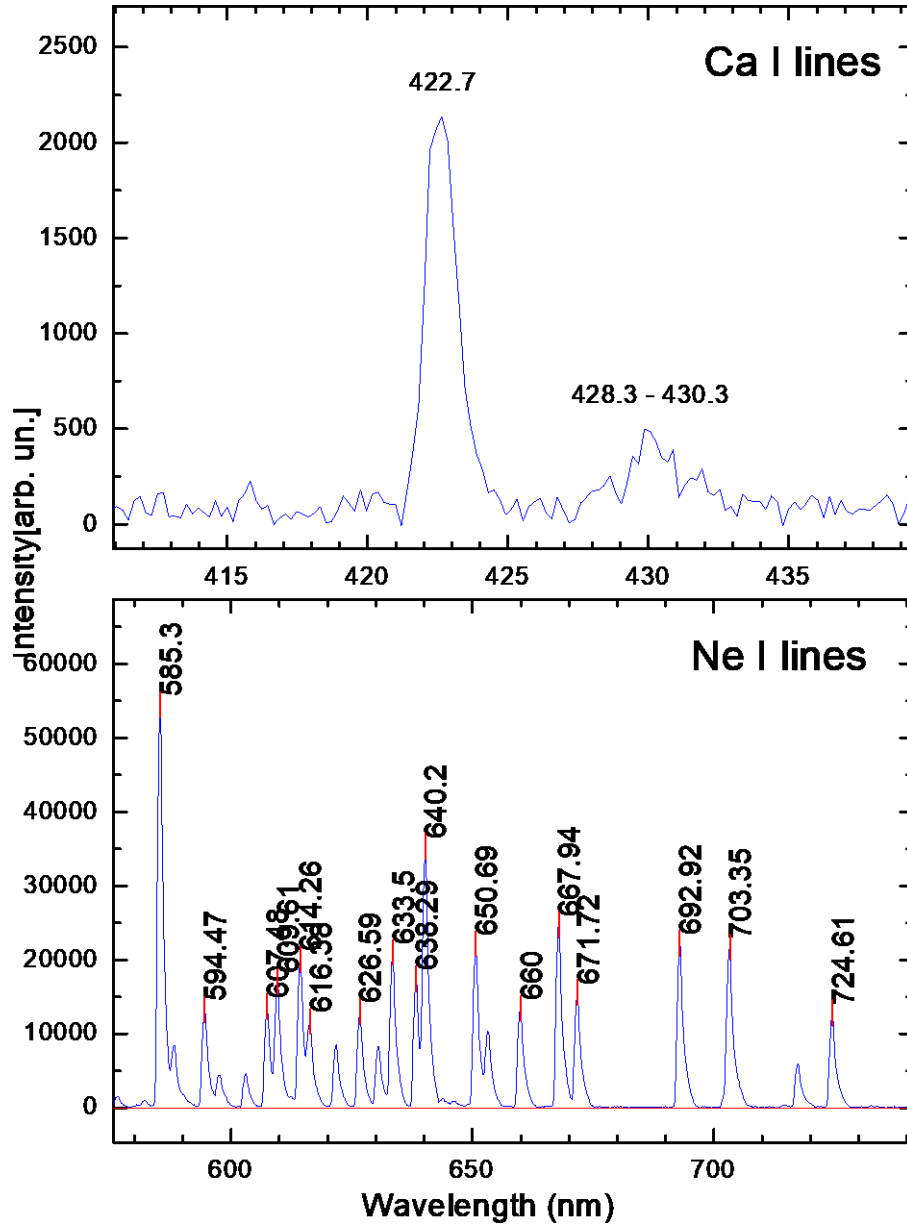


Figure 6.8 Identified Ne I and Ca I lines in Ca-Ne HCL using NIST database.

Table 6.1 and 6.2 show neon and calcium spectral lines, respectively, identified using NIST data base.

Table 6.1. Ne I spectral lines emitted from Ca-Ne HCL.

| Observed Wavelength (nm) | $A_{ki}$ (s$^{-1}$) | Upper energy level (eV) | Lower Level Conf., Term | | Upper Level Conf., Term | |
|---|---|---|---|---|---|---|
| 585.24878 | 6.82e+07 | 18.96595353 | $2s^2 2p^5(^2P^\circ_{1/2})3s$ | $^2[^1/_2]^\circ$ | $2s^2 2p^5(^2P^\circ_{1/2})3p$ | $^2[^1/_2]$ |
| 594.48340 | 1.13e+07 | 18.70407102 | $2s^2 2p^5(^2P^\circ_{3/2})3s$ | $^2[^3/_2]^\circ$ | $2s^2 2p^5(^2P^\circ_{1/2})3p$ | $^2[^3/_2]$ |
| 607.43376 | 6.03e+07 | 18.71137652 | $2s^2 2p^5(^2P^\circ_{3/2})3s$ | $^2[^3/_2]^\circ$ | $2s^2 2p^5(^2P^\circ_{3/2})3p$ | $^2[^1/_2]$ |
| 609.61630 | 1.81e+07 | 18.70407102 | $2s^2 2p^5(^2P^\circ_{3/2})3s$ | $^2[^3/_2]^\circ$ | $2s^2 2p^5(^2P^\circ_{1/2})3p$ | $^2[^3/_2]$ |
| 614.30627 | 2.82e+07 | 18.63679141 | $2s^2 2p^5(^2P^\circ_{3/2})3s$ | $^2[^3/_2]^\circ$ | $2s^2 2p^5(^2P^\circ_{3/2})3p$ | $^2[^3/_2]$ |
| 616.35937 | 1.46e+07 | 18.72638130 | $2s^2 2p^5(^2P^\circ_{1/2})3s$ | $^2[^1/_2]^\circ$ | $2s^2 2p^5(^2P^\circ_{1/2})3p$ | $^2[^1/_2]$ |
| 626.64952 | 2.49e+07 | 18.69335927 | $2s^2 2p^5(^2P^\circ_{1/2})3s$ | $^2[^1/_2]^\circ$ | $2s^2 2p^5(^2P^\circ_{1/2})3p$ | $^2[^3/_2]$ |
| 633.44276 | 1.61e+07 | 18.57583585 | $2s^2 2p^5(^2P^\circ_{3/2})3s$ | $^2[^3/_2]^\circ$ | $2s^2 2p^5(^2P^\circ_{3/2})3p$ | $^2[^5/_2]$ |
| 638.29914 | 3.21e+07 | 18.61270512 | $2s^2 2p^5(^2P^\circ_{3/2})3s$ | $^2[^3/_2]^\circ$ | $2s^2 2p^5(^2P^\circ_{3/2})3p$ | $^2[^3/_2]$ |
| 640.2248 | 5.14e+07 | 18.55510789 | $2s^2 2p^5(^2P^\circ_{3/2})3s$ | $^2[^3/_2]^\circ$ | $2s^2 2p^5(^2P^\circ_{3/2})3p$ | $^2[^5/_2]$ |
| 650.65277 | 3.00e+07 | 18.57583585 | $2s^2 2p^5(^2P^\circ_{3/2})3s$ | $^2[^3/_2]^\circ$ | $2s^2 2p^5(^2P^\circ_{3/2})3p$ | $^2[^5/_2]$ |
| 659.89528 | 2.32e+07 | 18.72638130 | $2s^2 2p^5(^2P^\circ_{1/2})3s$ | $^2[^1/_2]^\circ$ | $2s^2 2p^5(^2P^\circ_{1/2})3p$ | $^2[^1/_2]$ |
| 667.82766 | 2.33e+07 | 18.70407102 | $2s^2 2p^5(^2P^\circ_{1/2})3s$ | $^2[^1/_2]^\circ$ | $2s^2 2p^5(^2P^\circ_{1/2})3p$ | $^2[^3/_2]$ |
| 671.70430 | 2.17e+07 | 18.69335927 | $2s^2 2p^5(^2P^\circ_{1/2})3s$ | $^2[^1/_2]^\circ$ | $2s^2 2p^5(^2P^\circ_{1/2})3p$ | $^2[^3/_2]$ |
| 692.94672 | 1.74e+07 | 18.63679141 | $2s^2 2p^5(^2P^\circ_{1/2})3s$ | $^2[^1/_2]^\circ$ | $2s^2 2p^5(^2P^\circ_{3/2})3p$ | $^2[^3/_2]$ |
| 703.24128 | 2.53e+07 | 18.38162308 | $2s^2 2p^5(^2P^\circ_{3/2})3s$ | $^2[^3/_2]^\circ$ | $2s^2 2p^5(^2P^\circ_{3/2})3p$ | $^2[^1/_2]$ |
| 724.51665 | 9.35e+06 | 18.38162308 | $2s^2 2p^5(^2P^\circ_{3/2})3s$ | $^2[^3/_2]^\circ$ | $2s^2 2p^5(^2P^\circ_{3/2})3p$ | $^2[^1/_2]$ |

Table 6.2. Calcium spectral lines (Ca I and Ca II) emitted from Ca-Ne HCL.

| Ion | Observed Wavelength (nm) | $A_{ki}$ (s$^{-1}$) | $E_k$ (eV) | Lower Level Conf., Term | | Upper Level Conf., Term | |
|---|---|---|---|---|---|---|---|
| Ca II | 393.366 | 1.47e+08 | 3.150984 | $3p^64s$ | $^2$S | $3p^64p$ | $^2$P° |
| Ca II | 396.847 | 1.4e+08 | 3.123349 | $3p^64s$ | $^2$S | $3p^64p$ | $^2$P° |
| Ca I | 422.673 | 2.18e+08 | 2.9325119 | $3p^64s^2$ | $^1$S | $3p^64s4p$ | $^1$P° |
| Ca I | 428.301 | 4.34e+07 | 4.7797840 | $3p^64s4p$ | $^3$P° | $3p^64p^2$ | $^3$P |
| Ca I | 428.936 | 6.0e+07 | 4.7690283 | $3p^64s4p$ | $^3$P° | $3p^64p^2$ | $^3$P |
| Ca I | 429.899 | 4.66e+07 | 4.7690283 | $3p^64s4p$ | $^3$P° | $3p^64p^2$ | $^3$P |
| Ca I | 430.253 | 1.36e+08 | 4.7797840 | $3p^64s4p$ | $^3$P° | $3p^64p^2$ | $^3$P |

Seven calcium spectral lines are identified; two of them are emitted by calcium ions (Ca II) and five by calcium atoms (Ca I). Four calcium atom's lines, marked in Table 6.2, are not resolved. Only one Ca I line (the ultimate line Ca I 422.67 nm) can be used for investigation of intensity vs. current relation. Similar was done to Sb HCL. Figure 6.9 shows identified peaks from Ne spectra in Sb HCL using the NIST database. There are the same lines identified in Ca-Ne HCL. No one spectral line of antimony atom or ion is identified.
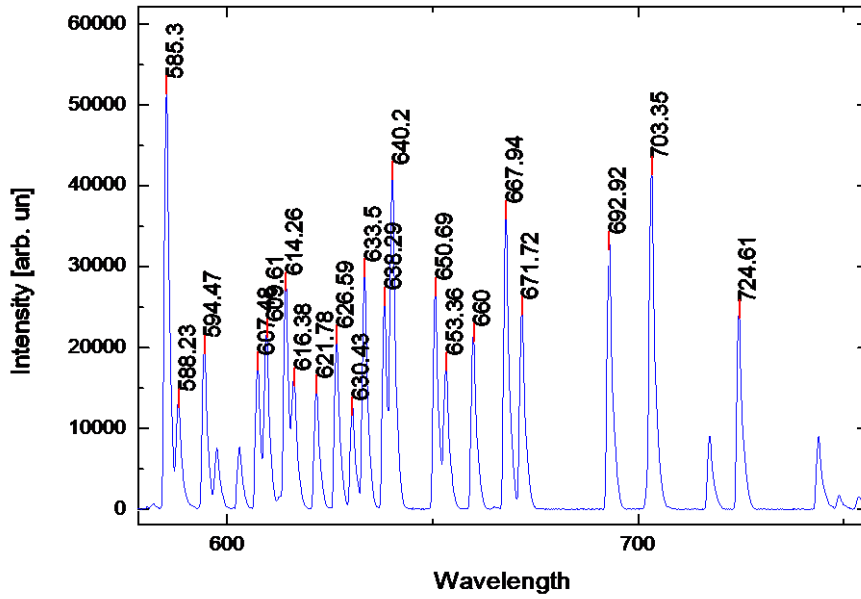
Figure 6.9 Identified Ne I lines in Sb-Ne HCL using NIST database.

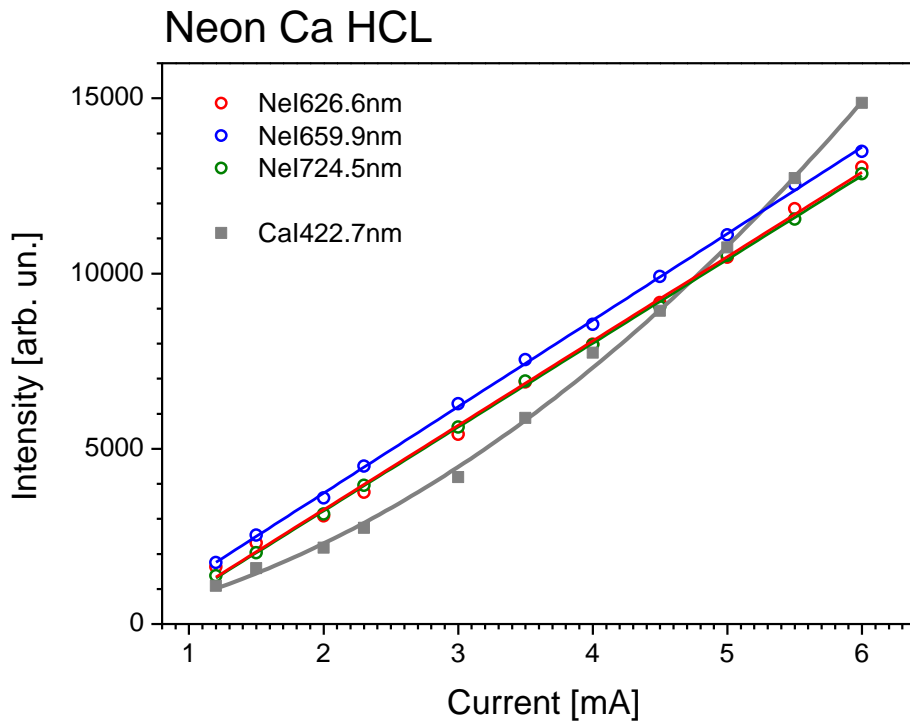Line intensity vs. current graphs for Ne I and Ca I lines are shown in Figure 6.10



Figure 6.10 Line intensity vs. discharge current for, Ca-Ne HCL

All data for Ne I lines are fitted using linear function while data for Ca I line are fitted using a square fit function. According to the graph Ne I line are produced in a single

step by electron collisions, while Ca I line is formed in a two-step process. In the case of Sb-Ne HCL line intensity vs. discharge current is presented for Ne I lines only. Linear dependence is again proven.
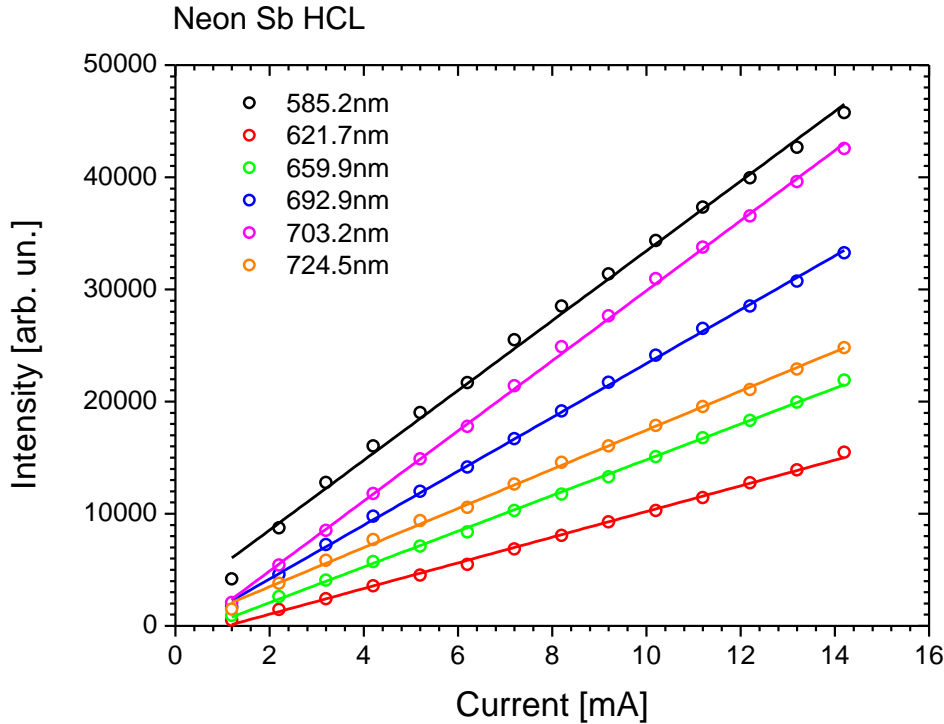


Figure 6.11 Line intensity vs. discharge current for Ne I lines from Sb-Ne HCL.

## 6.3 Optogalvanic effect

Figures 6.12 and 6.13 show the optogalvanic signals for the different discharge current 0.5 – 6.0 mA. Together with the OGSs, the driving current for the laser diode is presented. Two OGSs per one period of the ramp mode driving current are shown, one for increasing laser light wavelength (increasing current) and one for the deceasing wavelength. Analyzing the figures, one can see that the asymmetry of the OGS is the largest for the lowest HCL current (0.5 mA). Figure 6.12 also shows that asymmetry of the OGS is equal for increasing and decreasing of the laser light wavelength, clearly showing that the OGS's shape cannot be directly explained using some of the spectral broadening mechanisms. The OGS intensity is primarily governed by electron collisional excitation, radiative depopulation and electron collisional ionization occurring within the plasma of the hollow cathode discharge

lamp. The OGS shape during the decay phase is, beside the mentioned processes, also governed by the plasma discharge relaxation and the response of the electrical circuit.
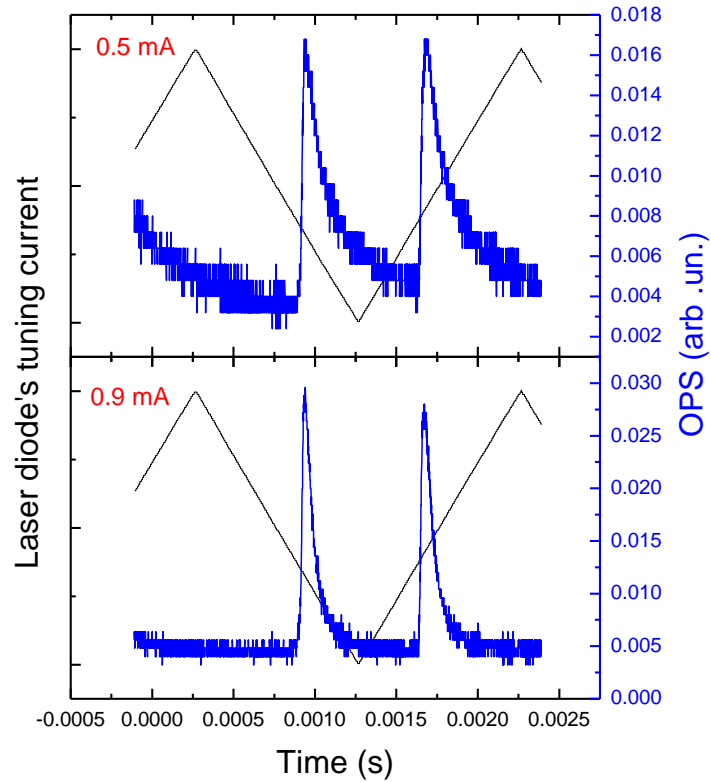


Figure 6.12 Optogalvanic signal for the discharge current I = 0.5 mA and I = 0.9 mA.

Figure 6.13 shows signals for current which was increased from 3 and 6 mA. The results for this range show less transition effects.
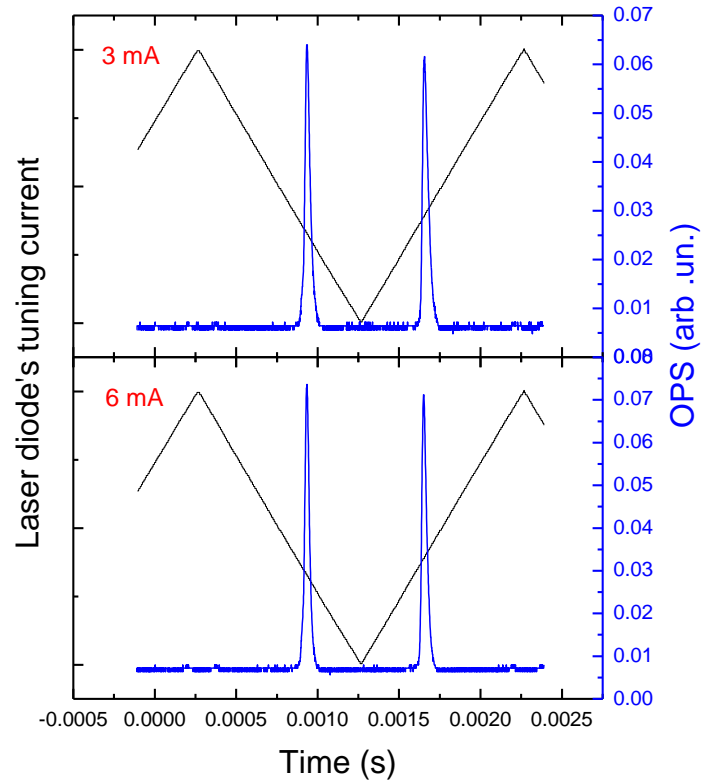
Figure 6.13 Optogalvanic signal forthedischarge current I = 3 mA and I = 6 mA.

The analysis of the OGS has to include dependences of its maximal value (measured in microamperes) and width (or relaxation time – in microseconds) on the discharge current. Here, it can be noticed that the relaxation time decreases with increasing current, indicating the expected increase in the rates of electron collision processes in the plasma as the current increases. However, the OGS relaxation time depends on many relaxation processes which cannot be easily taken into consideration, especially for the commercial HCL which is not designed for OGS investigation. Namely, the hollow cathode discharges used for the OGE research have the cathode open at both ends allowing the laser beam to precisely illuminate different discharge regions. In the commercial HCL, the laser beam reflects at the cathode closed end illuminating, in an unpredictable way, the whole hollow cathode interior i.e. all different discharge regions.

Taking the previously mentioned into account, only OGS intensity (i.e. $\Delta I_{OG}$ expressed as a maximal value) dependence on the current is presented in Figure 6.14 [64]. Fitting of experimental data was done according to equation (3.4), where $\Delta n_{pG}$

was estimated according to equation (3.5). Hence, the experimental data are fitted using the fitting function 6.4 and a very good agreement between them is obtained.

$$\Delta I_{OG}(I) = I \frac{1}{1-G} \gamma_p \frac{AI(1+CI)}{1+BI} \tag{6.4}$$

where $A$, $B$ and $C$ are the constants. Constant $A$ depends on one-stage excitation, $C$ on the relative importance of two and one-stage excitation, and $B$ on the relative importance of collisional and radiative de-excitation.
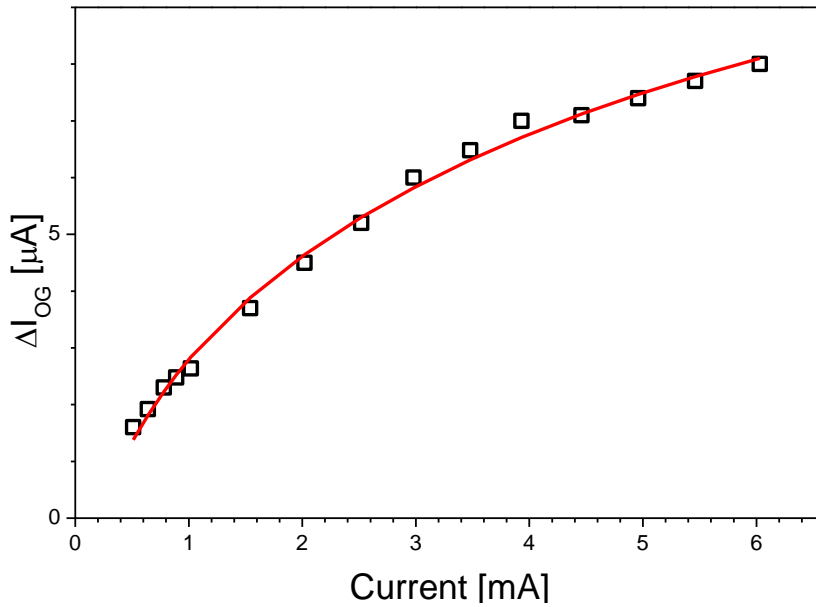


Figure 6.14 Optogalvanic signal (presented as a maximal value of $\Delta I_{OG}$) dependence on the discharge current in Ca neon HCL. Solid line is the fit obtained using fitting function (6.4) [64].

## 6.4 Oscillations in the discharge - self-generated and laser induced

In these experiments, dynamics of the discharge is observed through (i) relation between anode-cathode voltage and discharge current, (ii) relation between the oscillation frequency and discharge current and (iii) temporal profile of laser induced oscillations trough the OG effect. Initially, after igniting the discharge in the HCL, the current was decreased to the lowest value where the discharge still operates. From the standpoint of voltage-current characteristic, the HCL is operated as an abnormal glow discharge. With the discharge current increase, four different ranges

are observed: two with the stable current and two with the self-sustained oscillating current.

Current ranges describe the following states:

State I:  0.4 mA ≤ I ≤ 3.1 mA, self-sustained oscillations

State II: 3.2 mA ≤ I ≤ 3.9 mA, stable current region

State III:4.0 mA ≤ I ≤ 7.5 mA, self-sustained oscillations

State IV: I≥ 7.6 mA, stable current region.

In the State I the oscillations change their frequency with the current increasing. In the State II the discharge works without oscillations (DC or stable-current mode) until it reaches 4 mA. After that, the oscillations start again and prolong till I = 7.5 mA, but with different frequency than in the State I. Finally, for I ≥ 7.6 mA a new stable current state occurred. Figure 6.15 shows the current oscillations angular frequency ω vs. current. Figure 6.15 also shows that self-sustained oscillation frequencies have similar behavior in both current regions. They increase with the current increase and after reaching the maxima (at the middle of the regions) decrease to the values lower than the starting ones.
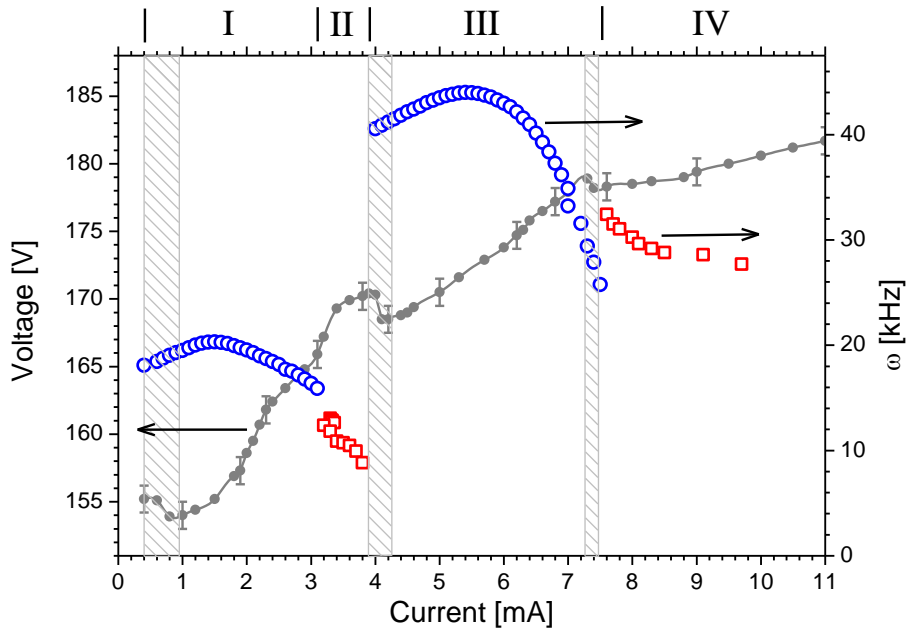
Figure 6.15 Steady state voltage-current characteristic of the Sb HCL (solid circles with error bars), and graph of current oscillations angular frequency vs. current (open circles and open squares). Self-sustained oscillations are marked by circles while laser induced oscillations are marked by squares. States I to IV and regions with negative differential resistance are also marked on the graphs [64].

The latter is especially pronounced in the second region where angular frequency rapidly decreases to the value more than 35% lower than the starting one. Examples of self-sustained current oscillations are presented in Figure 6.16.
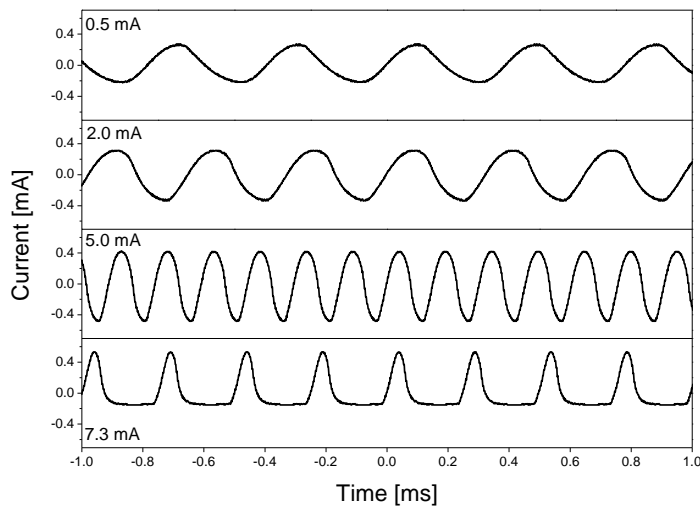


Figure 6.16 Example of steady-state oscillations for different discharge currents.

Analyzing the Figure 6.16 one can conclude that amplitudes of the self-sustained current oscillations cannot be approximated as small (e.g. they can be larger than 50% of the steady state current), so formulas (4.34) and (4.35) cannot be applied. In that case, as already mentioned, the transient model for all current values, represented by Eqs (4.8) and (4.9) have to be used and equations have to be numerically solved. Numerical solutions are beyond the scope of this thesis, so the self-sustained current oscillations presented in Figure 6.16 are not fitted

In many articles it is noted that the current oscillations are strongly related to the negative differential resistance, dV/dI < 0 [52, 54-58]. The regions of the negative differential resistance have been observed in the I - V curve for various hollow cathode discharges [52,55,56]. The physical cause of the negative differential resistance is that increased current leads to increased ionization which, in turn, serves to reduce voltage.
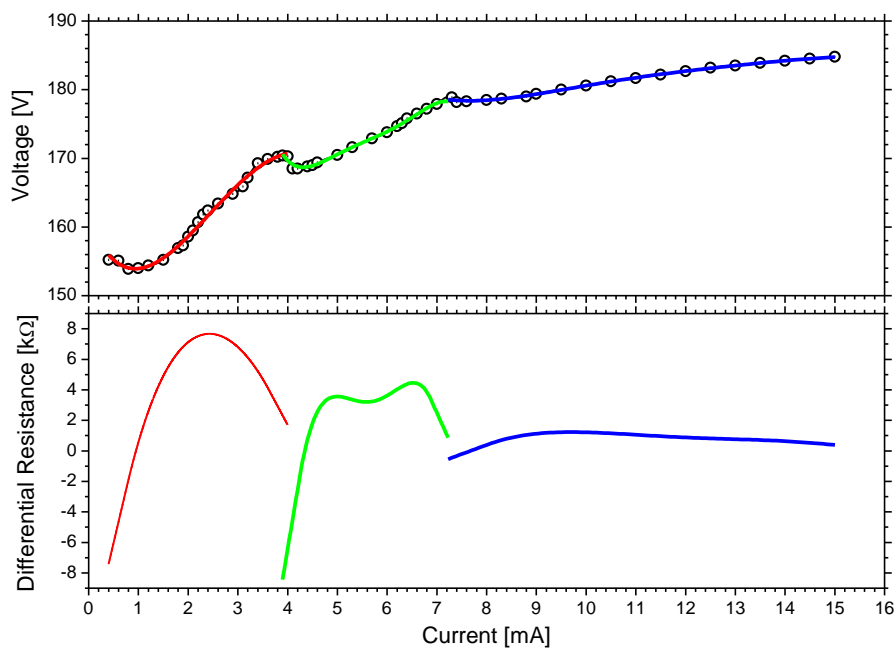
Figure 6.17 I–V characteristic (upper graph) and differential resistance ($R_D = dV/dI$), curve of Sb neon HCL (lower graph) [64].

Namely, as the ionization begins, charge carriers are produced and the potential decreases. This decrease leads to a decrease in the kinetic energy of the ions/electrons which are then less effective at promoting collisional ionization. The number of charge carriers decreases, the voltage increases, and the process begins

again [59]. Three regions used for calculation of differential resistance are marked in Figure 6.17 [64]. Using part by part fitting with polynomial functions (upper graph in Figure 6.17) and differentiating them, differential resistances as functions of the steady-state current are obtained (lower graph in Figure 6.17). Relating the differential resistances with $\omega^2$ for self-sustained oscillations ($\alpha = 0$ for undamped oscillations) two graphs are drown and presented in Figure 6.18 [64]. Analyzing these graphs one can conclude that the linear dependence of $\omega^2$ on the differential resistance (associated with $R_D$) predicted by eq. 4.36 is valid only for $R_D < 0$. The large discrepancy between the theory and the experiment shows that the theory is only qualitative at these currents, presumably because of large space-charge effects that violate the assumptions of $\gamma$ dependence on current and voltage in the form of the first-order model see eq. 4.2.



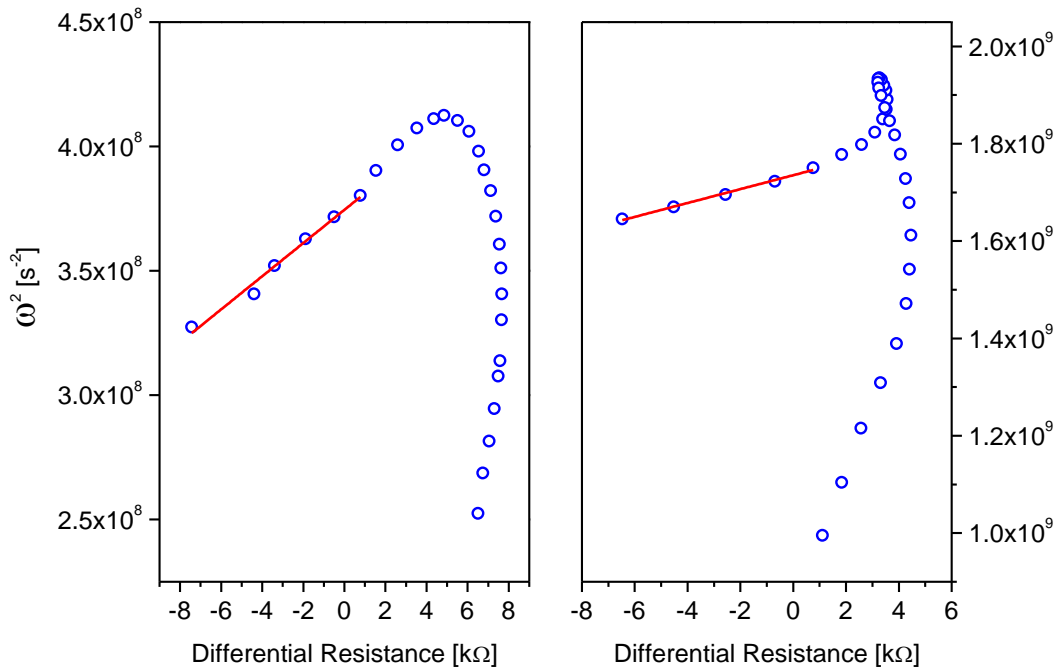Figure 6.18 $\omega^2$ dependence on differential resistance for self-sustained oscillations in two current regions, see Figure 6.17 top [64].

The analysis of the OGS has to include dependences of its maximal value (measured in microamperes) and width (or relaxation time – in microseconds) on the discharge current. Here, it can be noticed that the relaxation time decreases with increasing

current, indicating the expected increase in the rates of electron collision processes in the plasma as the current increases. However, the OGS relaxation time depends on many relaxation processes which cannot be easily taken into consideration, especially for the commercial HCL which is not designed for OGS investigation. For the OGE research the cathode is opened at both ends allowing the laser beam to precisely illuminate different discharge regions, while in the commercial HCL the laser beam reflects at the cathode closed end illuminating the whole hollow cathode interior.

Examples of the laser induced current oscillations are presented in Figures 6.19 - 6.22. The current oscillations in the State II are presented in Figures 6.19 and 6.20. Figures 6.21 and 6.22 show the current oscillations in State IV – stable current region. On all diagrams rectangular signals are the laser diode's tuning currents. This type of the tuning current produces the LD radiation turn-on at the wavelength of the neon line and the LD radiation turn-off.
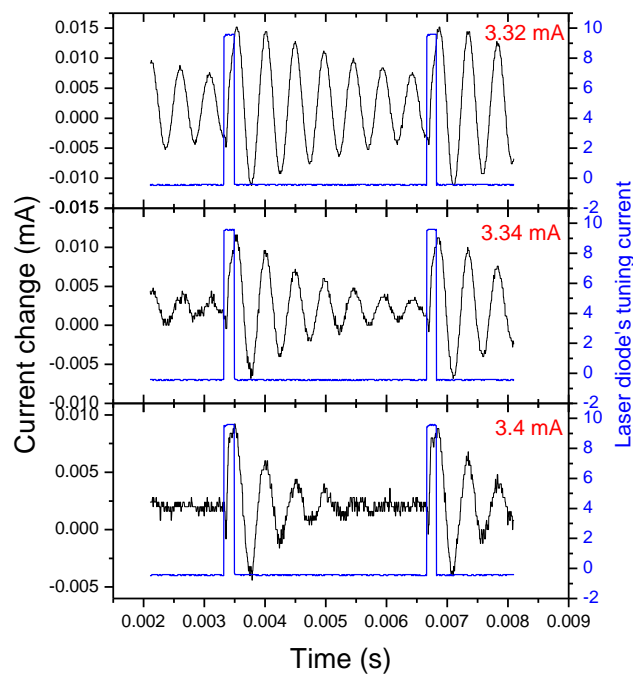


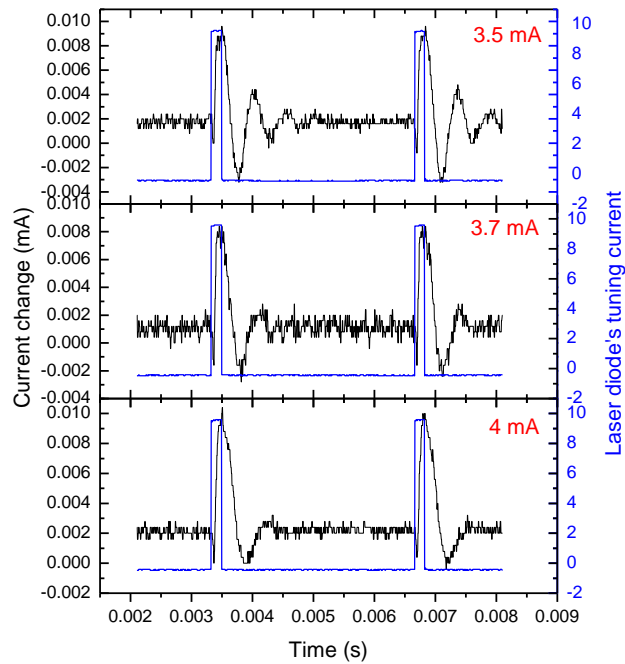Figure 6.19 Under-damped oscillations for I = 3.32 mA, I = 3.34 mA and I = 3.4 mA.

Figure 6.20 Under-damped oscillations for I = 3.5 mA, I = 3.7 mA and I = 4 mA

As explained earlier in this chapter, it can be seen in Figures 6.19 and 6.20 that in State II discharge works without oscillations (DC or stable-current mode) until it gets 4 mA.
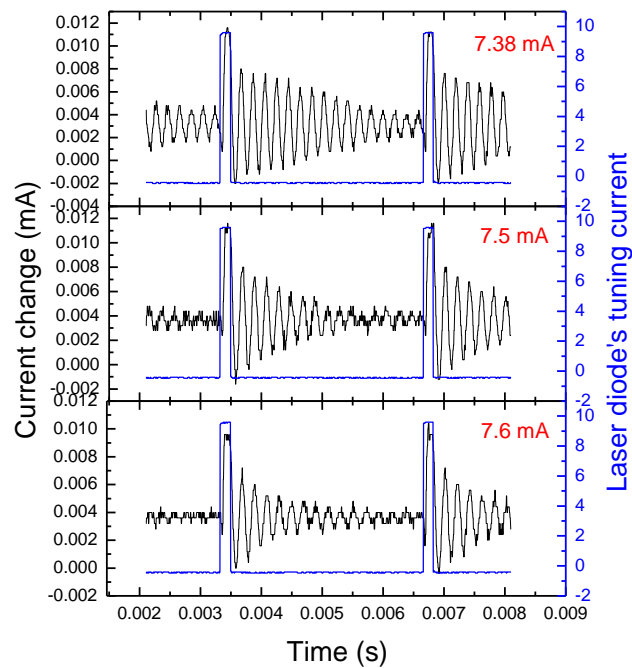


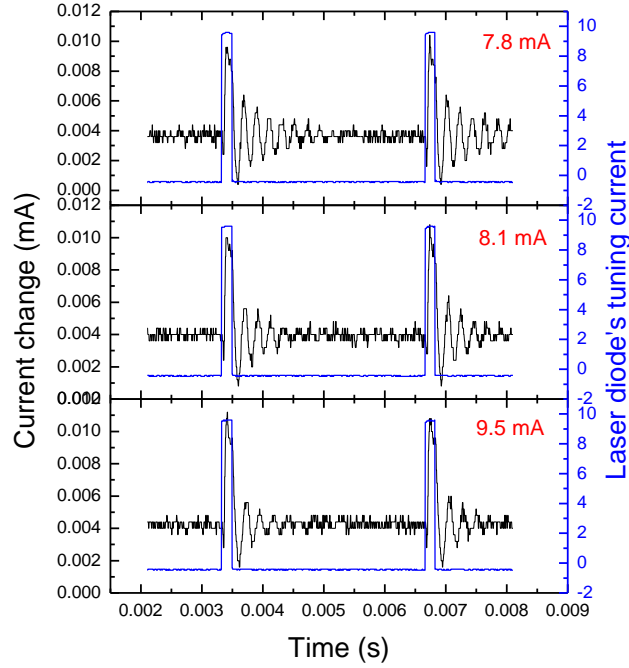Figure 6.21 Under-damped oscillations for I = 7.38 mA, I = 7.5 mA and I = 7.6 mA.

Figure 6.22 Under-damped oscillations for I = 7.8 mA, I = 8.1 mA and I = 9.5 mA.

After further increasing the current, and when the current reaches I = 7.6 mA, State IV of stable current region occurs. As it can be seen on Figures 6.21 and 6.22 they have different frequencies than in the State II. It can be seen on the figures that the dumping increases with increase of current.

The detailed quantitative description of the OGE is difficult, mainly because it is impossible to give a complete set of rate equations for all the levels and processes involved in the discharge. However, laser induced current oscillations can be fitted using SineDamp function, which describes quasi-sinusoidal oscillations with damping nature. Basically, it is a damped sine wave, a sinusoidal function whose amplitude decays as time increases. SineDamp is a function which includes phase shift, time period, decay constant, amplitude and offset, as it is given in equations (6.6-6.8).

$$y = y_0 + A * exp\left(-x/t_0\right)^* sin(\pi * (x - x_c)/w) \tag{6.6}$$

$$V = V_0 + V_0 exp\left(-t/\tau\right) sin(\omega t + \theta) \tag{6.7}$$

$$\Delta V = V_0 exp\left(-t/\tau\right) sin(\omega t + \theta) \tag{6.8}$$

Where $x = t$, $A = V_0$, $y = V(t)$, $\theta = \pi x_c/\omega$, and $\alpha/\omega_0 = \omega/\pi t_0$, $\alpha = 1/t_0$ is the damping factor and $\omega_0$ is frequency of oscillations.

The experimental data of the damping constant $\alpha$ and the angular frequency $\omega$ for the laser induced current oscillations are acquired by fitting recorded OGSs by dumped sinus function (Eq. 4.30) using ORIGIN 8.5 software. Some examples of the fitting are presented in figures 6.23 – 6.26. Obtained results for under-damped OG oscillations are separated in three current regions according to $\alpha/\omega_0$ values:

1) 3.30 mA $<$I $<$3.60 mA for $0.0240 < \alpha/\omega_0 < 0.2286$; $\alpha/\omega_0 \ll 1$

2) 3.70 mA $<$I $<$4.00 mA for $0.3000 < \alpha/\omega_0 < 0.3847$; $\alpha/\omega_0 < 1$

3) 7.38 mA $<$I $< 9.50$ mA for $0.0160 < \alpha/\omega_0 < 0.1000$; $\alpha/\omega_0 \ll 1$

If $\alpha \to 0 => \omega \to \omega_0$ the discharge response on the OGE tends to induce the current oscillations without damping, and the oscillations become highly sensitive and unstable. Damping factor influences on amplitude by gradually decreases it to zero. The results show two different cases of under-damped oscillations. For $\alpha/\omega_0 \ll 1$, low-current oscillations in the region II (figures 6.23 - 6.24) show smaller number of peaks, as compared to the oscillations in the region IV (figures 6.25 - 6.26). Since $\alpha/\omega_0 \approx 0$ the oscillatory behavior tends to critical damping, which occurs if the system is designed to return an oscillator to its equilibrium. If the damping is increased, the oscillations die away quicker and eventually return to the rest position with no overshoot oscillation. When $\alpha/\omega_0 < 1$ results confirmed the theoretical condition required for under-damped oscillations. Both $\alpha$ and $\omega_0$ depend highly on discharge current. The ratio $\alpha/\omega_0$ decreases with increment in negative dynamic resistance ($R_d < 0$). In this case, discharge inductance and capacitance remain fairly invariant upon resonant excitation.

Graphs in figures 6.23 - 6.26 show fits for different current regions. The experimental data are fitted using fitting functions 6.4 - 6.7. In all regions $\alpha$ increases and $\omega$ decreases with the current growth as one can see in Figure 6.27.
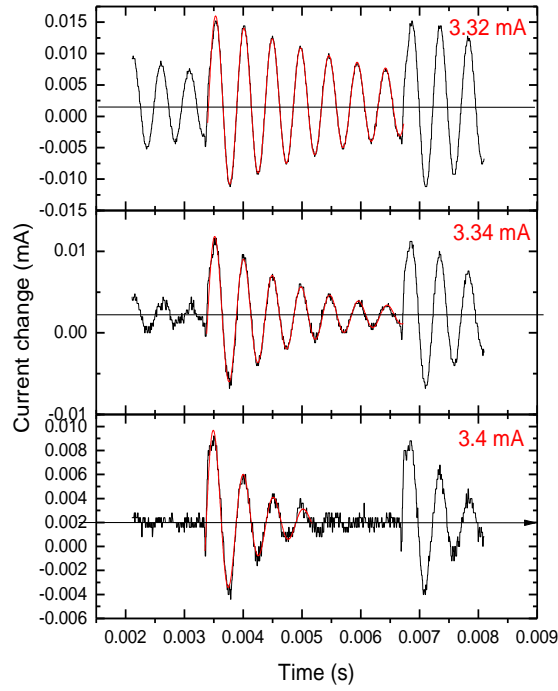
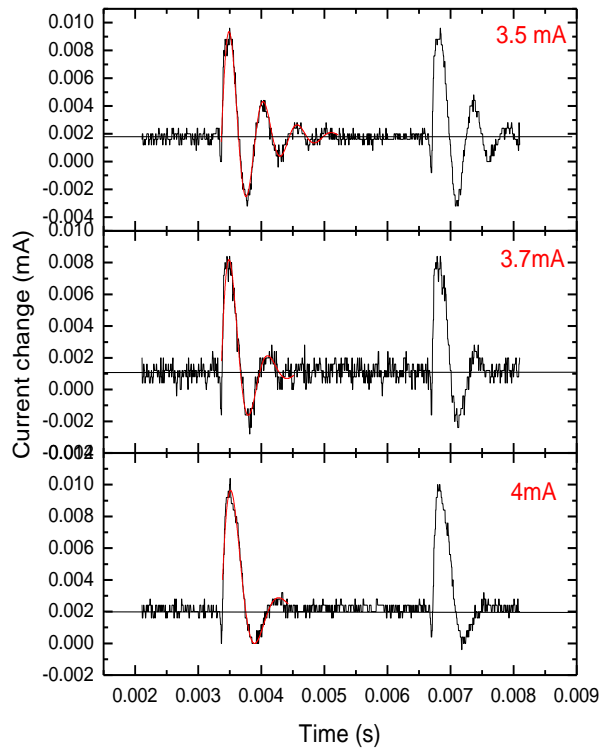Figure 6.23 SineDamp fit for I = 3.32 mA, I = 3.34 mA and I = 3.4 mA



Figure 6.24 SineDamp fit for I = 3.5 mA, I = 3.7 mA and I = 4.0 mA
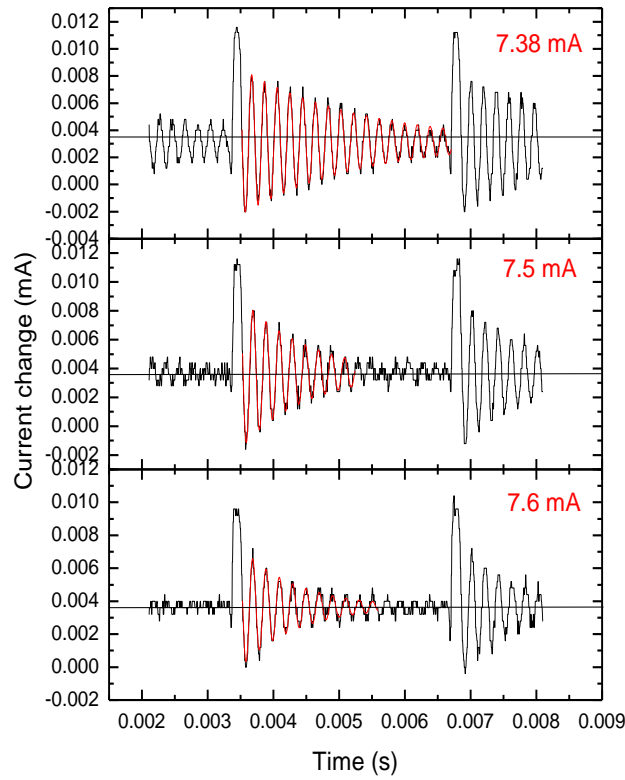
Figure 6.25 SineDamp fit for I = 7.38 mA, I = 7.5 mA and I = 7.6 mA


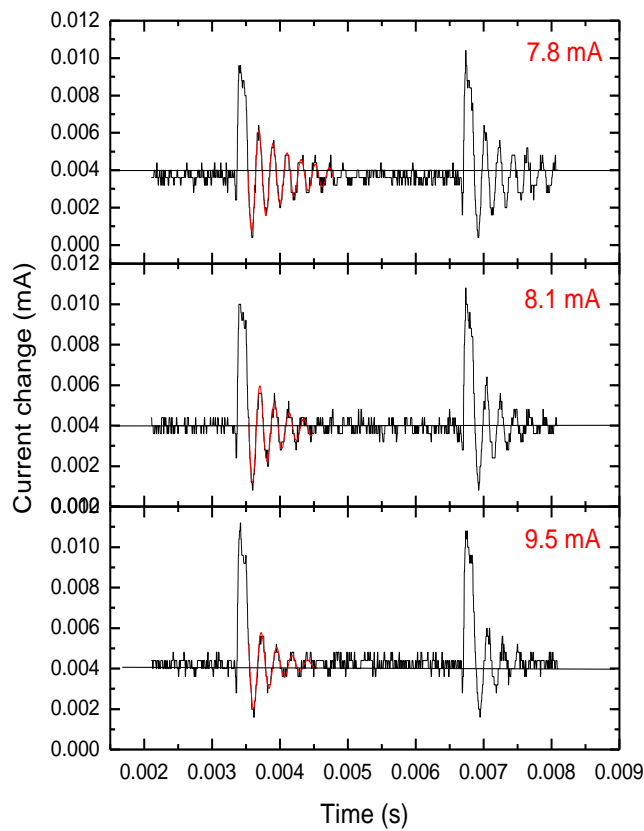
Figure 6.26 SineDamp fit for I = 7.8 mA, I = 8.1 mA and I = 9.5 mA

The fitting functions are presented in Figure 6.27. However, "constants" in the fitting functions, calculated from the equations 4.34 and 4.35, are different for two data sets.
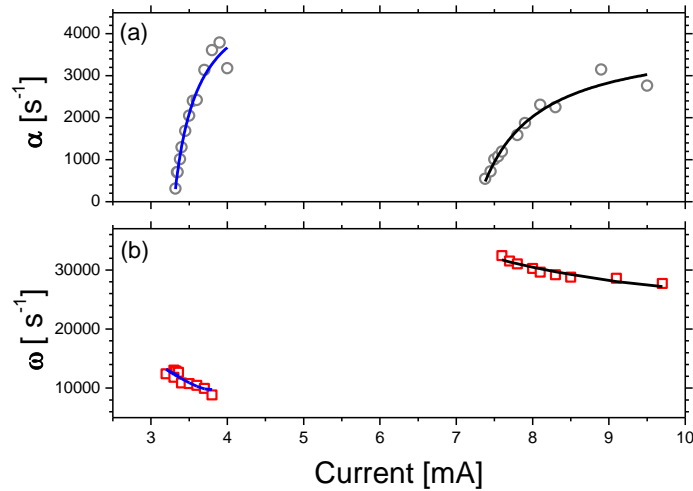


Figure 6.27. (a) The damping constant α and (b) the angular frequency ω, for the laser induced current oscillations. Appropriate fits for α(I) and ω(I) for two current regions are presented with different colors.

Upper graph in the figure shows a quite good agreement between the data of α and the fitting function, assigned with different colors for different current regions. Using previously acquired fitting functions α(I) (eq. 4.34), the fitting functions ω(I) (eq. 4.35) are created and fairly good agreement is obtained, see lower graph in Figure 6.27.

## 7 Exercises

Aims of the exercises are to correlate and compare some of mechanisms contributing to the HCD in relation to a varied range of operating conditions and parameters. Main objectives are studying voltage-current characteristics, emission spectra, OG signals and self-sustained and laser induced current oscillations in commercial HCL. Purpose of the exercises is to present the mentioned phenomena to undergraduate students by using relatively simple and accessible HCLs and current/temperature controlled laser diode. Four experimental exercises are given as a potential work for students at the universities studying plasma physics. Exercises included measurements of a) I-V neon hollow cathode discharge characteristics, b) emission spectrum of the lamp c) optogalvanic effect and d) laser diode induced oscillations in hollow cathode lamps. Each exercise is conducted in step-by-step manner; the theory related to the experiment is presented at first, experimental setup is given as a second part of the exercise, in the third part students are guided how to conduct experiments. After the laboratory work is done, students should use any data processing program (e.g ORIGIN) for graphical presentation, for comparing, analyzing and plotting the results. Finally, students have to comment present results.

## Experimental exercise 1: I-V neon hollow cathode discharge characteristics

### Theory

This part presents a theory of the glow discharge applied on a hollow cathode configuration. It is based on using Townsend's ionization equations with suitable boundary conditions in conjunction with Poisson's equation. If the mean free path for the charge transfer is λ than the potential $V'$ at the distance λ from the cathode is

$$V' = V(0)\left[\frac{2\lambda}{d} - \left(\frac{\lambda}{d}\right)^2\right] \qquad \text{(E1.1)}$$

Where V(0) = V at x = 0, and d is dark space thickness. The metastable atom concentration in the dark space is much lower than in the negative glow which gives equation

$$\frac{j^+(0)}{j} = \frac{1 - G_p - G_m}{1 + \gamma_i} \tag{E1.2}$$

$j^+(0)$ is ion current density at the survey of cathode, $\gamma_i$- , $G_p$ is the secondary emission coefficient due to radiation from the glow and $G_m$ is the secondary emission coefficients due to metastable produced in the glow. They must depend on the parameters of the dark space

$$j = 2\varepsilon_0 \sqrt{\frac{e\lambda}{m}} \frac{V(0)^{\frac{3}{2}}}{d^{\frac{5}{2}}} \frac{1 + \gamma_i}{1 - G_p - G_m} \tag{E1.3}$$

which gives a fitting function for I - V graphs for the hollow cathode discharge in the forms:

$$I(V) = k_1 V^{\frac{3}{2}} \frac{1}{1 - G} \tag{E1.4}$$

$$G(V) = k_2 V e^{-k_3 \sqrt{\frac{1}{V}}} \tag{E1.5}$$

where: $k_1 = 2\varepsilon_0 \sqrt{\frac{e\lambda}{m}} \frac{1+\gamma_i}{d^{\frac{5}{2}}} S$ (S – the cathode surface)

$k_2 = \gamma_p \eta_p b_p + d_g \gamma_m \eta_d b_m$

$k_3 = \bar{s} d \sqrt{V_e}.$

$\gamma_p$ and $\gamma_m$ are coefficients which represents efficiency of the secondary electron emission from the cathode surface for the impact of photons and metastable atoms, respectively, $\eta_p$ is a number of active quanta per one volt produced by one electron in the glow and $b_p V(0)$ is the average energy of fast electrons at the entrance of the glow. Here it is assumed that d and $\bar{s}$ dependence on V is of secondary importance (insignificant) in comparison with G dependence on V (e.g. $d \sim lnG$).

### Experiment

The experiment is based on studying the correlation between current and voltage, by measuring voltage-current characteristic using commercial hollow cathode lams (HCLs). It includes measurements of voltage and current on different hollow cathode lamps. For some HCLs I-V characteristics has a negative dynamic resistance in narrow regions of the discharge current. In the regions of negative dynamic

resistance current oscillations could be observed. Figure Ex.1.1 shows schema of the electrical circuit with for voltage and current measurement of the HCL.
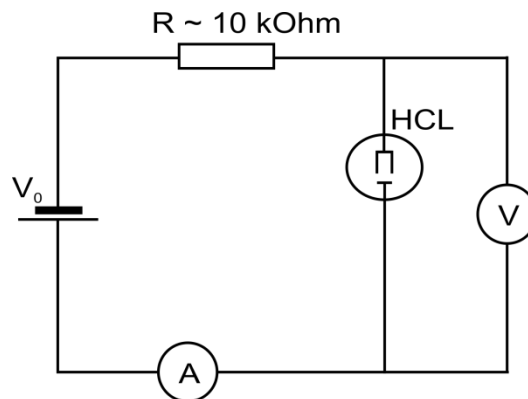


Figure Ex.1.1 Schema of electrical circuit for I-V measurement.

The experiment is conducted in the following way:

1. Form the electrical circuit using schema in Figure Ex.1.1. The ballast resistor has ~ 10 kΩ. Power supply use in a regime of voltage stabilization.

2. Increase the voltage until the discharge is ignited, then decrease the voltage to the minimal value necessary for stable working.

3. Measure discharge current and voltage increasing the voltage in steps of 1 V and make following table.

| I (mA) | V (V) |
|--------|-------|
| . | . |
| . | . |
| . | . |
| . | . |
| . | . |

4. Make V=f(I) and I=f(V) plots and notice, if exist, region with negative dynamic resistance. An example of I-V graph should is presented in Figure Ex.1.2

5. Fit the results using the formulas E1.4 and E1.5 and obtain values for $k_1$ and $k_2$. $k_3$ is fixed to a value reasonable for the neon at ~ 4 mbar pressure, because it does not depend on the cathode material and size.

6. Present I=f(V) graph together with the fit using, for example ORIGIN 8.5. The graphs should be similar to the graphs which are presented in Figure Ex.1-3.
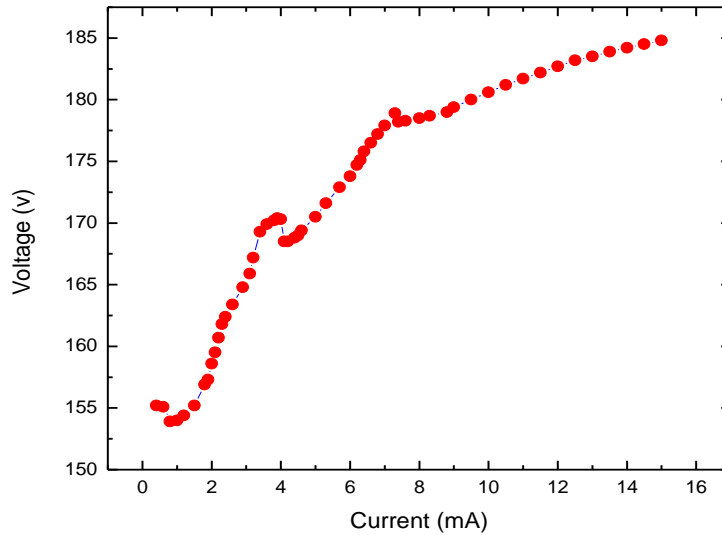
7. Comment the obtained results.



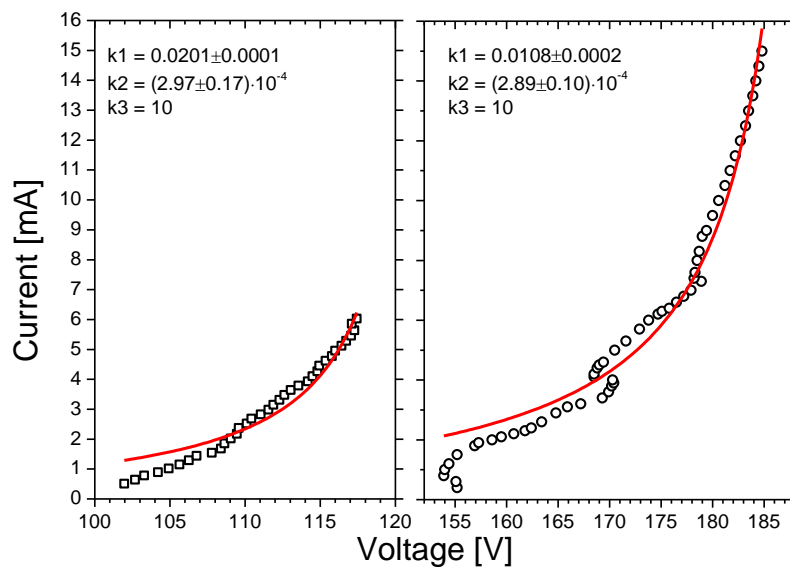Figure Ex.1.2 I-V characteristic of the Sb-Ne HCL.

**Example:**



Figure Ex1.3 Current-voltage characteristics of HCL with appropriate fits.

## Experimental exercise 2: Spectroscopy of hollow cathode lamps

The spectroscopy of HCL includes measurements of emission spectrum from HCL for different discharge currents. Figure Ex.2.1 presents experimental setup for recording of emission spectrum of neon HCL using UV-VIS spectrometer which covers the wavelength range 200 – 900 nm. Two types of lenses are used for image projection. The achromatic lens (f= 150 mm) is used to eliminate chromatic aberration in the visible range of spectra while quartz lens is used for recording UV range of spectra.
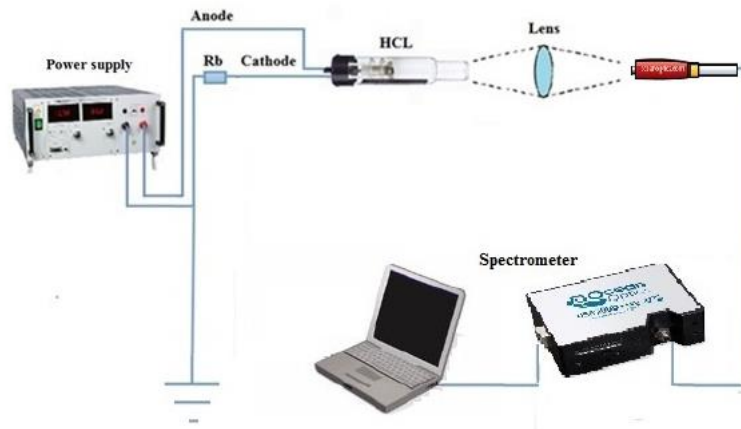


Figure Ex2.1 Experimental setup for spectroscopy measurement of hollow cathode lamp.

### Theory

HCL is a type of a glow discharge tube that uses a hollow cathode to enhance the emission intensity. Due to the hollow cathode effect emission line intensity significantly increases. Each specific HCL has the hollow cathode made of characteristic materials (metals or alloys) with specific current settings. Emission spectrum of a HCL contains atomic lines specific to the element from which the cathode is comprised and from the gas filled the lamp (argon or neon). Intensity of a particular spectral line depends on excitation and de-excitation processes connected to its upper and lower atomic energy levels. In general intensity of atomic line (vs. the discharge current $i$) in a HCL has the form:

$$I(i) = \frac{Ai(1 + Ci)}{1 + Bi} \tag{E.2.1}$$

where *A* depends on the magnitude of single-step excitation, *B* on the relative importance of collisional and radiative de-excitation and *C* on the relative importance

of two-stage and single-stage excitation. The number density of electrons is, at a given pressure and discharge configuration, approximately proportional to the discharge current. If an energy level may be populated from the ground state, in a single step by electron collisions, and if it is de-populated by radiation, than intensity of the line originated from this level is proportional to the discharge current. This is often characteristic of an atomic line of gas filled the HCL. On the other side, intensity of an atomic line of cathode material depends on a two-step process – sputtering of the cathode material and excitation of sputtered atom's line. As each of two the processes is approximately proportional to the discharge current it is expected that intensity of sputtered atoms' line is proportional to the square of the current. The purpose of the spectroscopy measurements is to investigate line intensity – discharge current relations in different HCLs.

**Experiment**

1. Focus the radiation from the negative glow region of a HCL onto entrance of the optical fiber connected to a wide range spectrometer. For focusing the radiation use quartz lens. Record spectra using appropriate software and identify all recorded lines using NIST spectra database (http://physics.nist.gov/PhysRefData/ASD/lines_form.html). An example of recorded spectrum and characteristic atomic lines is presented in Figure Ex.2.2.

2. Increase voltage in steps of 1 V on power supply and record spectra for each discharge current. The highest current is limited by the specification of HCL.

3. Plot graphs atomic line intensity vs. the discharge current for several gas lines and sputtered material lines. (See the example Figure Ex.2.3).
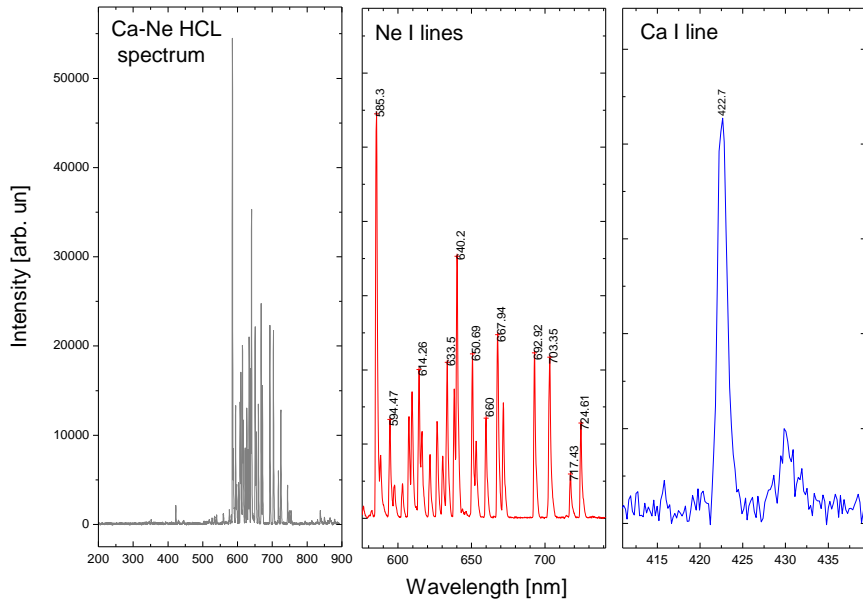
4. Comment the results.

Figure Ex2.2 Emission spectrum from Ca-Ne HCL and spectra of identified atomic neon lines and atomic calcium line.
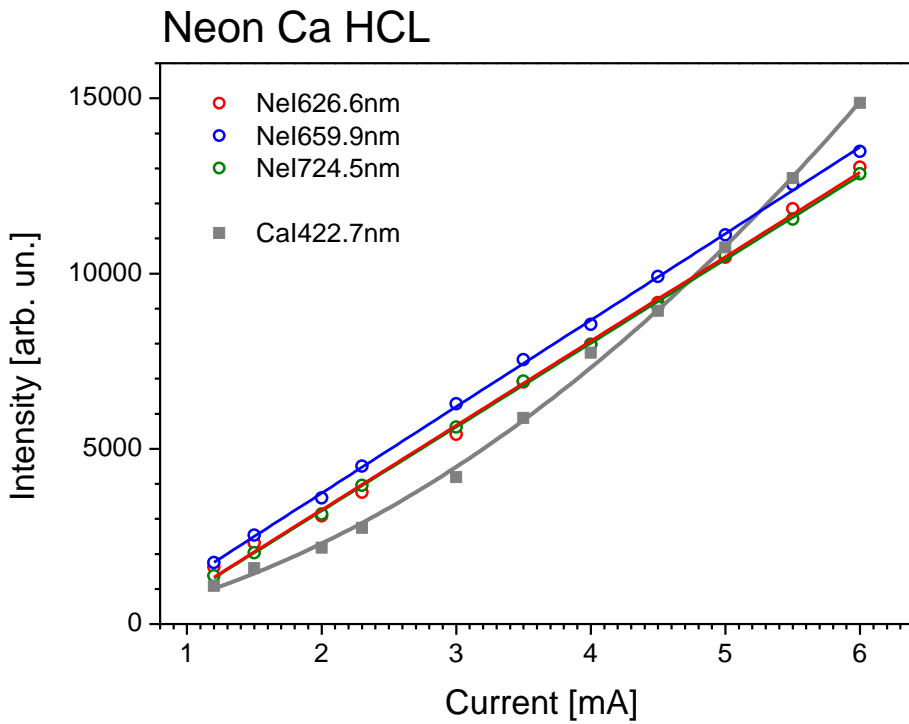
**Example**



Figure Ex2.3. Line intensity vs. discharge current for Ca-Ne HCL.

## Experimental exercise 3: Optogalvanic effect (OGE)

The schematic of the experimental setup of optogalvanic effect in neon hollow cathode discharge is shown in Figure Ex3.1. HCL with the cathode made of Ca and filled with neon at low pressure should be used. To run the discharge, a 0 – 1000 V and 0 – 100 mA voltage stabilized power supply is used. A ballast resistor of 9.85 kΩ should be placed in series with the discharge and power supply. Laser diode controller is used for controlling temperature and current of the laser diode. For tuning the laser wavelength a function generator should be used to generate saw tooth signal and square pulse for modulation of the laser diode current. The laser beam needs to be focused by a lens (f = 250 mm) to the hollow cathode filling all its interior space. Four channels, wideband oscilloscope is needed for measurements and recording the signals.
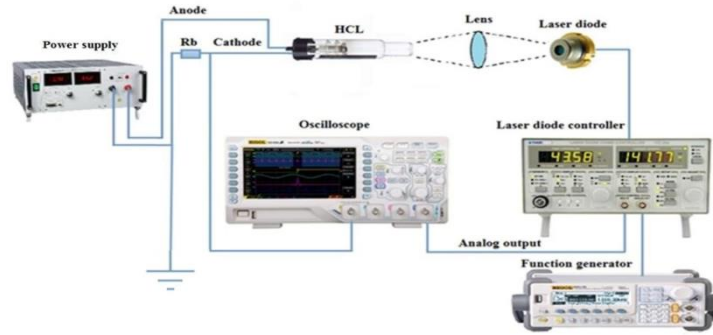


Figure Ex3.1 Experimental setup of OGE in neon HC.

### Theory

For modeling OG signal we use generalized theory for a hollow cathode discharge. In our case when the laser radiation excites 3s – 3p neon transition (659.89 nm) the variation of energetic photon densities $\Delta n_p^d$ and $\Delta n_p^g$ and the variation of the metastable density $\Delta n_m^d$ and $\Delta n_m^g$ induce a perturbation $\Delta I$ of the discharge current:

$$\Delta I = \frac{\partial I}{\partial n_p^d} \Delta n_p^d + \frac{\partial I}{\partial n_p^g} \Delta n_p^g + \frac{\partial I}{\partial n_m^d} \Delta n_m^d + \frac{\partial I}{\partial n_m^g} \Delta n_m^g \qquad \text{(E3.1)}$$

During the change of the radiative level $\Delta n_m^d$ and $\Delta n_m^g$ can be neglected. Also, during irradiation of the negative glow region $\Delta n_p^d$ can be neglected. Finally, OG signal is:

$$\Delta I = \frac{\partial I}{\partial G_p} \Delta G_p \tag{E3.2}$$

Where $\Delta G_p = \gamma_p \Delta n_p^g$.

Accordingly, taking into account E1.4:

$$\Delta I = I \frac{1}{1 - G} \gamma_p \Delta n_p^g \tag{E3.3}$$

In the equation (Ex3.3) G is the secondary emission coefficient which gives a fitting function for I - V graphs for the hollow cathode lamps in the form:

$$G(V) = k_2 V e^{-k_3 \sqrt{\frac{1}{V}}} \tag{E3.4}$$

where $k_2 = \gamma_p \eta_p b_p + d_g \gamma_m \eta_d b_m (f_g \approx 1$ for the hollow cathode discharge) and $k_3 = \overline{s} d \sqrt{V_e}$. Here it is assumed that the dark space thickness d and average ionization coefficient $\overline{s}$ dependence on V is of secondary importance (insignificant) in comparison with G dependence on V (e.g. $d \sim \ln G$).

It is necessary to estimate value of $\Delta n_p^g$ for fitting. Here we suppose that the change of energetic photons has the same dependence on current $I$ as the intensities of emitted atomic lines in the neon hollow cathode discharge.

$$\Delta n_p^g = \frac{AI(1 + CI)}{1 + BI} \tag{E3.5}$$

where A, B and C are the constants. Constant A depends on one-stage excitation, C on the relative importance of two and one-stage excitation, and B on the relative importance of collisional and radiative de-excitation. Finally, the fitting function for OG signal is:

$$\Delta I = I \frac{1}{1 - G} \gamma_p \frac{AI(1 + CI)}{1 + BI} \tag{E3.6}$$

## Experiment

To conduct the experiment on OGE, take the following steps:

1. Focus laser diode radiation to the central region of HCL (negative glow region).

2. Set the laser diode to be appropriate with neon line wavelength using laser diode controller by changing temperature and current.

3. Laser diode radiation wavelength has to be continuously increase (or decrease) so the LD has to be driven by saw tooth current signal.

4. Change the current discharge in steps of 0.5 mA and measure OG signal. An example of recorded OG signal is presented in Figure Ex.3.2.

5. Plot a graph intensity of OG signal vs. discharge current ($\Delta I = f(I)$) and use the formula E3.5 for fitting.

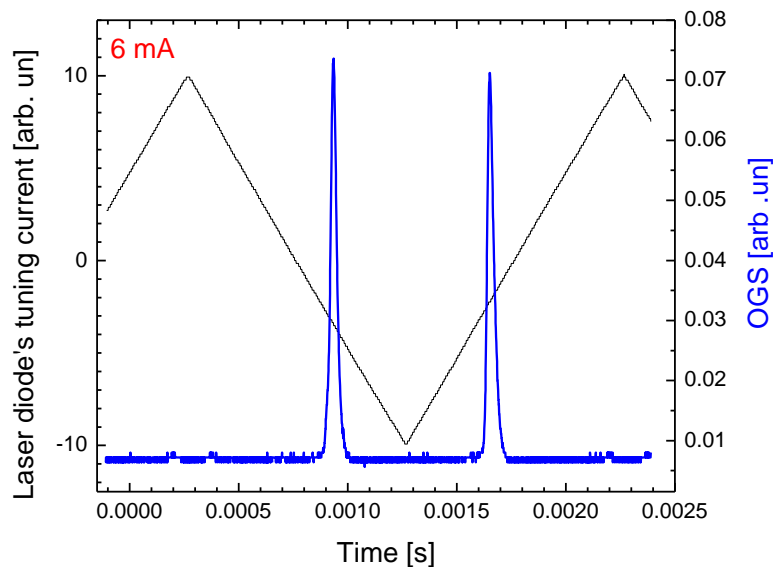6. Comment the obtained results.



Figure Ex3.2. An example of optogalvanic signal in Ca-Ne HCL. The discharge current I = 6mA.
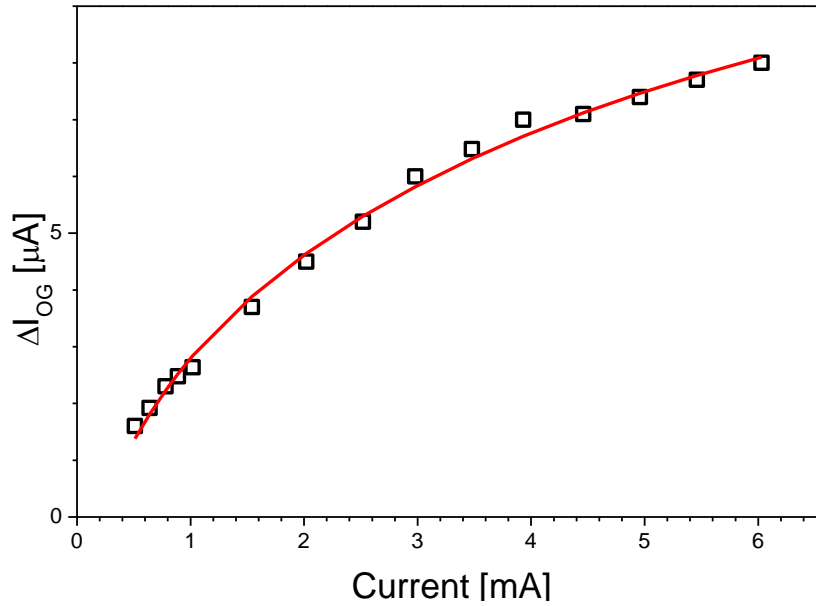
Figure Ex3.3 An example of optogalvanic signal vs. discharge current dependence in Ca neon HCL. Solid line is the fit obtained using fitting function.

## Exercise 4: Laser induced oscillations in hollow cathode lamps

### Theory

The low-current oscillations usually occur in the transition region between the Townsend and the normal glow regimes, i.e. in the subnormal region. Beside the self-sustained oscillations which are formed for some ranges of the discharge current, damped oscillations can be induced by the application of external voltage pulses, photoelectron initiated avalanches and resonant laser light absorption i.e. OGE.

Association of the electron current $I$ at the cathode (at time $t+T$) with the current at the time $t$ is given by equation:

$$I^e(0, t + T) = I^p(0, t + T) + \gamma_i I^e(0, t)\left(e^{\alpha_i(t)d} - 1\right)$$
$$+ G_m I^e(0, t)\left(e^{\alpha_m(t)d} - 1\right) \qquad \text{(E4.1)}$$

where $I^p(0, t + T)$ is the photoelectric current produced by irradiation of the cathode, $\gamma_i$ is the effective yield of electrons per ion arriving at the cathode, $G_m$ is the effective yield of electrons per metastable atom arriving at the cathode, $\alpha_i(t)$ and

$\alpha_m(t)$ are ionization and metastable excitation coefficients. Ions produced by backscattered electrons arriving at the anode could be neglected in the electrode configuration of the commercial HCL. The electron current at the cathode can also be written as an expansion in time about the time t.

$$I^e(0, t + T) = I^e(0, t) + T\frac{dI^e(0,t)}{dt} \tag{E4.2}$$

Relation for the total current at the cathode is:

$$I^e(0, t) = I(t)\frac{\gamma_i + G_m + G_p}{1 + \gamma_i} \tag{E4.3}$$

By deriving Eq. (Ex4.3) it is obtained:

$$\frac{dI^e}{dt} = \frac{dI}{dt}\frac{\gamma_i+G_m+G_p}{1+\gamma_i} + I\frac{1}{(1+\gamma_i)^2}\left[\left(\frac{\partial\gamma_i}{\partial V}\frac{dV}{dt} + \frac{\partial\gamma_i}{\partial I}\frac{dI}{dt}\right)\left(\gamma_i + G_m + G_p\right) + (1+\gamma_i)\left[\left(\frac{\partial\gamma_i}{\partial V} + \right.\right.\right.$$

$$\left.\left.\left.\frac{\partial G_m}{\partial V} + \frac{\partial G_p}{\partial V}\right)\frac{dV}{dt} + \left(\frac{\partial\gamma_i}{\partial I} + \frac{\partial G_m}{\partial I} + \frac{\partial G_p}{\partial I}\right)\frac{dI}{dt}\right]\right] \tag{E4.4}$$

and after substitution of $I^e$ with $I$, the following equation is obtained:

$$\left[\frac{\gamma_i+G_m+G_p}{1+\gamma_i} + \frac{1}{(1+\gamma_i)^2}\left[\left(1 - G_m - G_p\right)k_{iI} + (1+\gamma_i)\left(k_{mI} + k_{pI}\right)\right]I\right]\frac{dI}{dt} = \frac{I^p}{T} +$$

$$\frac{g-1}{T}\frac{\gamma_i+G_m+G_p}{1+\gamma_i}I - \frac{1}{(1+\gamma_i)^2}\left[\left(1 - G_m - G_p\right)k_{iV} + (1+\gamma_i)\left(k_{mV} + k_{pV}\right)\right]I\frac{dV}{dt} \tag{E4.5}$$

Where $k_{iI}$, $k_{iV}$, $k_{mI}$, $k_{mV}$, $k_{pI}$, $k_{pV}$ are coefficients for ions, metastable atoms and photons.

Another equation which connects the discharge voltage V and the discharge current I with the circuit componentsshown in Fig. Ex4.1a is:

$$\frac{dV(t)}{dt} = \frac{1}{RC}[V_0(t) - V(t) - RI(t)] \tag{E4.6}$$

where $V_0$ is a power supply voltage, R is a series resistance and C includes the capacitance of cables, high voltage connections and the discharge electrodes.
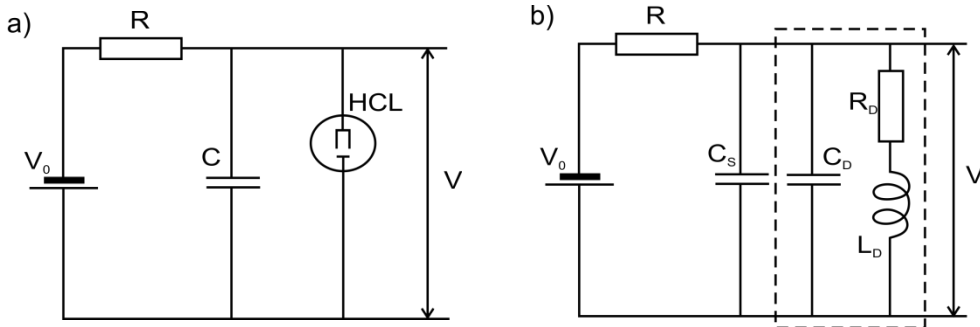
Figure Ex 4.1. (a) Schema of the electrical circuit with an idealized discharge tube. HCL – hollow cathode lamp (b) Schema of electrical circuit with an approximate equivalent circuit of the discharge enclosed in the dashed rectangle.

Analytical solutions of equations for small changes of voltage and current (equations Ex4.5 and Ex 4.6) are given with formulas (E4.7) and (E4.8).

$$V(t) = V_{ss} + \beta v(t) \tag{E4.7}$$

$$I(t) = I_{ss} + \beta i(t) \tag{E4.8}$$

Where $v(t)$ and $i(t)$ are time dependent components of current and voltage. Equations (E4.9) and (E4.10) are coupled linear first-order differential equations and are readily solved for $i(t)$ and $v(t)$.

$$(a + b_I I_{SS}) \frac{di}{dt} = \frac{\frac{\partial g}{\partial v}}{T} a I_{SS} v - \frac{\frac{\partial g}{\partial i}}{T} a I_{SS} i + b_V I_{SS} \frac{dv}{dt} \tag{E4.9}$$

$$\frac{dv}{dt} = -\frac{1}{RC} v - \frac{1}{C} i \tag{E4.10}$$

For our present purposes we need only the roots of the determinant which occurs using the Laplace transform technique. Without method of Laplace transform, the system of linear differential equations is given with formulas:

$$C(a + b_I I_{SS}) \frac{d^2 v}{dt^2} + \left[ \frac{(a + b_I I_{SS})}{R} + \frac{C}{T} \frac{\partial g}{\partial I} a I_{SS} + b_V I_{SS} \right] \frac{dv}{dt}$$
$$+ \frac{a I_{SS}}{T} \left[ \frac{\partial g}{\partial V} + \frac{1}{R} \frac{\partial g}{\partial I} \right] v = 0 \tag{E4.11}$$

$$i = -\frac{v}{R} - C \frac{dv}{dt} \tag{Ex4.12}$$

The first of above equations presented model of damped harmonic oscillator. At intermediate $I$ss the roots are complex and the current i(t) and voltage v(t) vary as

$$i(t) = i(0)e^{-\alpha t} \sin(\omega t + \phi_1) \qquad \text{(Ex4.13)}$$

$$v(t) = v(0)e^{-\alpha t} \sin(\omega t + \phi_2) \qquad \text{(Ex4.14)}$$

Where $\alpha$ and $\omega$ are the damping constant and the angular frequency. $\phi_1$ and $\phi_2$ are phase shifts that will be not measured in the experiment. $\omega^2$ and $\alpha$ have to be expressed as functions on $I = I$ss to use them for fitting of the experimental data:

$$\alpha(I) = \frac{a_1 + a_2 I}{1 + a_3 I} \qquad \text{(Ex4.15)}$$

$$\omega(I) = \sqrt{\frac{b_1 I}{1 + b_2 I} - \alpha(I)^2} \qquad \text{(Ex4.16)}$$

The detailed quantitative description of the OGE is difficult mainly because it is impossible to give a complete set of rate equations for all the levels and processes involved in the discharge.

However, laser induced current oscillations can be fitted using SineDamp function, which describes quasi-sinusoidal oscillations with damping nature,. Basically, it is a damped sine wave, a sinusoidal function whose amplitude decays as time increases. SineDamp is a function which includes phase shift, time period, decay constant, amplitude and offset, as it is given in equations (E4.17-E4.19).

$$y = y_0 + A * exp\left(-x/t_0\right)^* \sin(\pi * (x - x_c)/w) \qquad \text{(Ex4.17)}$$

$$V = V_0 + V_0 exp\left(-t/\tau\right) \sin(\omega t + \theta) \qquad \text{(Ex4.18)}$$

$$\Delta V = V_0 exp\left(-t/\tau\right) \sin(\omega t + \theta) \qquad \text{(Ex4.19)}$$

Where $x = t$, $A = V_0$, $y = V(t)$, $\theta = \pi x_c/\omega$, and $\alpha/\omega_0 = \omega/\pi t_0$, $\alpha = 1/t_0$ is the damping factor and $\omega_0$ is frequency of oscillations.

### Experiment

To conduct the experiment on laser induced current oscillations by using OGE, take the following steps:

1. Focus laser diode radiation to the central region of HCL (negative glow region).

2. Set the laser diode radiation to be at neon line wavelength using laser diode controller by changing temperature and current.

3. Laser diode's current has to be tuned to rectangular mode to record current oscillations.

4. Plot the results using for example ORIGIN 8.5. (Examples for I = 3.34 mA and I = 4 mA are presented in Figure Ex4.2).

5. Do fitting using SinDamp function according to equations E4.17 - E4.19 for all currents where induced oscillations are obtained. (Example of SineDump fit for I = 3.32 mA is given in Figure Ex4.3)

6. Find relation between damping factor $\alpha$ and discharge current (An example is given in Figure Ex4.4)
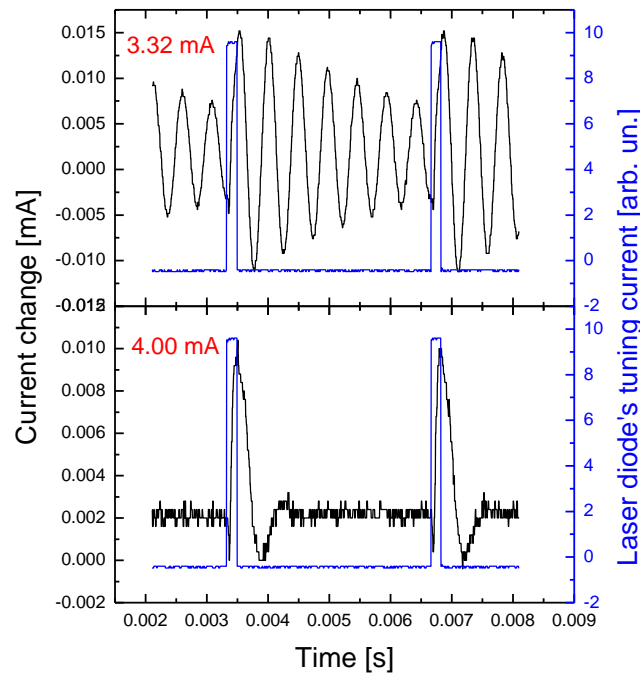
7. Comment the results.



Figure Ex4.2 Under-damped oscillations for I = 3.32 mA and I = 4.00 mA.
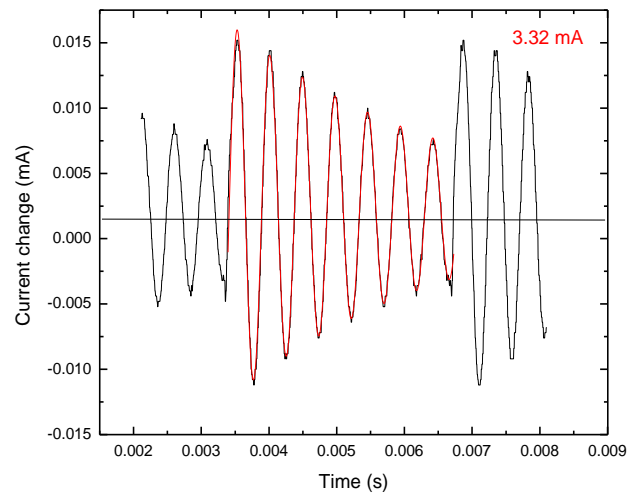
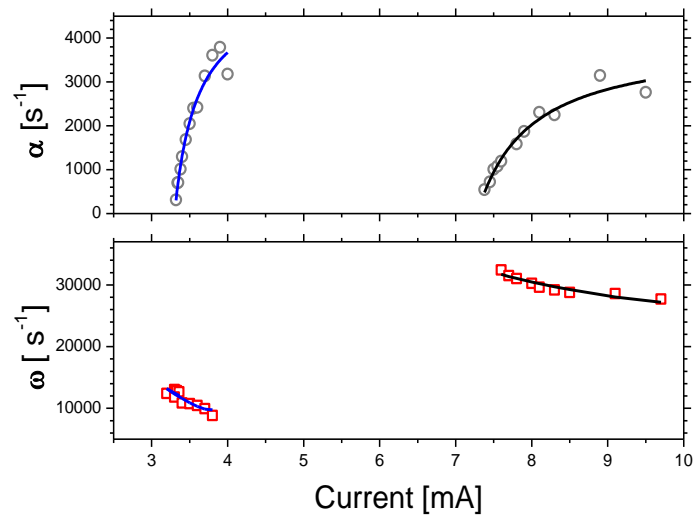Figure Ex4.3 SineDamp fit of induced current oscillations for I = 3.32 mA.



Figure Ex4.4. An example of the damping constant $\square$ and the angular frequency $\omega$ and for the laser induced current oscillations with appropriate fits.

## 8 Conclusion

The scientific expertise in various research topics is the guideline for education in physics of ionized gases and plasmas, providing research opportunities for students. There are many problems related to teaching and learning in the physics of ionized gases and plasma regarding availability and presence of facilities, poorly equipped laboratories, and the extent to which the university is conductive for practical activities. It is also a fact that many universities cannot afford to perform research in plasma physics with their own resources. Although most of the equipment is expensive, there are some commercial equipment which can be used for demonstration of phenomena in physics of ionized gases. One of such equipment is a hollow cathode lamp (HCL) and it could be used to conduct the experiments on the glow discharge. Other reasons are that HCL offer spectral purity, stable operation, low noise, long life, and high output intensity. For the purpose of demonstration of different phenomena in gas discharges, commercial HCLs with Ca and Sb cathode, filled with neon were investigated. The main goal of the study is to present the obtained results on investigating different phenomena related to HCL as experimental exercises for motivated graduated students in physics. In order to follow experiments students are expected to be familiar with some theory, laboratory equipment and experimental work in a laboratory, as well as graphical presenting and analyzing of the results.

The experiments in the thesis use HCLs and current/temperature controlled laser diode. The research is based on tracking down the current oscillations from the occurrence until they decrease to zero, so the laboratory work itself consisted in registering I-V characteristics and frequency-current (f-I) dependence, to determine points of stability and current oscillations. Namely, their voltage-current characteristics were recorded, and current oscillations and optogalvanic effect (OGE) were studied. Voltage-current characteristics of the lamps were explained using the classical theory of the hollow cathode discharge. The OGE in HCL is produced by a commercial laser diode radiated at the wavelength that corresponds to the neon transition $1s^2$-$2p^2$ at 659.89 nm. The OG signal in the Ca-Ne HCL is theoretically treated as a small perturbation of discharge current and obtained functional dependence of the OG intensity on the current is used as a fitting function for the

measured data. In the Sb-Ne HCL, self-sustained as well as laser induced current oscillations are observed in the two regions of voltages. Laser induced oscillations, two orders smaller than the self-sustained ones, are theoretically treated using the phenomenological model. Obtained functional dependences of frequency and dumping constant on the current are used for fitting of the experimental data. The phenomenological model could only qualitatively treat the large self-sustained oscillations, although linear dependence of square of the oscillation frequency on negative differential resistance is confirmed.

As the thesis outcome, four experimental exercises are given as work for students at the universities studying physics of ionized gases. Each exercise is conducted in step-by-step manner; the theory related to the experiment is presented at first, experimental setup is given as a second part of the exercise, in the third part students are guided how to conduct experiments. After the laboratory work is done, students should use a program for graphical presentation (e.g. Origin) for comparing, analyzing and plotting the results. Finally, they have to comment presented results.

First experimental exercise presents measurements of I-V neon hollow cathode discharge characteristics. For some current values students will observe self-sustained oscillations and will record them using a digital oscilloscope. The phenomenological approach for describing the self-sustained current oscillations is explained in terms of equivalent circuit elements. Second experimental exercise includes measurements of emission spectrum emitted from the Ne HCL. Students are guided to setup the experiment, record spectra, for different HCL currents, export data and plot the results. Also, students have to identify spectral lines using NIST spectra database taking into account the lines are produced by exited gas atoms and atoms of sputtered cathode material. Finally, they have to plot line intensity as a function of current and comment the results.

Third experimental exercise is a demonstration and measurement of the optogalvanic effect in HCL. The experiment includes measurement of OG signals for different current values. Students will use laser diode radiation having wavelength matched to a neon atoms transition in neon field HCL. The laser diode radiation, tuned to appropriate wavelength (659.9 nm) is directed to the center of the HCL. The OG signals are measured as a function of the discharge current and obtained results are fitted using the fitting function presented in the theoretical part of the exercise.

Fourth experimental exercise deals with the laser diode induced oscillations. The experiment includes measuring of time dependent current oscillations and modeling them by dumped harmonic oscillator. Theory in the exercise is presented only through basic formulas. Experimental setup for the exercise is the same as for exercise 3 except that the laser diode is tuned by a rectangular current signal. Results have to be prepared using graphical interface and results should be commented.

This thesis shows that using affordable and simple equipment, experiments for undergraduate students can be formed in the field of physics of ionized gases.

# References

[1] R. Keller, A.; B. Warner, E.; E. Zalewski, F.; P. Dyer; R. Engleman; Jr.; B. Palmer, A., The mechanism of the optogalvanic effect in a hollow-cathode discharge, J. Phys. Colloques 44 (1983) C7-23-C7-33.

[2] S.B. Rai; D.K. Rai, Review article: optogalvanic spectroscopy, Proceedings of Indian National Science Academy 62 (1996) 475-512.

[3] P.D. Foote; F.L. Mohler, Photo-Electric Ionization of Caesium Vapor, Physical Review 26 (1925) 195-207.

[4] A. Terenin, Photoionization of Salt Vapors, Physical Review 36 (1930) 147-148.

[5] S.S. Joshi; V. Narasimham, A light effect in chlorine under electrical discharge, Current Science 9 (1940) 535-536.

[6] R.B. Green; R.A. Keller; G.G. Luther; P.K. Schenck; J.C. Travis, Galvanic detection of optical absorptions in a gas discharge, Applied Physics Letters 29 (1976) 727-729.

[7] R.B. Green; R.A. Keller; P.K. Schenck; J.C. Travis; G.G. Luther, Opto-galvanic detection of species in flames, Journal of the American Chemical Society 98 (1976) 8517-8518.

[8] H.A. Bachor; P.J. Manson; R.J. Sandeman, Optogalvanic detection as a quantitative method in spectroscopy, Optics Communications 43 (1982) 337-342.

[9] P. Misra; I. Misra; X.L. Han, Laser optogalvanic spectroscopy of neon at 659.9 nm in a discharge plasma and nonlinear least-squares fitting of associated waveforms, Nonlinear Analysis: Theory, Methods & Applications 71 (2009) e661-e664.

[10] B. Barbieri; N. Beverini; A. Sasso, Optogalvanic spectroscopy, Reviews of Modern Physics 62 (1990) 603-644.

[11] C. Haridass; H. Major; P. Misra; X. Han, Laser Optogalvanic Spectroscopy of Discharge Plasmas in the Ultraviolet Region, in Ultraviolet Spectroscopy And Uv Lasers, CRC Press: 2002.

[12] X.L. Han; V. Wisehart; S.E. Conner; M.C. Su; D.L. Monts, Collisional Ionization of Excited State Neon in a Gas Discharge Plasma, Contributions to Plasma Physics 35 (1995) 439-452.

[13] R.S. Stewart; K.I. Hamad; K.W. McKnight, Optogalvanic Spectroscopy, in Optogalvanic Spectroscopy, R.S. Stewart; J.E. Lawler, Eds. Institute of Physics: Inst. Phys. Conf., Bristol, UK, 1990; Vol. 113, p 89.

[14] X.L. Han; M.C. Su; C. Haridass; P. Misra, Collisional dynamics of the first excited states of neon in the 590-670 nm region using laser optogalvanic spectroscopy, Journal of Molecular Structure 695–696 (2004) 155-162.

[15] D. Marić; N. Škoro; G. Malović; Z.L. Petrović; V. Mihailov; R. Djulgerova, Hollow cathode discharges: Volt-ampere characteristics and space-time

resolved structure of the discharge, Journal of Physics: Conference Series 162 (2009) 012007.

[16]     D. Zhechev; N. Bundaleska; J.T. Costello; D. Todorov, Photoelectron emission and its instrumental effect on optogalvanic measurements in a hollow cathode discharge, Opto - Electronics Review Vol. 13, No. 3 (2005) 193-196.

[17]     D. Murnick; O. Dogru; E. Ilkmen, 14C analysis via intracavity optogalvanic spectroscopy, Nuclear Instruments and Methods in Physics Research Section B: Beam Interactions with Materials and Atoms 268 (2010) 708-711.

[18]     M. Blosser; X.L. Han; R.F. Garcia-Sanchez; P. Misra, Laser Optogalvanic Spectroscopy and Collisional State Dynamics Associated with Hollow Cathode Discharge Plasmas, in Applied Spectroscopy and the Science of Nanomaterials, P. Misra, Ed. Springer Singapore: Singapore, 2015; pp 21-40.

[19]     C.P. Ausschnitt; G.C. Bjorklund; R.R. Freeman, Hydrogen plasma diagnostics by resonant multiphoton optogalvanic spectroscopy, Applied Physics Letters 33 (1978) 851-853.

[20]     D.K. Doughty; J.E. Lawler, Spatially resolved electric field measurements in the cathode fall using optogalvanic detection of Rydberg atoms, Applied Physics Letters 45 (1984) 611-613.

[21]     J.E.M. Goldsmith; J.E. Lawler, Optogalvanic spectroscopy, Contemporary Physics 22 (1981) 235-248.

[22]     C.R. Webster; C.T. Rettner, Laser optogalvanic spectroscopy of molecules, Laser Focus 19 (1983) 41-52.

[23]     V.V. Zhurin, Industrial Ion Sources: Broadbeam Gridless Ion Source Technology, Weinheim Wiley-VCH-Verlag: 2012.

[24]     A. Ben-Amar; G. Erez; R. Shuker, Pulsed resonant optogalvanic effect in neon discharges, Journal of Applied Physics 54 (1983) 3688-3698.

[25]     D. Zhechev; N. Parvanova, Anomalous optogalvanic signal. Spectrometric applications, Opto-electronics review 11 (2003) 31-34.

[26]     V. Steflekova; D. Slavov; D. Zhechev; G. Todorov, Self-sustained unstable modes for operation of glow discharge. An application., Publ. Astron. Obs. Belgrade 84 (2008) 361-364.

[27]     G. Schaefer; K.H. Schoenbach, Basic Mechanisms Contributing to the Hollow Cathode Effect, in Physics and Applications of Pseudosparks, M.A. Gundersen; G. Schaefer, Eds. Springer US: Boston, MA, 1990; pp 55-76.

[28]     P.F. Little; A. von Engel, The Hollow-Cathode Effect and the Theory of Glow Discharges, Proceedings of the Royal Society of London. Series A. Mathematical and Physical Sciences 224 (1954) 209-227.

[29]     A. Günther-Schulze, Die Stromdichte des normalen Kathodenfalles, Zeitschrift für Physik 19 (1923) 313-332.

[30]     V.I. Kolobov; L.D. Tsendin, Analytic model of the hollow cathode effect, Plasma Sources Science and Technology 4 (1995) 551.

[31] R.R. Arslanbekov; A.A. Kudryavtsev; R.C. Tobin, On the hollow-cathode effect: conventional and modified geometry, Plasma Sources Science and Technology 7 (1998) 310.

[32] K.H. Becker; K.H. Schoenbach; J.G. Eden, Microplasmas and applications, Journal of Physics D: Applied Physics 39 (2006) R55.

[33] R. Mavrodineanu, Hollow Cathode Discharges, Journal of Research of the National Bureau of Standards 89 (1984) 143-185.

[34] J. Hu. Experimental investigations of pseudospark discharge and pseudospark produced intense electron beams, Ph.D. Thesis, Missouri University of science and technology, Missouri, USA, 2012.

[35] V.K. Mehta; R. Mehta, Principles of Electronics, S. Chand: 2008.

[36] C.F. Gallo, Corona-A Brief Status Report, IEEE Transactions on Industry Applications IA-13 (1977) 550-557.

[37] V.A. Lisovskiy; V.A. Koval; E.P. Artushenko; V.D. Yegorenkov, Validating the Goldstein–Wehner law for the stratified positive column of dc discharge in an undergraduate laboratory, European Journal of Physics 33 (2012) 1537.

[38] http://studentsrepo.um.edu.my/1668/4/BAB_1.pdf (31/08/2015),

[39] Atomic-Absorption and Emission Analysis. http://intranet.tdmu.edu.ua/data/kafedra/internal/pharma_2/classes_stud/en/pharm/prov_pharm/ptn/analytical%20chemistry/2%20course/21%20atomic-absorption%20and%20emission%20analysis.htm (07/05/2017),

[40] Sanyo 2003 Red laser diode DL-3147-060, Ver.1. http://eelinux.ee.usm.maine.edu/courses/ele467/Reference%20Material/DL-3147-060%20Specs.pdf (28/08/2015),

[41] Heraeus Nobelight 2015 Hollow cathode lamp. http://www.heraeus-noblelight.com/en/productsandsolutions/opticalanalysis/hollow_cathode_lamps.aspx (29/08/2015),

[42] SpectroLamps 2015 Hollow Cathode Lamps HCL. http://www.spectrolamps.com.au/hollow_cathode_lamps.html (29/08/2015),

[43] http://www.hamamatsu.com/ (08/05/2017),

[44] A. von Engel, Ionized Gases, Clarendon Press: Oxford, 1965.

[45] A.J. Lucero; Y.C. Chung; S. Reilly; R.W. Tkach, Saturation measurements of excited-state transitions in noble gases using the optogalvanic effect, Opt. Lett. 16 (1991) 849-851.

[46] D.E. Murnick; J.O. Okil, Use of the optogalvanic effect (OGE) for isotope ratio spectrometry of 13CO2 and 14CO2, Isotopes in Environmental and Health Studies 41 (2005) 363-371.

[47] M.N. Reddy, Laser Optogalvanic Spectroscopy: Experimental Details and Potential Applications, R&D Defense Science Journal 44 (1994) 279-293.

[48] R. Shuker; A. Ben-Amar; G. Erez, Theoretical and Experimental Study of the Resonant Optogalvanic Effect in Neon Discharges, J. Phys. Colloques 44 (1983) C7-35-C7-44.

[49]     E. DeMarinis; A. Sasso; E. Arimondo, Optogalvanic investigations in the cathodic region of a neon glow discharge, Journal of Applied Physics 63 (1988) 649-655.

[50]     C. Howard; M.E. Pillow; E.B.M. Steers; D.W. Ward, Intensities of some spectral lines from hollow-cathode lamps, Analyst 108 (1983) 145-152.

[51]     I. Poole, Laser Diode Types. http://www.radio-electronics.com/info/data/semicond/laser_diode/types-laser-diodes.php (06/08/2015),

[52]     Z. Donkó, Modelling of low-current self-generated oscillations in a hollow cathode discharge, Journal of Physics D: Applied Physics 32 (1999) 1657.

[53]     Z.L. Petrović; A.V. Phelps, Oscillations of low-current electrical discharges between parallel-plane electrodes. I. dc discharges, Physical Review E 47 (1993) 2806-2815.

[54]     B.M. Jelenković; K. Rózsa; A.V. Phelps, Oscillations of low-current electrical discharges between parallel-plane electrodes. II. Pulsed discharges in H2, Physical Review E 47 (1993) 2816-2824.

[55]     S.P. Lee; E.W. Rothe; G.P. Reck, Influence of electrical resonance on the interpretation of optogalvanic data, Journal of Applied Physics 61 (1987) 109-112.

[56]     L.F.M. Braun; J.A. Lisbôa, Observation of damped oscillations in the optogalvanic effect in a subnormal glow discharge, Optics Communications 108 (1994) 302-310.

[57]     V.K. Saini, Laser-induced optogalvanic signal oscillations in miniature neon glow discharge plasma, Appl. Opt. 52 (2013) 4404-4411.

[58]     Z. Petrovic, Lj.; I. Stefanovic; S. Vrhovac; J. Zivkovic, Negative Differential Resistance, Oscillations and Constrictions of Low Pressure, Low Current Discharges, J. Phys. IV France 07 (1997) C4-341-C4-352.

[59]     A.V. Phelps; Z.L. Petrović; B.M. Jelenković, Oscillations of low-current electrical discharges between parallel-plane electrodes. III. Models, Physical Review E 47 (1993) 2825-2838.

[60]     T. Donahue; G.H. Dieke, Oscillatory Phenomena in Direct Current Glow Discharges, Physical Review 81 (1951) 248-261.

[61]     K. Tochigi; S. Maeda; C. Hirose, Optogalvanic Observation of Ionization Waves in Hollow-Cathode Discharges, Physical Review Letters 57 (1986) 711-714.

[62]     X.L. Han; M.C. Blosser; P. Misra; H. Chandran, Abrupt changes in neon discharge plasma detected via the optogalvanic effect, Thin Solid Films 521 (2012) 155-157.

[63]     J.R. Nestor, Optogalvanic spectra of neon and argon in glow discharge lamps, Appl. Opt. 21 (1982) 4154-4157.

[64]     M.S.A. Eldakli; S.S. Ivković; B.M. Obradović, Optogalvanic effect and laser-induced current oscillations in hollow-cathode lamps, European Journal of Physics 38 (2017) 025210.

Appendix 1

## Laser diode as optical source for optogalvanic spectroscopy

Laser diodes (LDs) operating in the infrared, and more recently in the visible red, green, blue, or violet, have found many commercial applications, including use in fiber optic communications systems, laser printers, and remote sensing, and in consumer products such as compact disk players, home security systems, and remote control devices. Because of their low cost, modest power requirements, and reliability, diode lasers are rapidly replacing older gas lasers such as the HeNe laser and tunable dye lasers in many scientific applications in the red and infrared region of the optical spectrum. Laser diodes are electrically pumped semiconductor devices in which the gain is generated by an electrical current flowing through a p–n junction. This process can be spontaneous, but can also be stimulated by incident photons, in effect leading to optical amplification, and with optical feedback in a laser resonator to laser oscillation. Typical LD structure (example of double hetero structure) is given in Figure A.1.



metal contact
p-type (material A)
p-type (material B)
quantum well (material C)
n-type (material B)
n-type (material A)
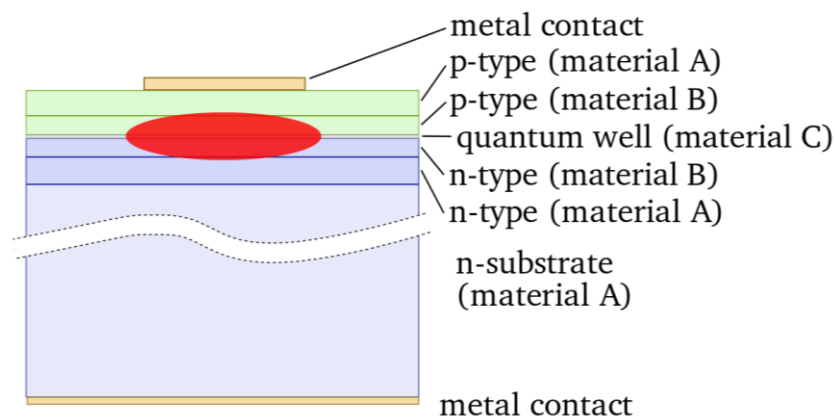n-substrate (material A)
metal contact

Figure A.1 Laser diode structure.

LDs operate in two different ways, although many of the concepts used within them are very similar. The Injection LD has many factors in common with light emitting diodes. The main difference is that LDs are manufactured having a long narrow channel with reflective ends. This acts as a waveguide for the light. In operation, current flows through the p-n junction, and light is generated using the same process that generates light in a light emitting diode. However, the light is confined within the waveguide formed in the diode itself. Here the light is reflected and then amplified because of stimulated emission before exiting though one end of

the laser diode as the external beam. For the optically pumped semiconductor laser the optical gain is provided by stimulated emission. This approach offers several advantages, particularly in wavelength selection and lack of interference from internal electrode structures.

Laser diodes differ from conventional lasers in several ways:

1)      Small size and weight: A typical laser diode measures less than 1 mm across and weighs a fraction of a gram, making it ideal for use in portable electronic equipment.

2)      Low current, voltage, and power requirements: Most laser diodes require only a few mW of power at 3 to 12 V DC and several mA. Therefore, they can operate using small battery power supplies. Overall efficiencies greater than 30% are typical in the case of LDs.

3)      Low power- few mW: Its coherent output results in high efficiency and ease of modulation for communications and control applications.

4)      Wide-angle beam: A laser diode produces a "cone" rather than a "pencil" of visible light or IR, although this "cone" can be collimated using convex lenses.

5)      Since LDs are made of semiconductor materials, they do not require the fragile glass enclosures or mirror alignment typical of gas lasers. The resulting ruggedness and small size allow laser diodes to be used in environments and spaces in which other types of lasers cannot operate.

The advantage of LDs is that they can be directly modulated at high frequencies. By modulating the drive current, the output of the laser diode is modulated with frequencies up to several GHz in high-speed data communications. Coherence and single wavelength characteristics of laser diodes enable the outputs of these devices to be focused to a diffraction limited spot size. The size of the resultant spot is dependent on the wavelength of the laser - the shorter the wavelength of light, the smaller the size of the spot that can be generated. Most LDs are built as edge-emitting lasers, where the laser resonator is formed by coated or uncoated end facets of the semiconductor wafer. They are often based on a double hetero-structure, which restricts the generated carriers to a narrow region and at the same time serves as a waveguide for the optical field. Some modern kinds of LDs are of the surface-

emitting type, where the emission direction is perpendicular to the wafer surface, and the gain is provided by multiple quantum wells.

There are very different kinds of LDs, operating in very different regimes of optical output power, wavelength, bandwidth, and other properties. there are several types of LDs: 1) Small edge-emitting LDs generate between a few mW and up to roughly 0.5 W of output power in a beam with high beam quality. The output may be emitted into free space or coupled into a single-mode fiber. Such lasers can be designed to be either index guiding with a waveguide structure guiding the laser light within the LD, or gain guiding where the beam profile is kept narrow via preferential amplification on the beam axis. 2) Small LDs made as distributed feedback lasers (DFB lasers) or distributed Bragg reflector lasers (DBR lasers) with short resonators can achieve single-frequency operation, sometimes combined with wavelength tenability. 3) External cavity diode lasers contain a laser diode as the gain medium of a longer laser resonator, completed with additional optical elements such as laser mirrors or a diffraction grating. They are often wavelength-tunable and exhibit a small emission line width. 4) Broad area laser diodes generate up to a few watts of output power. The beam quality is significantly poorer than that of lower-power LDs, but better than that of diode bars. Tapered broad-area lasers can exhibit an improved beam quality and brightness. 5) Slab-coupled optical waveguide lasers, containing a multi-quantum well gain region in a relatively large waveguide, can generate a watt-level output in a diffraction-limited beam with a nearly circular profile. 6) High-power diode bars contain an array of broad-area emitters, generating tens of watts with poor beam quality. Despite the higher power, the brightness is lower than that of a broad area LD. 7) Monolithic surface-emitting semiconductor lasers typically generate a few mW with high beam quality. There are also external-cavity versions of such LDs, which can generate much higher powers with still excellent beam quality.

According to Poole [51] some of the main types of LD include the following 1) Double hetero structure LD is made up by sandwiching a layer of a low band gap material with a layer on either side of high band gap layers. This makes the two hetero junctions as the materials themselves are different and not just the same material with different types of doping. The advantage of the double hetero junction LD over other types is that the holes and electrons are confined to the thin middle layer, which acts as the active region. By containing the electrons and holes within this area more

effectively more electron-hole pairs are available for the laser optical amplification process. 2) Quantum well LD uses a very thin middle layer; this acts as a quantum well where the vertical component of the electron wave function is quantized. As the quantum well has an abrupt edge, this concentrates electrons in energy states that contribute to laser action, and this increases the efficiency of the system. In addition to the single quantum well LD, multiple quantum well LDs also exist. The presence of multiple quantum wells improves the overlap between the gain region and the optical waveguide mode. 3) Quantum cascade LD is a form of hetero junction laser diode, which the difference between well energy levels is used to provide the laser light generation. This allows the LD to generate relatively long wavelength light - the actual wavelength can be adjusted during fabrication by altering the LD layer thickness. 4) Separate confinement hetero structure LD overcomes the problem that in many other forms of LD the thin laser layer is too thin to confine the light effectively. This LD overcomes the problem by adding another two layers with a lower refractive index on the outside of the existing ones. This effectively confines the light to within the diode. 5) Distributed feedback LDs are used in forms of telecommunications or data transmission using optical systems. Here the laser diode wavelength is important, but laser diodes are not particularly stable in this respect with wavelength varying with temperature, voltage, ageing, etc. A diffraction grating is etched close to the p-n junction of the diode to assist in stabilizing the wavelength of the generated light signal; this acts like an optical filter causing a single wavelength to be fed back to the gain region. The pitch of the grating is set during manufacture, and this only varies slightly with temperature. 6) Vertical-Cavity Surface-Emitting LDs are a form of surface emitting laser and they emit the laser radiation in a direction perpendicular to the wafer, delivering a few mW with high beam quality.

The optical characteristics, small size, and ruggedness of LDs have allowed many new uses to be commercialized. LDs are used in a variety of applications that require small sizes in addition to low power consumption with long operating lifetimes. LDs are ideal for applications such as life science, industrial, or scientific instrumentation, in addition to laser line generation or machine vision. As they are available in a wide variety of wavelengths, output powers, or beam shapes LDs are used in optical fiber systems, compact disc players, laser printers, remote-control devices, and intrusion detection systems. Figure A.2 presents several commercial

laser diodes. Figure A.2 a) presents semiconductor LD; Figure A.2 b) presents external cavity LD; Figure A.2 c) presents high-reliability, high-power, monolithic stack pulsed LDs.
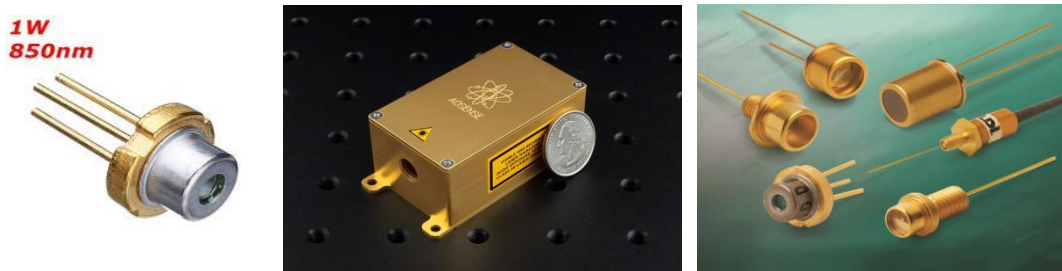


Figure A.2 a) Semiconductor LD; b) External cavity LD; c) High-Reliability, High Power, Monolithic Stack Pulsed LDs

Main characteristics of LDs that were considered in this research are the following:

Optoelectronic Characteristics

The most important parameter of LDs to be measured is the degree to which they emit light when current is injected into the device. This generates the Output Light vs. Input Current Curve, more commonly referred to as the L.I. curve. The efficiency of the LD in converting electrical power to light power is determined by the slope of the L.I. curve that is shown in Figure A.3.
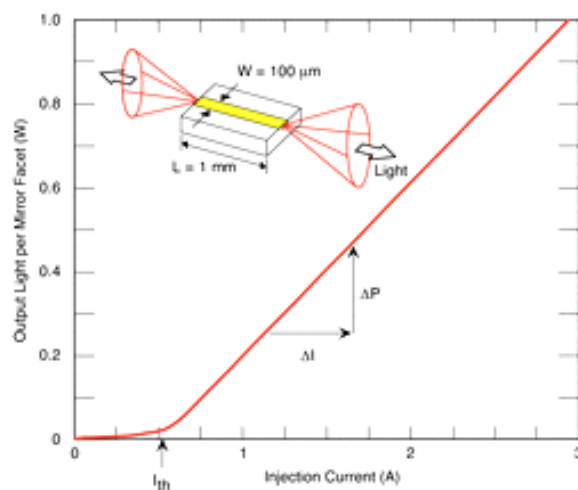


Figure A.3 Light power vs. Current curve.

As the injected current is increased, the laser first demonstrates spontaneous emission that increases very gradually until it begins to emit stimulated radiation, which is the onset of laser action. The first parameter of interest is the exact current value at which this phenomenon takes place. This is typically referred to as the threshold current. A threshold current is one measure used to quantify the performance of a laser diode.

1) Characteristic Temperature

The ability of the LD to perform well at elevated temperatures is of great interest. It is important for the semiconductor crystal to be robust enough so as not to suffer from device deterioration at high temperatures. In order to measure the characteristic temperature of a laser diode it is necessary experimentally measure the L.I. curve of a laser at various temperatures. Typically, these measurements are performed at temperatures ranging from 15 $^0$C up to about 80 $^0$C, and at 5 or 10-degree increments.

2) Spectral Characteristics of Laser Diodes

The optical spectrum of LDs depends on the characteristics of the laser's optical cavity. The optical wave propagating through the laser cavity forms a standing wave between the two mirror facets of the laser. The center wavelength of a LD is directly proportional to its operating temperature. The reason for this is that the refractive index and the length of the active zone, respectively the resonator, increase with increasing temperature. Beyond a certain temperature the mode does not fit anymore into the resonator and another mode, which faces more favorable conditions will start to oscillate. As the distance between two successive modes is very large for the extremely short resonator (typical 300 μm), the jump is about 0.3 nm. Lowering the temperature gets the laser jumping back in his wavelength. After this the laser must not be necessarily in the departing mode. The laser radiation of the diodes has distinct direction of polarization, the ratio of polarization, vertical polarization to horizontal polarization, depends on the output power since for higher laser power the ratio of spontaneous to stimulated emission is changing (Fig A.4).
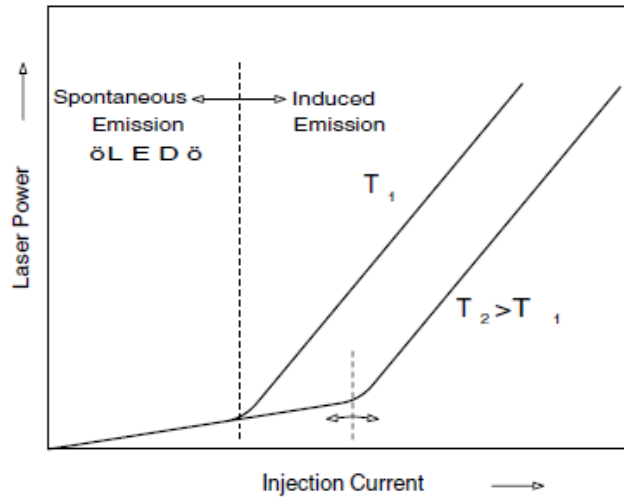
Figure A.4 Laser light power vs. Injection current curves for two temperatures.

In this work, a similar behavior is observed for the variation of the injection current and in consequence for the laser output power.

Several factors govern the change in lasing wavelength of laser diodes. The rate of temperature change in the active layer depends on a transient phenomenon determined by heat conduction. This behavior shows the active layer temperature increase as a function of the current pulse width. A tuning of LD is possible only in a narrow spectral band. The maximum tuning range is typically 10 nm for lasers where $\lambda \approx 650$ nm and 15 nm for $\lambda \approx 750$ nm. Spectrum of used laser diode is shown on Figure A.5, while graphs given in Figures A.6-A.8 show results on our experiments conducted to the laser diode at different temperatures and at different injection current. Different curves represent different peaks in LD spectrum.
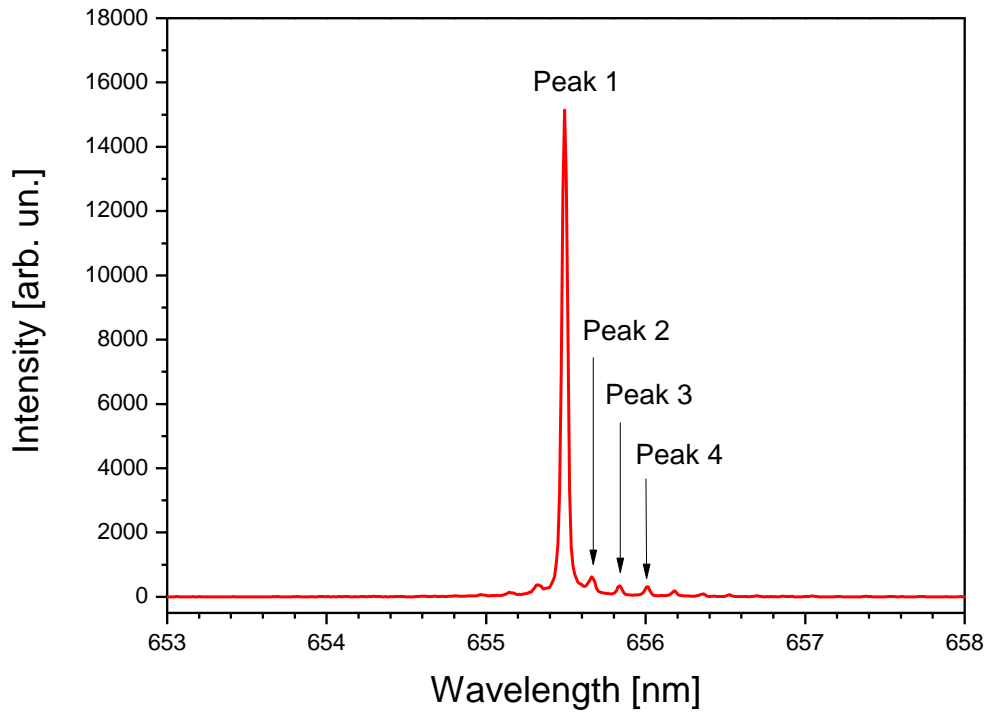
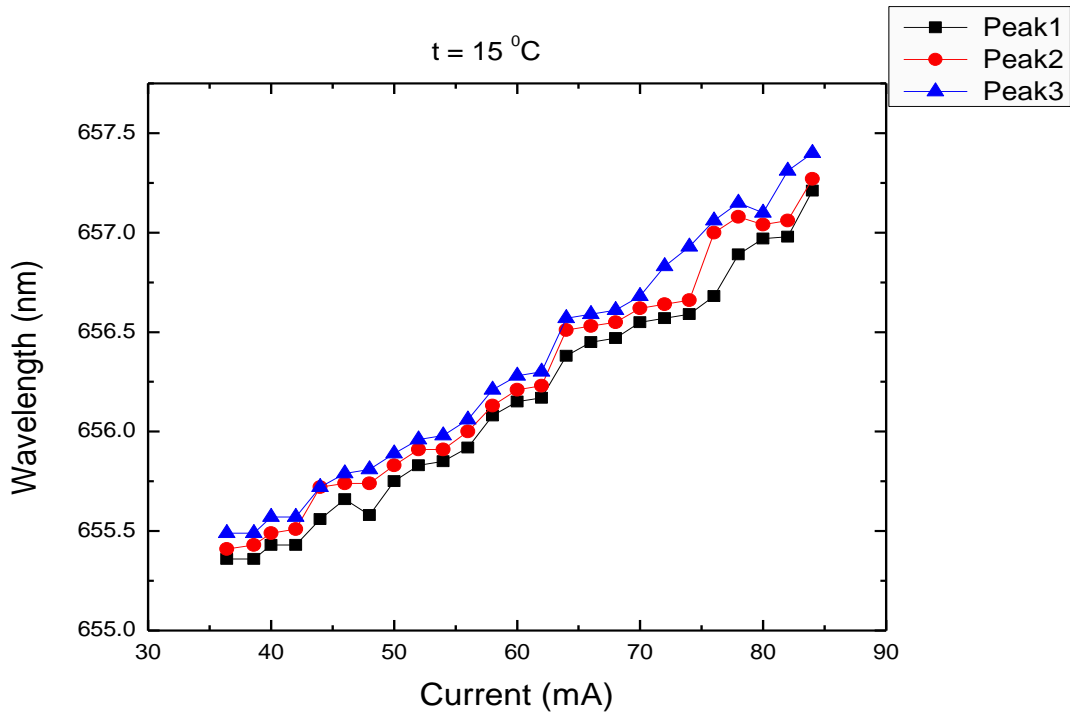Figure A.5 Spectrum of used LD in the experiments.
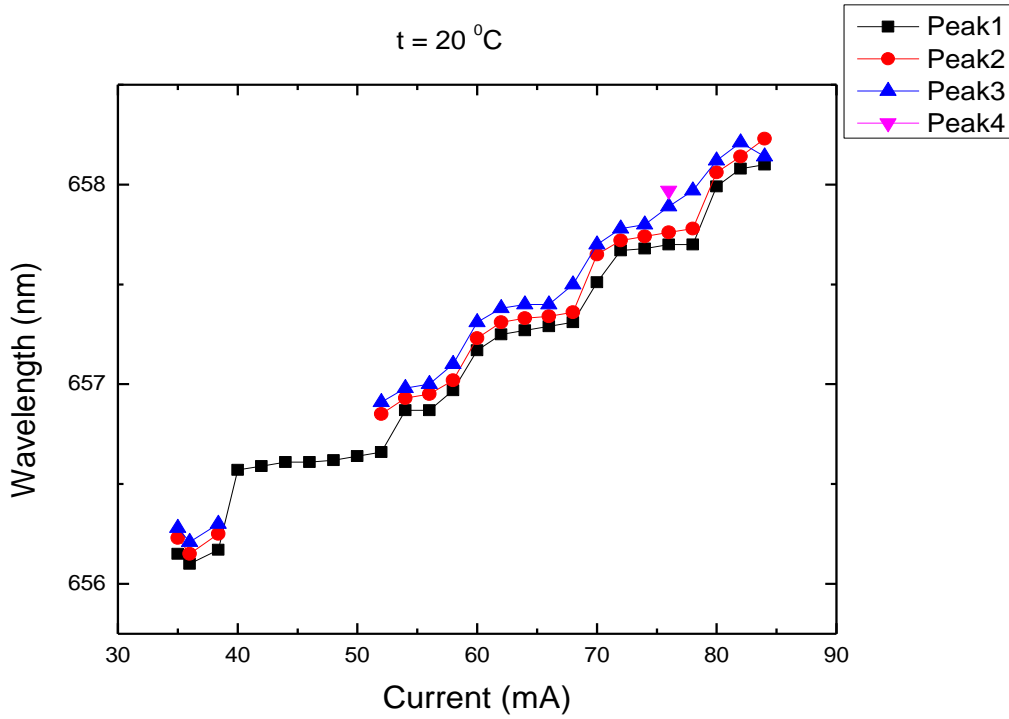


Figure A.6 Wavelengths vs. Current (t = 15 $^0$C).
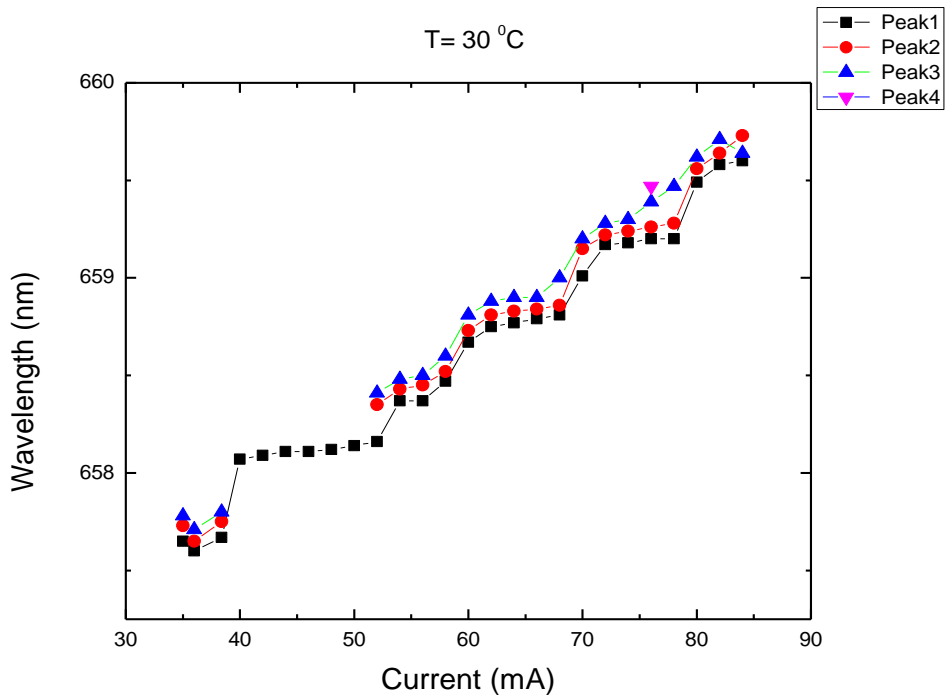
Figure A.7 Wavelengths vs. Current (t = 20 $^0$C).



Figure A.8 Wavelengths vs. Current (t = 30 $^0$C).

Results of experiments conducted to the laser diode at different temperatures and on the injection current of laser show movement of spectral band towards higher wavelengths with the increase of temperature, which is in compliance with theory. Comparing the spectral bands of LD in Figures A.6-A.8 one can see that spectral band is moved from 655.25-657.5 nm range to 656.0 – 658.25 nm range with the increase in temperature from 15°C to 20°C (Figure A.7), i.e. spectral band has moved to 657.0-659.75 nm range with the increase in temperature to 30°C (Figure A.8).

# CURRICULUM VITAE - Eldakli Mohsan S. A.

Date&Place of birth: 14.03.1981 Alajimyal – Libya

Contacts                 : E-mail: mohsan.eldakli@ff.bg.ac.rs

## The topic of PHD research
- Transfer of knowledge from scientific experiments to student laboratory –Hollow cathode discharge and optogalvanic effect

## Education
- 1998 Graduated at High School in Libya
- 2002 BSc degree in Physics, AlZawiya University, Libya
- 2011 MSC degree in Physics, Faculty of Physics, University of Belgrade, Serbia
- currently - PhD candidate at Faculty of Physics, University of Belgrade, Serbia

## Professional experience
- Taught Electromagnetic Physics and Optical Physics Courses from 2003 to 2008 at Faculty of Physics, Al Zawiya university, Libya .

## Research interests
- Theoretical Physics
- Teaching Physics

## List of Publications
- D. V. Redzic, M. S. A. Eldakli, and M. D. Redzic, An Extension Of The Kelvin Image Theory To The Conducting Heaviside Ellipsoide. Progress in Electromagnetics Research M, Vol.18, 233-246, 2011.
- D. V. Redzic, M. S. A. Eldakli, and M. D. Redzic, Image charge inclusion in dielectric sphere revisited, Eur.J.Phys.33, 1751-1759, 2012
- M. S. A. Eldakli, S. S. Ivković, B. M. Obradović,Optogalvanic effect and laser-induced current oscillations in hollow-cathode lamps, European Journal of Physics, 38, 025210, 2017

**Прилог 1.**

# Изјава о ауторству

Потписани-а  Mohsan S. A. Eldakli

број уписа  D14/2012

**Изјављујем**

да је докторска дисертација под насловом

TRANSFER OF KNOWLEDGE FROM SCIENTIFIC EXPERIMENT TO STUDENT
LABORATORY - HOLLOW CATHODE DISCHARGE AND OPTOGALVANIC EFFECT

- резултат сопственог истраживачког рада,
- да предложена дисертација у целини ни у деловима није била предложена за добијање било које дипломе према студијским програмима других високошколских установа,
- да су резултати коректно наведени и
- да нисам кршио/ла ауторска права и користио интелектуалну својину других лица.

Потпис докторанда

У Београду,  17.10.2017

**Прилог 2.**

# Изјава о истоветности штампане и електронске верзије докторског рада

Име и презиме аутора _Mohsan S. A. Eldakli_

Број уписа _D14/2012_

Студијски програм _Настава физике_

Наслов рада _TRANSFER OF KNOWLEDGE FROM SCIENTIFIC EXPERIMENT TO STUDENT LABORATORY - HOLLOW CATHODE DISCHARGE AND OPTOGALVANIC EFFECT_

Ментор _Проф. др Братислав Обрадовић_

Потписани _Mohsan S. A. Eldakli_

изјављујем да је штампана верзија мог докторског рада истоветна електронској верзији коју сам предао/ла за објављивање на порталу **Дигиталног репозиторијума Универзитета у Београду.**

Дозвољавам да се објаве моји лични подаци везани за добијање академског звања доктора наука, као што су име и презиме, година и место рођења и датум одбране рада.

Ови лични подаци могу се објавити на мрежним страницама дигиталне библиотеке, у електронском каталогу и у публикацијама Универзитета у Београду.

**Потпис докторанда**

У Београду, _17.10.2017_

**Прилог 3.**

# Изјава о коришћењу

Овлашћујем Универзитетску библиотеку „Светозар Марковић" да у Дигитални репозиторијум Универзитета у Београду унесе моју докторску дисертацију под насловом:

**TRANSFER OF KNOWLEDGE FROM SCIENTIFIC EXPERIMENT TO STUDENT LABORATORY - HOLLOW CATHODE DISCHARGE AND OPTOGALVANIC EFFECT**

која је моје ауторско дело.

Дисертацију са свим прилозима предао/ла сам у електронском формату погодном за трајно архивирање.

Моју докторску дисертацију похрањену у Дигитални репозиторијум Универзитета у Београду могу да користе  сви који поштују одредбе садржане у одабраном типу лиценце Креативне заједнице (Creative Commons) за коју сам се одлучио/ла.

1. Ауторство

2. Ауторство - некомерцијално

3. Ауторство – некомерцијално – без прераде

4. Ауторство – некомерцијално – делити под истим условима

5. Ауторство –  без прераде

6. Ауторство –  делити под истим условима

(Молимо да заокружите само једну од шест понуђених лиценци, кратак опис лиценци дат је на полеђини листа).

Потпис докторанда

У Београду, 17.10.2017